AD-A108 416 TORONTO UNIV DOWNSVIEW (ONTARIO) INST FOR AEROSPACE --ETC F/G 20/4
AN EXPERIMENTAL INVESTIGATION OF RISE TIMES OF VERY WEAK SHOCK --ETC(U)
MAR 81 O HOLST-JENSEN AFOSR-77-3303
UNCLASSIFIED UTIAS-TN-229 AFOSR-TR-81-0781 NL

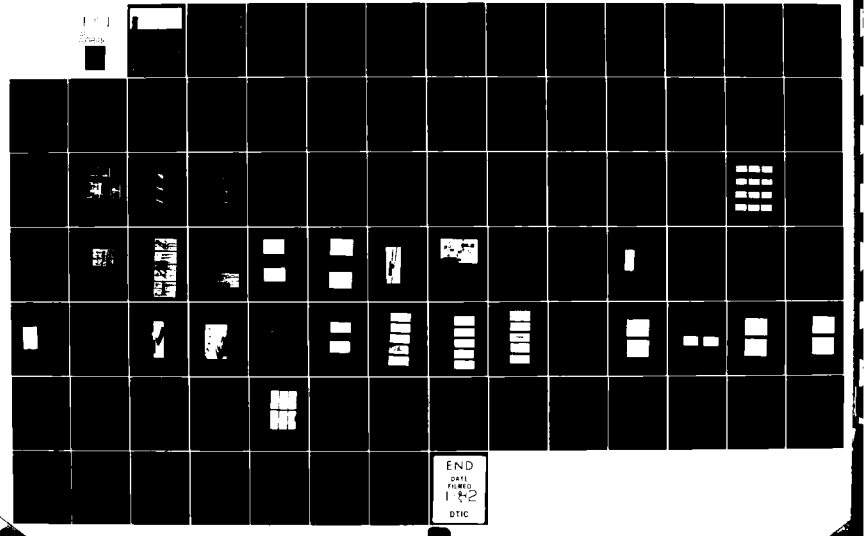

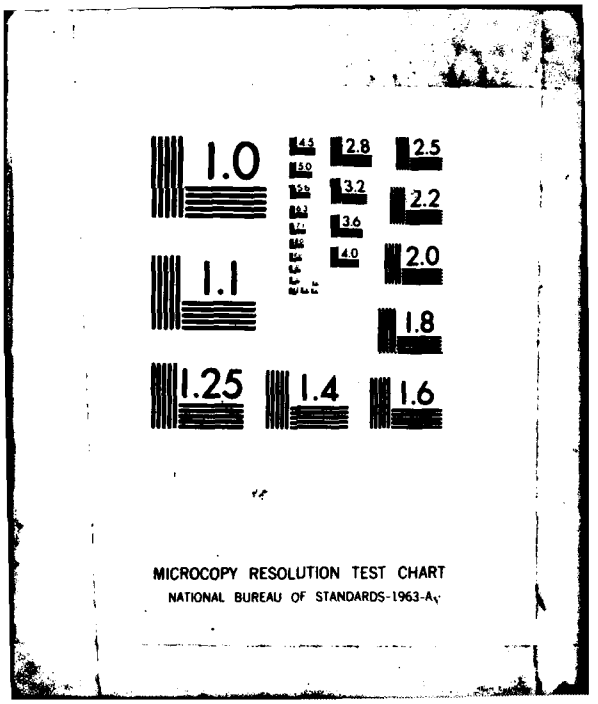
1.0
1.1
1.25
1.4
1.6
2.8
3.2
3.6
4.0
2.5
2.2
2.0
1.8
MICROCOPY RESOLUTION TEST CHART
NATIONAL BUREAU OF STANDARDS-1963-A

INSTITUTE
FOR
AEROSPACE STUDIES
UNIVERSITY OF TORONTO

AFOSR-TR- 81-0781

AN EXPERIMENTAL INVESTIGATION OF RISE TIMES OF VERY WEAK SHOCK WAVES

by

Ole Holst-Jensen

March, 1981

TN-229
UTIAS-Technical Note No. 229
CN ISSN 0082-5263

UNCLASSIFIED

SECURITY CLASSIFICATION OF THIS PAGE (When Data Entered)

REPORT DOCUMENTATION PAGE		READ INSTRUCTIONS BEFORE COMPLETING FORM
1. REPORT NUMBER AFOSR-TR- 81 -0781	2. GOVT ACCESSION NO. AD-A1084 16	3. RECIPIENT'S CATALOG NUMBER
4. TITLE (and Subtitle) AN EXPERIMENTAL INVESTIGATION OF RISE TIMES OF VERY WEAK SHOCK WAVES		5. TYPE OF REPORT & PERIOD COVERED INTERIM 6. PERFORMING ORG. REPORT NUMBER
7. AUTHOR(s) OLE HOLST-JENSEN		8. CONTRACT OR GRANT NUMBER(s) AFOSR-77-3303
9. PERFORMING ORGANIZATION NAME AND ADDRESS UNIVERSITY OF TORONTO, INSTITUTE FOR AEROSPACE STUDIES, 4925 DUFFERIN STREET DOWNSVIEW, ONTARIO, CANADA, M3H 5T6		10. PROGRAM ELEMENT, PROJECT, TASK AREA & WORK UNIT NUMBERS 61102F 2307/A1
11. CONTROLLING OFFICE NAME AND ADDRESS AIR FORCE OFFICE OF SCIENTIFIC RESEARCH/NA BOLLING AIR FORCE BASE, DC 20332		12. REPORT DATE MAR 81 13. NUMBER OF PAGES 85
14. MONITORING AGENCY NAME & ADDRESS(if different from Controlling Office)		15. SECURITY CLASS. (of this report) UNCLASSIFIED 15a. DECLASSIFICATION/DOWNGRADING SCHEDULE

16. DISTRIBUTION STATEMENT (of this Report)

Approved for public release; distribution unlimited.

17. DISTRIBUTION STATEMENT (of the abstract entered in Block 20, if different from Report)

18. SUPPLEMENTARY NOTES

19. KEY WORDS (Continue on reverse side if necessary and identify by block number)

SONIC BOOM
N-WAVES
EXPLODING WIRES
EXPLODING SPARKS
TRAVELLING-WAVE SONIC-BOOM SIMULATOR

20. ABSTRACT (Continue on reverse side if necessary and identify by block number)

The present work has as its main contribution the development of the experimental technique of using exploding wires to generate N-waves. Consideration is also given to N-waves generated by sparks, in the UTIAS Travelling-Wave Sonic-Boom Simulator and from supersonic aircraft.

DD FORM 1 JAN 73 1473 EDITION OF 1 NOV 65 IS OBSOLETE

UNCLASSIFIED

SECURITY CLASSIFICATION OF THIS PAGE (When Data Entered)

Qualified requestors may obtain additional copies from the Defense Documentation Center, all others should apply to the National Technical Information Service.

Conditions of Reproduction:

Reproduction, translation, publication, use and disposal in whole or in part by or for the United States Government is permitted.

Approved for public release; distribution unlimited.

A

AIR FORCE OFFICE OF SCIENTIFIC RESEARCH (AFSC)
NOTICE OF TRANSMITTAL TO DDC
This technical report has been reviewed and is approved for public release IAW AFR 190-12.
Distribution is unlimited.
MATTHEW J. KERPER
Chief, Technical Information Division

AN EXPERIMENTAL INVESTIGATION OF RISE TIMES OF VERY WEAK SHOCK WAVES

by

Ole Holst-Jensen

Submitted October, 1980

March, 1981

UTIAS Technical Note No. 229
CN ISSN 0082-5263

Acknowledgements

I wish to thank Dr. I. I. Glass for his support and enthusiasm throughout the course of this work. The provision of data and discussions with Professor D. T. Blackstock, Mr. D. J. Maglieri and Mr. D. R. B. Webb are very much appreciated. Thanks are due to Dr. H. S. Ribner and Dr. G. W. Johnston for many constructive comments. I also wish to thank my wife and friends, without whose understanding and support this work could not have been completed.

The financial assistance received from the U.S. Air Force under Grant AFOSR 77-3303 and from the Canadian Ministry of Transport, Transportation Development Centre, is acknowledged with thanks.

Summary

The present work has as its main contribution the development of the experimental technique of using exploding wires to generate N-waves. Consideration is also given to N-waves generated by sparks, in the UTIAS Travelling-Wave Sonic-Boom Simulator and from supersonic aircraft.

Contents

1. INTRODUCTION AND REVIEW

Sonic booms have been studied since supersonic transports became a reality. Extensive measurements of sonic booms have been undertaken in the U.S.A. (Refs. 1-4), in the U.K. (Refs. 5-7) and in France (Ref. 8) to investigate the physical characteristics of the phenomenon. Typical shapes of sonic booms as measured at Edwards Air Force Base (Ref. 1) are shown in Fig. 1.1. The general shape, the peak overpressure and duration of a sonic boom can be predicted from the design of the aircraft, its altitude, Mach number and the variation of temperature and wind gradients of the atmosphere with altitude (see Refs. 9-11).

The present study was initiated on the basis that shock rise times in sonic booms have been reported to be 100 to 1000-fold longer than the rise times predicted by the weak-shock theory. Researchers have for a number of years been challenged to investigate the causes for this discrepancy.

The rise time of the sonic boom was shown by Zepler and Harel (Ref. 12), Johnson and Robinson (Ref. 13) and Niedzwiecki and Ribner (Refs. 14-16) to be an important parameter in the overall loudness of a wave. These subjective-loudness studies of N-waves have indicated that a decrease in rise time increases the loudness (Fig. 1.2, Ref. 14). For this reason it is important to be able to predict the fastest possible rise of any part of the sonic boom on an average day.

Some sonic boom measurements are presented below. They serve the purpose of showing very small sonic boom rise times, and the measured variations due to atmospheric turbulence.

During the program of supersonic overflights at Edwards Air Force Base (Ref. 1) numerous sonic booms were recorded. We have received previously unpublished (Ref. 17) oscilloscope traces from the measurement of a sonic boom generated by an F-104 fighter aircraft flying at M = 1.3 at an altitude of 9296 m. In this particular trace the time scales were expanded to show the front and the back of the boom (Fig. 1.3), which was not previously published. The front shock shows a rise time (10% to 90% peak overpressure) of t_f = 48 μs while the rear shock has a rise time of t_b = 40 μs. The microphone used for the measurements was a condenser microphone with an estimated rise time capability of 50 μs (Ref. 1). This indicates that the rise time of the oscilloscope traces in Fig. 1.3 are those of the monitoring system, which lead to the conclusion that the rise time of the shock fronts in the sonic boom may have been shorter than the measured values. It should be noted that Fig. 1.3 provides evidence of very short rise times in sonic booms.

This particular F-104 boom is classified as a spiked boom known to have the shortest rise times of all types of booms. Generally (Ref. 17) the sonic boom has a transition as shown in the pressure time histories of Figs. 1.4 and 1.5 (Ref. 1). The pressure rises quite rapidly to a value p_f equal to .8 or .9 amplitude followed by a comparatively slow increase until the peak pressure p_{max}. From what can be estimated from Figs. 1.4 and 1.5 the rise time t_f to p_f is at most 1/10 of the rise time t_{max} to p_{max}, which is the rise time tabulated in Ref. 1.

Measurements of sonic booms by SR-71 aircraft operating at Mach numbers up to 3.0 and altitudes to 24,384 metres is reported in Ref. 3. The obtained histograms of rise times per unit overpressure to maximum overpressure and to half amplitude are shown in Fig. 1.6. As reported, the most probable overpressure is 45 Pa. This implies that the typical rise time to maximum overpressure is 5 ms and to half overpressure 1.25 ms.

Sonic booms generated by the Concorde have been studied extensively by the Royal Aircraft Establishment (Refs. 5-7). One particular experiment of interest for rise time studies is the simultaneous measurement at five different altitudes, namely 593m, 420m, 287m, 144m and ground level. This has not been published previously (Ref. 7). Four microphones were attached to a balloon tether so that the diaphragms were mounted 20 inches from the tether and approximately horizontal, while one was mounted in a baffle at ground level. The purpose of the experiment was to study the rise time variation with altitude, and to determine its effects if possible. We have received data in digital form from one such experiment on a day with a clear blue sky, a gentle breeze and with microphones fitted with windscreens. The five microphone readings are reproduced in Fig. 1.7. At an altitude of 593m the pressure-time history of the front of the sonic boom is as shown in Fig. 1.7a.

First there is a steep rise to a pressure p_f = 29.3 Pa with a 10% to 90% rise time of t_f = 0.165 ms, then a much more shallow rise to the peak pressure p_{max} = 60.5 Pa, reached after a time t_{max} = 5.40 ms. The pressure-time history at 420m, Fig. 1.7b, shows a somewhat different picture, in that the pressure rises in a steep gradient to p_f = 42.9 Pa in t_f = .135 ms and the subsequent shallow rise to p_{max} = 62.0 Pa takes only t_{max} = 0.555 ms. At 287m the boom is spiked, Fig. 1.7c, i.e., the pressure rises to a maximum in one fast transition with t_{max} = 0.095 ms. The front of the boom measured at 144m altitude, Fig. 1.7d, shows the same character as that at 593m. The initial fast rise brings the pressure up to p_f = 27.1 Pa in t_f = 0.305 ms, and the subsequent shallow rise increases the pressure to p_{max} = 50.2 Pa after a total of t_{max} = 6.04 ms. At ground level, the front of the boom has been distorted as seen in Fig. 1.7e. The first rise to p_f = 22.7 Pa in t_f = 0.175 ms is followed by a comparatively irregular rise to maximum overpressure p_{max} = 91.7 Pa after a total of t_{max} = 1.20 ms. This measurement reads twice the incident sonic boom overpressure because of reflection from the baffle. All the stated data are computed from Ref. 7 and tabulated in Table 1.1.

It should be noted that the horizontal mounting of the microphones would most likely result in an angle of incidence of the front of the sonic boom of about 90°. The microphone used in the experiments was a Brüel & Kjaer type 4146 sonic boom microphone, which has a risetime capability at 90° incidence of t_m^{4146} (90°) = 105 μs. It should be noted that this conservative estimate of the capability is of the same order of magnitude as the rise times of the first front of the sonic boom (see column t_f in Table 1.1). We interpret the rise times t_f as being the limitation of the monitoring equipment, rather than the true rise time of the shocks. The fact that t_{max} = 0.095 ms in Fig. 1.7c probably arises from a less than 90° incidence.

The reported Concorde data, on a calm day, show a fairly steep front up to a point where the rise changes slope. Analysing the data of Fig. 1.7, we

find no definite trend in the variation of the shallow part of the booms with altitude.

It should be noted that the booms measured at the five altitudes have most likely propagated through different air masses of temperature, pressure, humidity, turbulence, and wind speeds. This is illustrated in Fig. 1.8 where the suspended microphones are seen as points 1 to 5. The sonic boom generated at altitude propagates along sound rays (r_1 to r_5). The figure shows that the five microphones are not necessarily located on the same sound ray. This explains the fairly large differences in the traces.

Sonic booms from Mirage III fighter planes have been measured in the exercise Jericho-Casbah (Ref. 8). The measured signals showed the general shape shown in Fig. 1.9. Note that we have adopted this definition of rise time, i.e., from 10% to 90% amplitude. Sample traces are shown in Fig. 1.10, the left column contains the full sonic boom, the middle and right columns show the front and rear shocks respectively on an expanded time scale. The measurements were performed with a Brüel & Kjaer 1/2" dia microphone with a rise time capability of ~ 25 μs. Note that the overpressures are in a range of 160-960 Pa, because the overflights were conducted at a low altitude of about 600m. For high altitude overflights of about 11,000m, the measurements listed in Table 3 (Ref. 8) show generally higher and measurable rise times, for overpressures in the range 99-131 Pa. It should be noted that four of the rise times are $\theta \sim 60$ μs.

The rise times reported in the American studies are defined as the time interval between the start and the peak of the pressure rise, see Fig. 1.11 (Ref. 1). In the French study (Ref. 8) the definition of rise time is the time elapsed from 10 to 90% of the pressure rise of the steepest part of the wave front, see Fig. 1.9. Note also in Fig. 1.9 that there is a great difference between the rise time and the time from start to peak. In Figs. 1.4, 1.7 and 1.10 are shown recordings of typical sonic booms in the U.S., U.K. and France, respectively. It is seen that the general shape of the shocks can be modeled by the wave form in the French study (Fig. 1.9). The rise time of the steepest part of the front has been shown (Ref. 16) to have the greatest influence on the subjective loudness. We have therefore adopted the French definition as the most useful one for sonic-boom rise-time assessments. An important result of the French measurements is that many rise times were found to be equal to the resolution of the measuring microphone, see Tables 1.1 and 1.2. It was therefore concluded (Ref. 7) that the rise time of the wave was shorter than the measured rise time.

The presented results indicate the physical existence of very fast pressure increases in sonic boom shock fronts. The true rise time of a sonic-boom shock can only be measured when microphones with very short response times are used. A suitable transducer for this measurement is the high-frequency microphone described in Ref. 18.

The sonic booms in Fig. 1.12 were measured along an 8,000 ft linear microphone array. The observed irregularities illustrate large deviations from the standard sonic booms shown above. We have found it relevant in the discussion of sonic-boom rise times also to include wave-interaction effects. A review of such observed effects is given below.

A laboratory experiment performed at UTIAS simulated the effect of a jet on a shock-tube driven N-wave. The convection of the N-wave in the jet causes a spike when it propagates upstream. Rounding of an N-wave occurs when it propagates downstream (Refs. 19, 20). Effects of diffraction and refraction of short N-waves were demonstrated by Davy and Blackstock (Ref. 21). Their experiments show that a soap bubble filled with helium can round the wavefronts considerably. When filled with argon, the wavefronts become spiked. Similar sound speed variations are speculated to arise in turbulent eddies in the atmosphere, thus affecting sonic booms.

Several laboratory experiments have been performed to study the influence of artificially generated turbulence on weak shocks. Tubb generated weak shocks in a shock tube and let them traverse a turbulent flow produced by a coarse grid (Ref. 20). A doubling of the shock rise time was found as a statistical mean value. Also Hesselink (Refs. 22, 23) studied the scattering of weak shocks by turbulent eddies experimentally. Considerable distortion of an M = 1.007 shock front after passing the random density region was found.

Bauer and Bagley (Refs. 24, 25) used supersonic projectiles to generate sonic booms. They also found large distortions of the shock fronts after passing through a turbulent jet.

Several authors have treated the theoretical problem of shock-interference with turbulence (Refs. 26-30). A conclusion by Ffowcs-Williams and Howe (Ref. 30) is that the small scale turbulence in the lower atmosphere is not likely to thicken a sonic boom shock by more than a factor of 2. Obermeier (Ref. 27) predicted large distortions by large turbulent eddies. The eddy motion introduced different propagation speeds for different parts of the wave front. When these parts merge at a later time, the phase difference between the parts results in large distortions of the fronts.

The above mentioned studies indicate that large scale turbulence does have the potential of a significant distortion effect on sonic boom shock fronts.

Refraction of the high frequencies due to temperature gradients close to the ground and due to the surface itself is speculated to be a cause for the measurement of long rise times in sonic booms. This effect has been observed at UTIAS when calibrating a portable sonic boom generator (Ref. 31). The shock propagated parallel to the ground and was measured at a distance of 30m from the source by two microphones, one located 1.64m above the ground and one 0.33m above ground level. The measured traces are shown in Fig. 1.13. In the top trace measured at 1.25m, the front has a short rise time, whereas the bottom trace shows a rise time several orders of magnitude larger. This effect may also be caused by ground reflection, as shown theoretically in Ref. 32.

The refraction effect has been observed to increase shock rise times in the 60m pyramidal shock tube at the Institute Franco-Allemand de Recherches de Saint-Louis (Refs. 33, 34), as shown in Figs. 1.14a and 1.14b. The top two oscillographs in Fig. 1.14 show the shocks with no temperature gradient, and they are indeed sharp. By introducing a temperature gradient across the horn as sketched, the shocks measured at points 3 and 3' now vary considerably.

The shock at the "cold" point, 3', is identical to the previous one, and the shock at the "hot" point, 3, has a considerably longer rise time. It should be noted that the overpressure of the shock is 1,050 Pa, a superboom, tenfold greater than normal sonic booms. Figure 1.14b shows in sketch (i) the influence of the temperature gradient on the shock fronts. The traces in (ii) show examples with two different temperatures.

The two different examples of increased rise time illustrate that near the ground a temperature gradient can cause an increase in measured rise time by orders of magnitude in sonic boom shocks propagating parallel to the ground. Most sonic boom measurements have been performed with the sensors mounted at ground level, where the direction of propagation is almost parallel to the ground. Therefore, we suspect that this was a significant factor in the reported measurements of apparently long rise times of sonic booms.

It should be noted that most NASA sonic-boom measurements were performed in a desert area where large near-ground temperature gradients are known to exist. This could well be the cause for the consistently longer N-wave rise-time data reported by NASA, compared with the rise-time data for the Mirage III and Concorde noted here.

These results imply that measured sonic boom shocks can have rise times about 100-1,000 times longer than what can be predicted by weak-shock theory. The explanation is to be found in the following effects:

(a) The above mentioned definition of rise time.
(b) Small and large scale turbulence.
(c) Thermal layers.
(d) Grazing ground effects.
(e) Real gas effects.

Because of the many effects causing the sonic boom rise time, it is not going to be a readily predictable parameter. It would, however, be useful to be able to predict the shortest possible rise time which would represent the worst case in a subjective loudness assessment, Ref. 16.

We assume that the shortest rise time will occur when none of the above mentioned wave-interactions have thickened the shock. The wave front is then a weak shock wave affected only by the nonlinearity of its propagation and the diffusion of the fluid within which it moves. Since the shock strength near the source (SST) is very large it is assumed that by the time they reach the ground they have evolved into an N-wave bounded by two weak shock waves.

The sonic-boom shocks are assumed to be quasisteady. This means that steepening and diffusion are balanced within the shock transition, and that a steady wave solution can give the theoretical transition for perfect and real gases. In the latter case, relaxation effects can cause very large rise times, especially for dispersed shock waves (Ref. 35).

The limitations of the Travelling-Wave Sonic-Boom Simulator in generating suitable N-waves will be discussed later. The spark and exploding wire techniques have the advantage of generating spherical N-waves that are free from distortion. However, they have the disadvantage that the durations are very

short. In studying the rise times of such fronts the weak, spherical shock wave transition problem must be solved numerically without introducing artificial viscous effects arising from the finite-difference equations. This can now be overcome by using the Random Choice Method and will be discussed in a later UTIAS report.

2. EXPERIMENTAL CONSIDERATIONS

The purpose of these experiments is to generate weak, fully-developed shock waves with overpressures below 100 Pa in air. Part of the experiments were used to investigate different ways of generating quasistable weak shock fronts in the laboratory. To obtain interference-free shock fronts in an N-wave is the main concern. This is readily done using the exploding-wire technique and partially so by the spark technique described below.

2.1 Monitoring Equipment

For the detection of weak shocks in the overpressure range 5-100 Pa, the condenser microphone is a good choice. The type used here was a Brüel & Kjaer (B & K) 4135 freefield 6.3 mm (1/4 in) dia microphone. The response of two such microphones was tested in the Travelling-Wave Simulator. They were mounted at the same distance from the apex, in the centre of the pyramid and only 50 mm apart. In this position they were exposed to very short-rise-time shocks. In Fig. 2.1 the times are from both microphones mounted with a protection grid and the shock is at 0-degree incidence. The ripple on top of the sharp part is at about 45 kHz, close to the resonance frequency of the cartridge. In Fig. 2.2 the protection grid of the one microphone has been removed. The lower trace shows that the 45 kHz ripple has disappeared. Hence the ripple is assumed to be due to diffraction introduced by the protection grid. In Fig. 2.3 both protection grids have been removed and the one microphone has been turned to a 90-degree incidence. This results in a poorer high frequency response (rise time) which is also seen in Appendix A, Fig. A.1, where the free-field response for 0 degree and 90 degree incidence are plotted. Based on these findings all measurements were performed without a protection grid at 0-degree incidence.

Note that in this setup a ripple of about 135 kHz was observed (see Fig. 2.4). The overpressure of this shock is 60 Pa, whereas the overpressures in the previous figures are about twice as much. This ripple is assumed to be due to diffraction phenomena because the frequency is much higher than the resonance frequency for this type of microphone. When measuring without its protective grid at zero angle of incidence, this microphone has an approximate minimum rise time $t = 2.9\ \mu s$, when mounted at the end of a 1m long 3/4 in (19 mm) copper tube (see Appendix A for details in obtaining this value). Amplification of the microphone signal was provided by a preamplifier, B & K 2619, and a power supply B & K 2807. According to the respective manuals, the upper limiting frequency -1 dB in the free-field response is the 140 kHz set by the microphone cartridge. As fairly long cables were used in the setup, the pulse response of a 60m RG 58/U cable was calculated as 100 ns for a 10% to 90% rise time of an "infinitely-steep" pulse propagated through the 60m of cable. Since no cables exceeded 60m it is assumed that the cables

did not limit the frequency response of the microphone system. The oscilloscopes used were Tektronix types 555 and 535 with a type D plug-in that has a bandwidth better than 300 kHz. It is seen that the microphone signal will be shown undistorted on the oscilloscope screen. The microphone was calibrated with a B & K Pistonphone type 4220, which gives a sound pressure level at 250 Hz of 124 dB. The accuracy according to the manual is better than $\epsilon_{cal} = \pm 4.7\%$.

All overpressures and time measurements were extracted from oscillographs. The values were obtained by measuring distances between parallel lines that were drawn through the points of interest. The distance was measured with a scale subdivided into 1/100 inch (0.25 mm). The accuracy is estimated to be 0.125 mm. A typical distance between lines, i.e., the distance to be measured, is 20 mm, where the accuracy becomes $\epsilon_{L1} \approx 0.6\%$. The lines used have a thickness of 0.15 mm and the location accuracy of the line is estimated to be ± 0.15 mm. As the reading was taken between two lines, the total error due to the location accuracy of the lines was for a typical measurement $\epsilon_{L2} = 0.30$ mm/20 mm = 1.5%. The total error in overpressure measurements consisted of two parts:

$$\epsilon_p = \epsilon_p \text{ (calibrator signal)} + \epsilon_p \text{ (measured signal)}$$

or

$$\epsilon_p = \epsilon_{cal} + \epsilon_{L1} + \epsilon_{L2} + \epsilon_{L1} + \epsilon_{L2}$$

or

$$\epsilon_p = 8.8\%$$

The calibration signal for the time base was the 60 Hz AC line frequency which was accurate to within $\epsilon_{AC} < 0.1\%$. The total error on the time signals is

$$\epsilon_t = \epsilon_t \text{ (calibration)} + \epsilon_t \text{ (measurement)}$$

or

$$\epsilon_t = \epsilon_{AC} + \epsilon_{L1} + \epsilon_{L2} + \epsilon_{L1} + \epsilon_{L2}$$

or

$$\epsilon_t = 4.3\%$$

Since some of the measurements were performed at 0°C the stability of the oscilloscopes was tested over an experimental period of a day. Variations were found to be less than 1%.

For the experiments in the horn the temperature detection was done using wide-range hygrosensors types 15-2011 and 15-2010 made by Hydrodynamics. These sensors in the four stations of the horn were coupled to a switch-box model No. 15-3050. The accuracies, according to the manual, were ± 1.5% on relative humidity and ± 1°C on temperature.

For the experiments in the ACV dome a sling psycrometer was used to measure the wet and dry bulb temperatures. The derived humidities were estimated to have an accuracy of ± 2%; the temperature was reliable to within ± 0.5°C.

2.2 Pyramidal Shock Tube

The UTIAS Travelling-Wave Sonic-Boom Simulator was used for part of the experiments. The facility consists of a 25m long horizontal concrete structure of pyramidal shape; it has a 3m x 3m base and a divergence angle of 7.2 degrees. Both ends of the horn are contained in simple structures shown in Fig. 2.5. The apex is in the so-called control room as shown in Fig. 2.6. In the experiments the horn was used in its shock-tube mode with three driver lengths: 0.21m, 0.46m and 1.58m. The diaphragm stations are shown in Fig. 2.6. It should be noted that the first 4 metres of the horn are made of 25mm thick steel. The interior of the horn is equipped with humidity and temperature sensors as shown in Fig. 2.7. There are four locations where the humidity and temperature can be measured, namely at distances of 6.10m, 12.2m, 18.3m and 24.4m from the apex. A complete description of the UTIAS Travelling-Wave Sonic-Boom Facility can be found in Refs. 36 and 37.

Shock-Tube Experiments with 1.58m Driver Length

The first experiments with the travelling-wave horn as a shock tube were done with a driver length of 1.58m. To generate waves with less than 100 Pa overpressure in the wide end, a weak and brittle diaphragm material was used. The material had to be weak to break at a sufficiently low overpressure in the driver and so brittle that cracks formed at the initial breaking point had a high propagation speed. A thin quality waxed typewriter carbon paper was found to have these properties pumping the driver section until the diaphragm burst by itself led to too-high overpressures, a breaker mechanism was designed. It consists of four levers that simultaneously press on the paper near the corners, see Fig. 2.8. This enhances crack formation along the edges which resulted in the cleanest initial wavefront. The signals were measured in the centre of the horn with a microphone on a movable stand. An average of 5 measurements were taken at seven locations along the axis of the horn. A typical oscillograph, taken at 2.13m from the apex of the horn is seen in Fig. 2.9. Note that the trace is not smooth, except for the initial part. Virtually all traces obtained with the 1.58m driver had the characteristic shown in Fig. 2.9. The measured peak overpressures $p\xi$ compensated for spherical spreading, i.e., multiplied by $\xi = x/x_o$, the distance from the apex over the driver length are plotted as a function of ξ in Fig. 2.10. The two sets of runs, series 1 and 2, were performed with the driver overpressures 1379 Pa and 1724 Pa, respectively. Note that the compensated overpressures are increasing with distance in both series. This is most unexpected, and we assume that the waves were not ideally-formed one-dimensional spherical waves.

According to Taylor's theory (Ref. 38), the overpressure multiplied by the rise time of a shock, $p \cdot t$, is constant if the total viscosity of the gas is constant. The behaviour of the parameter $p \cdot t$, as obtained from the measured waves in the horn, express whether the waves are steepening compression pulses or shocks. If $p \cdot t$ is decreasing as a function of the propagation distance, the wave is steepening. When $p \cdot t$ has reached a minimum value, a shock is formed which will persist beyond that point until its amplitude had decreased to an infinitesimal value. It is seen from the plot in Fig. 2.11 of $p \cdot t$ versus ξ for series 1, that the trend of $p \cdot t$ is to decrease. Hence the waves generated by the 1.58m driver are still steepening at the end of the horn, and cannot be regarded as fully-formed shocks. The reason why the shocks are not formed is that the rise time created by the breaking diaphragm is much longer than the

corresponding shock rise time, and the weak wave cannot steepen into a shock within the length of the horn.

Shock-Tube Experiments with Separator

To overcome the difficulty of weak waves with long rise times, the shorter driver lengths 0.21 and0.45m were employed. In this way the initial overpressure could be higher than with the 1.58m driver and still achieve the same wave overpressure at the base of the horn. The higher initial overpressure also provided for a faster breaking of the diaphragm, thereby creating a wave with a higher steepening potential. The initial wave fronts generated with the short drivers were irregular. The reason for this was taken to be due to transverse waves generated by the nonuniform pressure distribution across the diaphragm upon breaking. To avoid these modes a separator was introduced at the 1.58m section (Fig. 2.12). The wave transmitted through the separator material had a decreased overpressure and an increased rise time according to the material used. Thin PVC plastic was found to smooth the waveform suitably, and was used for the runs with the 0.21m and 0.46m drivers. An example of the variation of p·t versus ξ for one of a series (I to VI) with the 0.21m driver at an initial overpressure of 41,000 Pa is shown in Fig. 2.11. In each run the wavefront was measured at two locations in the horn, one at $\xi = 14.5$, the other on a movable stand. In this way the initial front could be checked for every run. For this series of runs the waves are steepening all the way down the horn.

At this point of the experiments it was desired to check the sphericity of the waves. This was done by locating two microphones at the same distance from the apex, one in the centre and the other at one sixth of the distance centre-wall from the wall. A typical measurement of the wavefront at 21.3m generated by the 0.46m driver at an initial overpressure of 15,500 Pa is shown in Fig. 2.13. Both the overpressure and the rise time varied considerably between the two measuring points at the same cross section. The nonuniformity of the wavefront implies that we cannot assume one-dimensional spherical waves. Another illustration is the differences in p·t versus ξ as shown in Fig. 2.14, where it appears that the difference between the two measuring points increases with distance. These final experiments in the Travelling-Wave Horn led to the conclusion that uniform one-dimensional spherical waves were impossible to establish when generated in the above manner.

It can be concluded that the experiments in the N-Wave Simulator established the difficulty in generating an ideally spherical shock front of overpressures lower than 100 Pa. One of the nonidealities was the uncontrolled curvature of the diaphragm upon breakage. If the curvature is different from the curvature given by the circle section with the driver length as radius, there will be a crosswise motion in the horn. The above assumes that the diaphragm is ruptured instantaneously along the rim. If we consider the breaking of the diaphragm to start at one point, there will at this point in the channel be a higher pressure relative to all other points at the diaphragm. This also causes transverse waves and a three-dimensional shock front. The separator did eliminate some of these nonidealities, but not all.

2.3 Air Cushion Vehicle Dome

The dome containing the UTIAS Air Cushion Vehicle (ACV) circular-track

facility was used as a still-air reservoir for part of the experiments. The facility is located in the field behind the UTIAS building as shown in Fig. 2.15. The interior of the 42.7m dia building appears in Fig. 2.16. The wooden track used for ACV experiments is readily seen. The need for waves free of interference with walls and non-ideal generation was fulfilled by the experiments designed to take place in the ACV dome. The first series used sparks as a source of N-waves. The sparks were generated by the energy release from a charged 7.5 μF capacitor. The maximum charging voltage was 8 kV and the releasing device was a thyratron. A sketch of the setup is seen in Fig. 2.17 where to the right the capacitor and thyratron are connected by a low-impedance cable to a resistor over which the spark jumps. To the left is the measuring microphone labelled 'm', and the trigger microphone labelled 't', both attached to the oscilloscope. Note that a typical wavelength is 50 mm, which means that the path length of any reflected signal must be longer than the direct path by 50 mm to avoid distorted recordings by the measuring microphone. This was achieved by elevating the source and microphone 1.8m above the floor.

One series consisted of six runs runs for at least three different charging voltages for several distances between the source and the receiver. Three runs were made with a fast 10 μs time-scale, the other three with a slower 50 μs time-scale. In this way the front shock and the full wave with the rear part could be studied (Fig. 2.18). Fairly extensive measurements were done in the temperature range of 275-277K and relative humidity range of 67-73%, where six source-receiver distances were employed with four different charging voltages. A total number of 106 oscillographs were obtained. Some of them are shown in Fig. 2.19 (a) to (c). The displayed oscillographs were picked so as to represent average measurements. In Fig. 2.19(a) all readings were obtained with S = 4.4 kV charge at five locations, 4.08m, 4.85m, 0.76m, 15.6m and 21.6m. Note that the first two oscillographs are taken with 20 μs/div, the third at 5 μs/div, and the last two at 10 μs/div. The maximum overpressures of the front P_f, and the rear P_r shocks are individually marked beside each picture together with the rise times t_f and t_r from 10% to 90% of the full amplitude. It should be noted that no rise time t_f is given in the first two pictures because it is assumed not to be a reliable replica of the shock rise time as the microphone does not respond fast enough (see Appendix A). In the last three pictures of Fig. 2.19(a) the shock rise time t_f of the front of the N-waves are recorded. The first two photos in Fig. 2.19(a), (b), (c) show the wave recorded at 20 μs/div, because the recording at 5 μs/div only shows that the microphone limits the front shock, $t_f < 5$ μs. We have therefore chosen to show the full wave in the first two oscillograms of Fig. 3.19(a), (b) and (c).

The oscillation at the frequency 143 kHz seen in the first three traces just after the first peak is caused by diffraction off the edge of the microphone capsule. It is not, as might be assumed, ringing because the pressure pulse response as mentioned in Appendix A does not show any ringing.

Since the rear part of the waves always showed a high degree of irregularity, it was concluded that well-formed shocks were not present there. Similar oscillographs are presented for charging voltages of S = 5 kV and S = 6 kV in Figs. 2.19(b) and (c), respectively. These show the same trend that the front shock is initially steeper than what the microphone can measure. When the peak overpressure reaches about 30 Pa the rise time has increased above the microphone response time of about 3 μs.

The pressure decay relative to the value at R_o = 4.08m multiplied by R/R_o is plotted against $\xi = R/R_o$ in Fig. 2.19(d). The experimental points from all spark experiments are averaged for each charging voltage.

Another source of N-waves is the exploding wire. By replacing the resistor in Fig. 2.17 by a thin wire, the sudden release of energy vaporizes the metal in the wire. The expansion of the metal vapour generates an N-wave in the far field as seen in Fig. 2.20. The wire material was 0.125 mm dia nickel. It is seen that the N-waves are much cleaner than those generated by a spark, especially the rear shock. Note that the wire length ℓ plays a significant role in shaping the rear shock wave. The top trace in Fig. 2.20 shows a record for R = 12.8m, S = 5.0 kV and ℓ = 25 mm. The rise time of the rear shock is much longer than the front. By increasing the wire length to ℓ = 60 mm the trace changes, as shown in the bottom trace. Now both ends of the wave look alike. We assume from this that the top trace is an N-wave with a shock in the front and a compression wave in the rear. The bottom trace is an N-wave with shocks in front and rear. A wire length of ℓ = 50 mm proved to generate the most symmetrical N-waves, and was used in all subsequent runs.

The length of the exploding wires had another effect, namely, the short wire acted as a point source and the long wire as a line source. This was measured by detecting the signals from wires 15 mm long as a function of the angle between the normal to the wire and the direction of the microphone; see Fig. 2.21(a). The signals for all angles were practically identical to the trace shown in Fig. 2.21(b), taken at an angle $\theta = 45°$. The experiment was repeated for a wire 150 mm long and the trace for an angle $\theta = 45°$ is shown in Fig. 2.21(c). It should be noted that the rear portion of the pressure trace has diminished. This is caused by the line-source effect, which has been treated in Ref. 42. We found that the flat part grows from zero to a maximum as θ varies from 0° to 90°. As our interest was in a symmetrical N-wave, all measurements were performed at an angle $\theta = 0°$.

Two runs at T = 280°K, RH = 85%, S = 4.6 kV and ℓ = 50 mm are shown in Fig. 2.22(a). The top trace is measured at R = 24.3m and the bottom trace at R = 29.3m. Note that the rear shocks have smaller overpressures and longer rise times than the front shocks. This slight asymmetry is assumed to be generated at the source and is not indicative of any real-gas or propagational effects.

Similar traces are found in Fig. 2.22(b) where the charging voltage was changed to S = 6.0 kV. It should be noted that the difference between the front and rear shocks is also present here. The rise time for the rear shock is, however, considerably larger than the front shock, which we interpret as caused by the difference in overpressure. In Fig. 2.22(a) and (b) it is seen that as the overpressure decreases the rise time increases as expected. Note, however, that the rear shocks for the N-waves generated by the 6.0 kV source strength have longer rise times than those generated by the 4.6 kV source strength. Additional data are presented in Appendix B.

3. CONCLUSIONS

A very considerable number of experiments are presented on the generation

of N-waves from exploding sparks and wires. These data should form an important and useful base for analytical and numerical studies of shock-wave structure of weak nonstationary spherical blast waves, including vibrational excitation of air. A comparison of such analyses and the experimental data will provide very worthwhile information on rise times due to vibrational relaxation. Such investigations are now underway.

REFERENCES

1. Anon. — "Sonic Boom Experiments at Edwards Air Force Base", NSBEO-1-67, AD0655310, Virginia, June 28, 1967.

2. Hilton, D. A.
Newman, J. W. — "Instrumentation Techniques for Measurement of Sonic Boom Signatures", J. Acoust. Soc. Amer., Vol. 39, No. 5, Part 2, 1966.

3. Maglieri, D. J.
Huckel, V.
Henderson, H. R. — "Sonic Boom Measurements for SR-71 Aircraft Operating at Mach-Numbers to 3.0 and Altitudes to 24384 Meters", NASA TN D-6823, 1972.

4. Maglieri, D. J.
Huckel, V.
Henderson, H. R.
Macleod, N. J. — "Variability in Sonic Boom Signatures Measured Along an 8000 ft Linear Array", NASA TN D-5040, 1969.

5. Webb, D. R. B.
Warren, C. H. E. — "Physical Characteristics of the Sonic Bangs and Other Events at Exercise Westminster", Ministry of Technology, R & M No. 3475, London, 1967.

6. Webb, D. R. B.
Hunt, F. L.
Pallant, R. J.
Walters, W. L. — "Sonic Bang Measurements During Exercise Summer Sky", Ministry of Aviation Supply, R & M No. 3659, London, 1971.

7. Webb, D. R. B. — Private Communications, March and May, 1977.

8. Rigaud, P.
Franke, R.
Matieu, G.
Evrard, G. — "Bang Sonique de Mirage III", ISL, Notice-Notiz N3/72, 1972.

9. Hayes, W. D.
Haefeli, R. C.
Kulsrud, H. E. — "Sonic Boom Propagation in a Stratified Atmosphere with Computer Program", NASA CR-1299, 1969.

10. Onyeonwu, R. O. — "Sonic Boom Signatures and Ray Focussing in General Manoeuvres: 1. Analytical Foundation and Computer Formulation, 2. A Numerical Study", J. Sound & Vibr., Vol. 42, Part 1, 1975, pp. 85-114.

11. Carlson, H. W. — "Simplified Sonic-Boom Prediction", NASA Technical Paper 1122, 1978.

12. Zepler, E. E.
Harel, F. R. P. — "The Loudness of Sonic Booms and Other Impulsive Sounds", J. Sound & Vibr., Vol. 2, 1965, p. 249.

13. Johnson, D. R.
Robinson, D. W. — "Procedure for Calculating the Loudness of Sonic Bangs", Acustica, Vol. 21, Heft 6, 1969, pp. 307-318.

14. Niedzwiecki, A. Ribner, H. S. "Subjective Loudness of Sonic Boom: N-Wave and Minimized ("Low-Boom") Signatures", UTIAS Technical Note No. 215, CN ISSN 0082-5263, November 1977.

15. Niedzwiecki, A. Ribner, H. S. "Subjective Loudness of N-Wave Sonic Booms", J. Acoust. Soc. America, Vol. 64(6), Dec. 1978, pp. 1617-1621.

16. Niedzwiecki, A. Ribner, H. S. "Subjective Loudness of 'Minimized' Sonic Boom Waveforms", J. Acoust. Soc. America, Vol. 64(6), Dec. 1978, pp. 1622-1626.

17. Maglieri, D. J. Private Communication, Noise Control Branch, NASA Langley, Oct. 14, 1976, June 2, 1977.

18. Wright, W. N. "High-Frequency Transducers for Use in Gases", Acoustics Research Laboratory, Harvard University, AD 276 637, April 1962.

19. Ribner, H. S. Morris, P. J. Chu, W. T. "Laboratory Simulation of Development of Superbooms by Atmospheric Turbulence", J. Acoust. Soc. America, Vol. 53, No. 3, 1973, pp. 926-928

20. Tubb, P. E. "Measured Effects of Turbulence on the Rise Time of a Weak Shock", AIAA Paper 75-543, March 1975.

21. Davy, B. A. Blackstock, D. T. "Measurements of the Refraction and Diffraction of a Short N-Wave by a Gas-Filled Soap Bubble", J. Acoust. Soc. America, Vol. 49, No. 3, Part 2, 1971.

22. Hesselink, L. "Propagation of Weak Shock Waves Through a Random Medium", Proc. Eleventh International Symposium on Shock Tubes and Waves, July 1977, pp. 82-90.

23. Hesselink, L. "An Experimental Investigation of Propagation of Weak Shock Waves in a Random Medium", Ph.D. Thesis, California Institute of Technology, Pasadena, California, May 24, 1977.

24. Bauer, A. B. "Sonic Boom and Turbulence Interactions – Laboratory Measurements Compared with Theory", AIAA Paper 71-618, July 1971.

25. Bauer, A. B. Bagley, C. J. "Sonic Boom Modeling Investigation of Topological and Atmospheric Effects", Report No. FAA-NO-70-10, Federal Aviation Administration Final Report, July 1970.

26. Beasley, J. A. "A Numerical Investigation of the Thickening of a Shock Wave on Passing Through Turbulence", RAE Reports and Memoranda No. 3793, Nov. 1974.

27. Obermeier, E. Zimmermann, G. "Das Streuverhalten eines Überschallknalles beim Durchgang durch eine Turbulente Schicht", MPI Strömungsforschung, Bericht 114, 1970.

28. Plotkin, K. J.
George, A. R.
"Propagation of Weak Shock Waves Through Turbulence", J. Fluid Mechanics, Vol. 54, Part 3, 1972, pp. 449-467.

29. Crow, S. C.
"Distortion of Sonic Bangs by Atmospheric Turbulence", J. Fluid Mechanics, Vol. 37, Part 1, 1969, p. 529.

30. Ffowcs-Williams, J. E.
Howe, M. S.
"On the Possibility of Turbulent Thickening of Weak Shock Waves", J. Fluid Mechanics, Vol. 58, Part 1, 1973, pp. 461-480.

31. Ellis, N. D.
Rushwald, I. B.
Ribner, H. S.
"A One-Man Portable Sonic Boom Simulator", J. Sound and Vibration, Vol. 40, Part 1, 1975, pp. 41-50.

32. Walker, E. I.
Doak, P. E.
"Effects of Ground Reflections on the Shapes of Sonic Bangs", Contributed Paper L55, 5e Congres Internationale D'Acoustique Liege, Sep. 7-14, 1965.

33. Peter, A.
Brunner, J. J.
"Etude d'un Tube a Choc Forme Pyramidale pour la Generation d'une Onde en N", Note Technique T 11/70, Isl Institute Franco-Allemand de Recherche de Saint Louis, 1970.

34. Thery, C.
Peter, A.
Schlosser, F.
"The ISL Bang Generator", Royal Aircraft Establishment, Library Translation No. 1629, December 1971.

35. Johannesen, N. H.
Hodgson, J. P.
"The Physics of Weak Waves in Gases", Rep. Prog. Phys., Vol, 42, 1979, pp. 629-676.

36. Glass, I. I.
Ribner, H. S.
Gottlieb, J. J.
"Canadian Sonic-Boom Simulation Facilities", Canadian Aeronautics & Space Journal, Vol. 18, No. 8, 1972, p. 235.

37. Gottlieb, J. J.
"Simulation of a Travelling Sonic Boom in a Pyramidal Horn", Progress in Aerospace Sciences, Vol. 17, 1976, pp. 1-66, Pergamon Press, Great Britain.

38. Taylor, G. I.
"The Conditions Necessary for Discontinuous Motion in Gases", Proc. of the Royal Society, Vol. 34, 1910, pp. 371-377.

39. Brüel & Kjaer
Instructions and Applications 4135/4136, Copenhagen, 1974.

40. Brüel & Kjaer
Instructions and Applications 4144, 4145, 4146, Copenhagen, April 1970.

41. Rudenko, O. V.
Soluyan, S. I.
Theoretical Foundations of Nonlinear Acoustics. Plenum Press, New York, 1977.

42. Howes, W. L.
"Farfield Spectrum of the Sonic Boom", J. Acoust. Soc., Vol. 41, No. 3, 1967, pp. 716-717.

Table 1.1

Data derived from RAE measured sonic booms generated by Concorde by an array of five microphones, four suspended from a balloon tether (Ref. 7)

Mic. Altitude (meters)	p_{max} (Pa)	p_f (Pa)	t_{max} (ms)	t_f (ms)
593	60.5	28.3	5.40	0.16
420	62.0	42.9	0.55	0.13
287	61.6	—	0.09	—
144	50.2	27.1	6.04	0.30
Ground	91.7	22.7	1.20	0.17

Table 1.2

Measured sonic booms from Mirage-III flying at altitude ~ 600m

Symbols refer to Fig. 1.9 (Ref. 9)

Vol. No.	Passage	T_N [ms]	First Shock				Second Shock			
			$\Delta\hat{p}_1$ [mbar]	θ_1 [μs]	Δp_1 [mbar]	$\frac{\Delta p_1}{\Delta\hat{p}_1}$	$\Delta\hat{p}_2$ [mbar]	θ_2 [μs]	Δp_2 [mbar]	$\frac{\Delta p_2}{\Delta\hat{p}_2}$
4	1	81.2	6.1	≈ 45	1.9	0.3	5.9	≈ 45	2.6	0.44
	2	78.3	3.2				4.3			
	3	81.3	5.3			6.3				
6	2	90.5	7.2	85	2.84	0.2	9.5	≤ 40	4.8	0.51
	3	80.4	4.1	≤ 25	1.5	0.38	3.8	≈ 70	1.6	0.42
	4	78.0	6.0	≤ 25	2.4	0.4	7.2	≤ 25	3.5	0.49
8	2	100.3	3.5				12.7	260	5.0	0.39
	3	91.3	9.1	≤ 25	6.8	0.75	7.2	≤ 25	2.5	0.35
	4	101.7	5.5				9.0	≤ 25	6.3	0.7
9	1	109.3	5.7	≤ 25	3.3	0.58	10.1	≤ 25	5.6	0.55
	2	-	1.6	-	-	-	2.3	-	-	-
	3	77.9	5.7	≤ 40	3.1	0.55	5.2	≤ 25	2.7	0.52
	4	79.55	6.9	≤ 30	3.7	0.54	5.9	≤ 30	2.7	0.46
11	1	77.6	3.2	≈ 80	1.7	0.53	3.9	120	1.9	0.48
	2	77	9.6	120	1.9	0.2	11.5	120	1.3	0.11
13	1	84	8.4	≤ 40	2.0	0.24	8.0	≤ 40	2.8	0.35
	2	82.6	5.3	≤ 30	2.7	0.51	5.9	≤ 25	2.0	0.34
	3	77.3	4.8	≤ 25	4.1	0.85	5.8	≤ 25	3.7	0.64
	4	78.7	4.4	≤ 35	4.0	0.91	4.5	≤ 25	3.0	0.67
14	2	107.5	3.2	640	2.0	0.62	6.5	640	5.3	0.82
	3	78.9	4.7	≤ 25	2.3	0.49	5.2	≤ 30	3.2	0.61

Table 1.3

Measured sonic booms from Mirage-III flying at altitude ~ 11,000m

Symbols refer to Fig. 1.9 (Ref. 9)

			First Shock				Second Shock			
Vol. No.	Passage	T_N [ms]	$\Delta\hat{p}_1$ [mbar]	ϑ_1 [μs]	Δp_1 [mbar]	$\frac{\Delta p_1}{\Delta\hat{p}_1}$	$\Delta\hat{p}_2$ [mbar]	ϑ_2 [μs]	Δp_2 [mbar]	$\frac{\Delta p_2}{\Delta\hat{p}_2}$
5	1	76.9	0.99	150	0.35	0.35	1.26	150	0.35	0.28
	2	77.0	1.13	150	0.75	0.66	1.22	110	0.9	0.74
10	1	74.5	1.06	700	0.95	0.9	1.14	700	1.05	0.92
	2	72.8	0.99	≈ 60	0.4	0.4	1.15	≈ 60	0.32	0.28
12	1	78.2	1.31		-		1.38	-	-	
	2	75.7	0.94	≈ 65	0.72	0.77	1.15	≈ 60	0.8	0.7

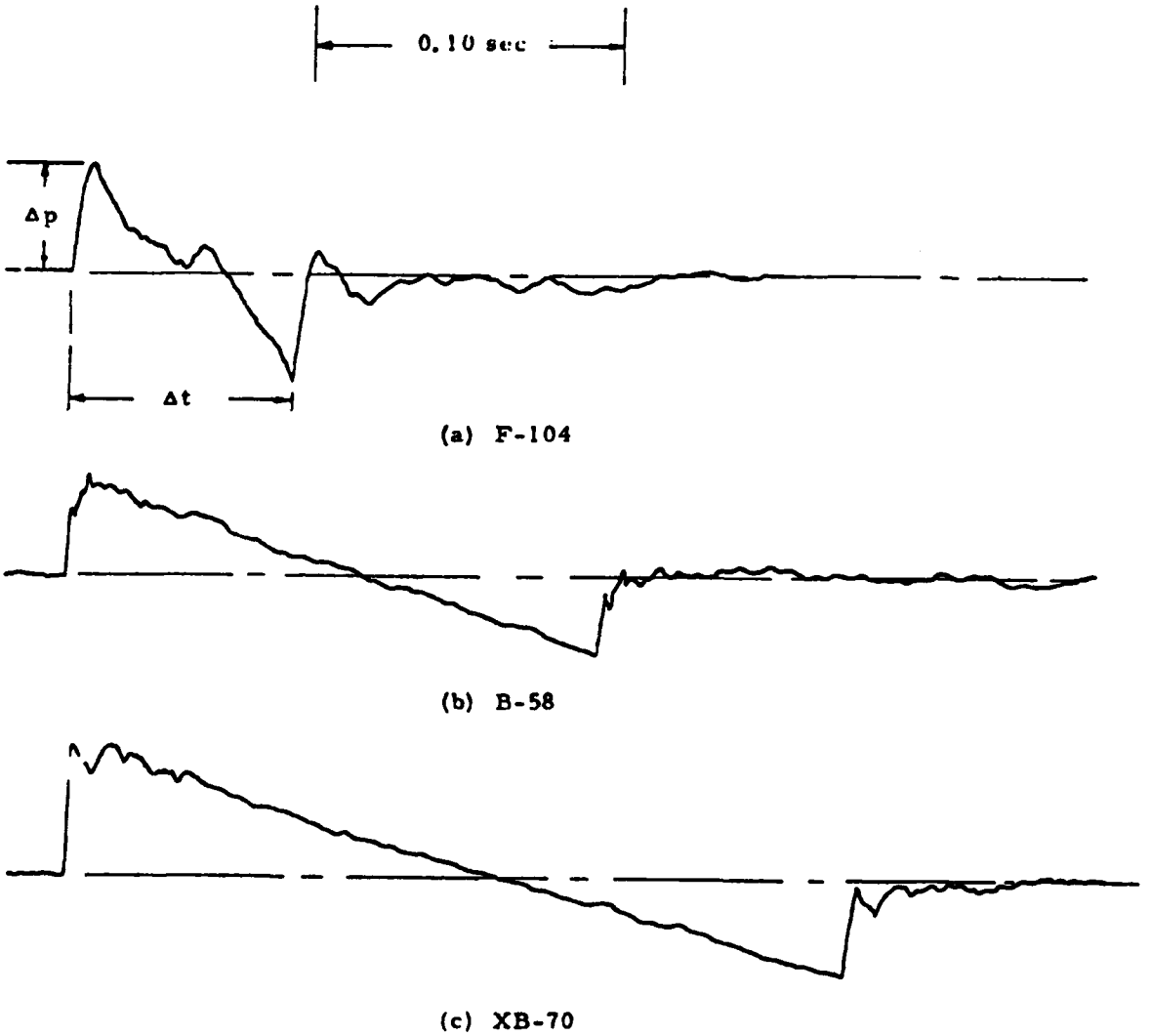

FIG. 1.1 TRACINGS OF SONIC BOOM SIGNATURES RECORDED DURING FLIGHTS OF THREE DIFFERENT AIRCRAFT (REF. 1).

(Δp and Δt values are listed.)

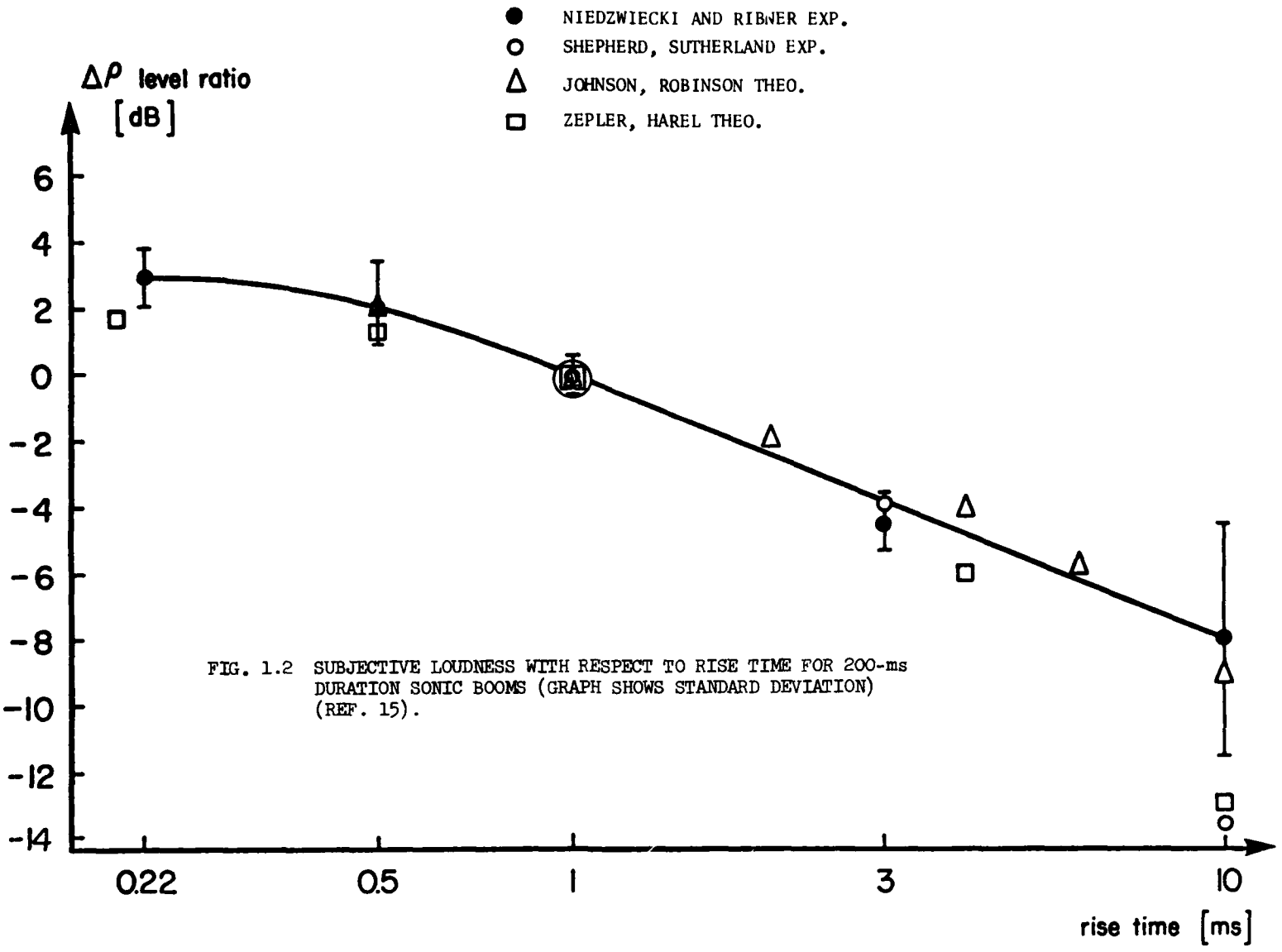

FIG. 1.2 SUBJECTIVE LOUDNESS WITH RESPECT TO RISE TIME FOR 200-ms DURATION SONIC BOOMS (GRAPH SHOWS STANDARD DEVIATION) (REF. 15).

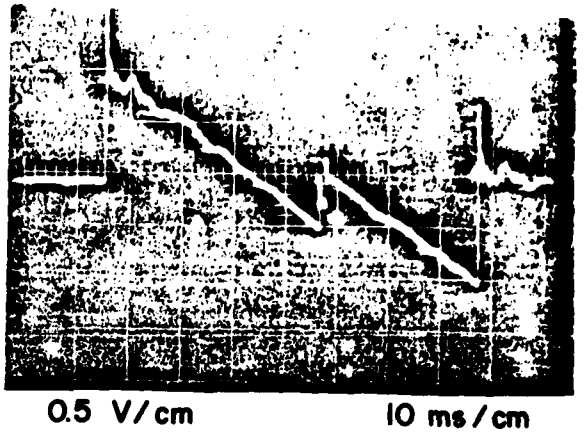

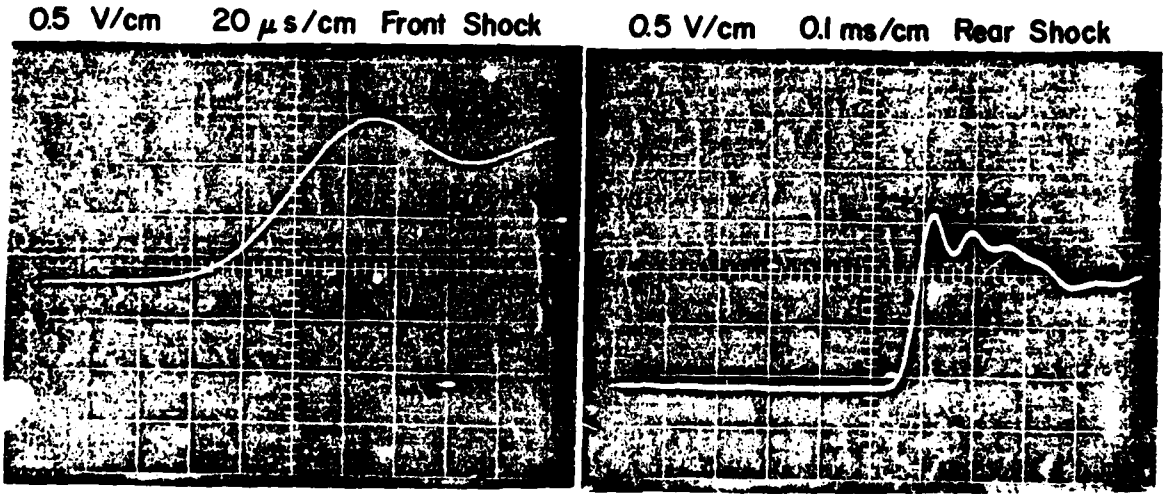

FIG. 1.3 SONIC BOOM FROM AN F-104 FIGHTER AT 9296m ALTITUDE AT M = 1.3 (REF. 3).

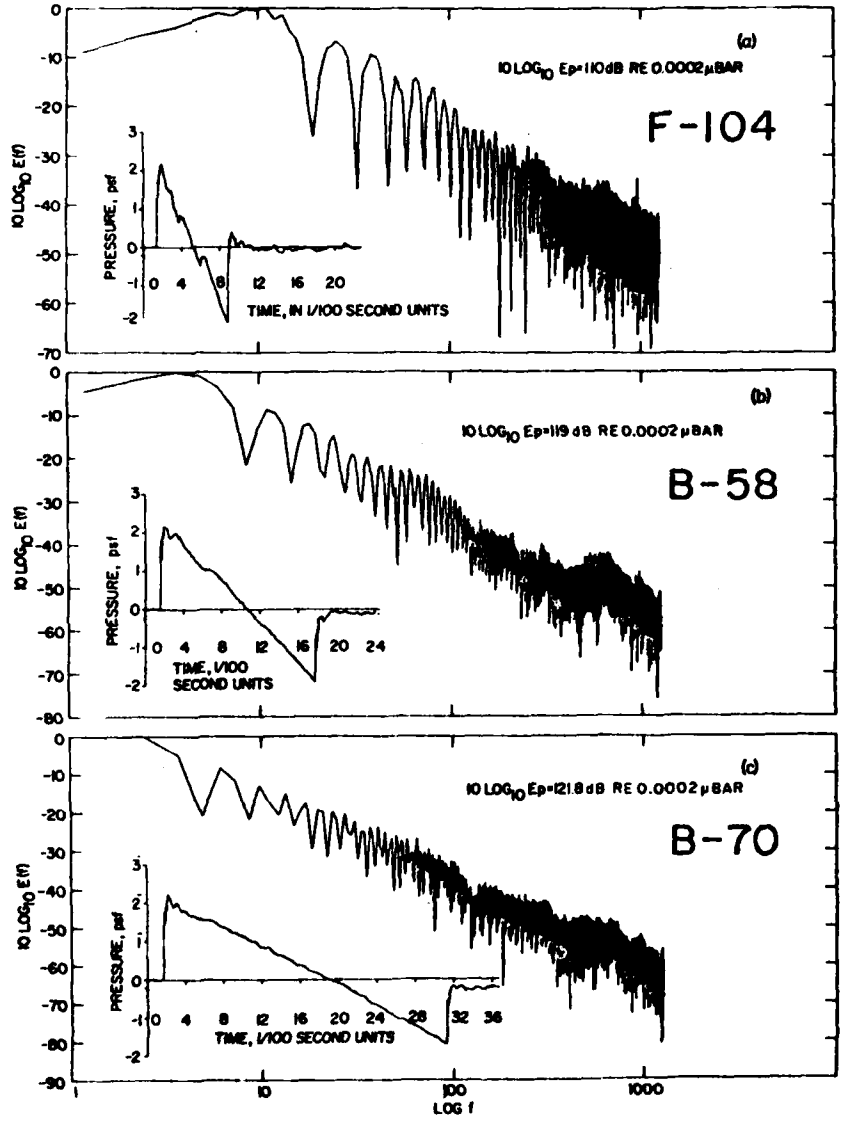

FIG. 1.4 PRESSURE-TIME AND E(f) PLOTS FOR THREE AIRCRAFT, F-104, B-58 AND B-70 (REF. 1).

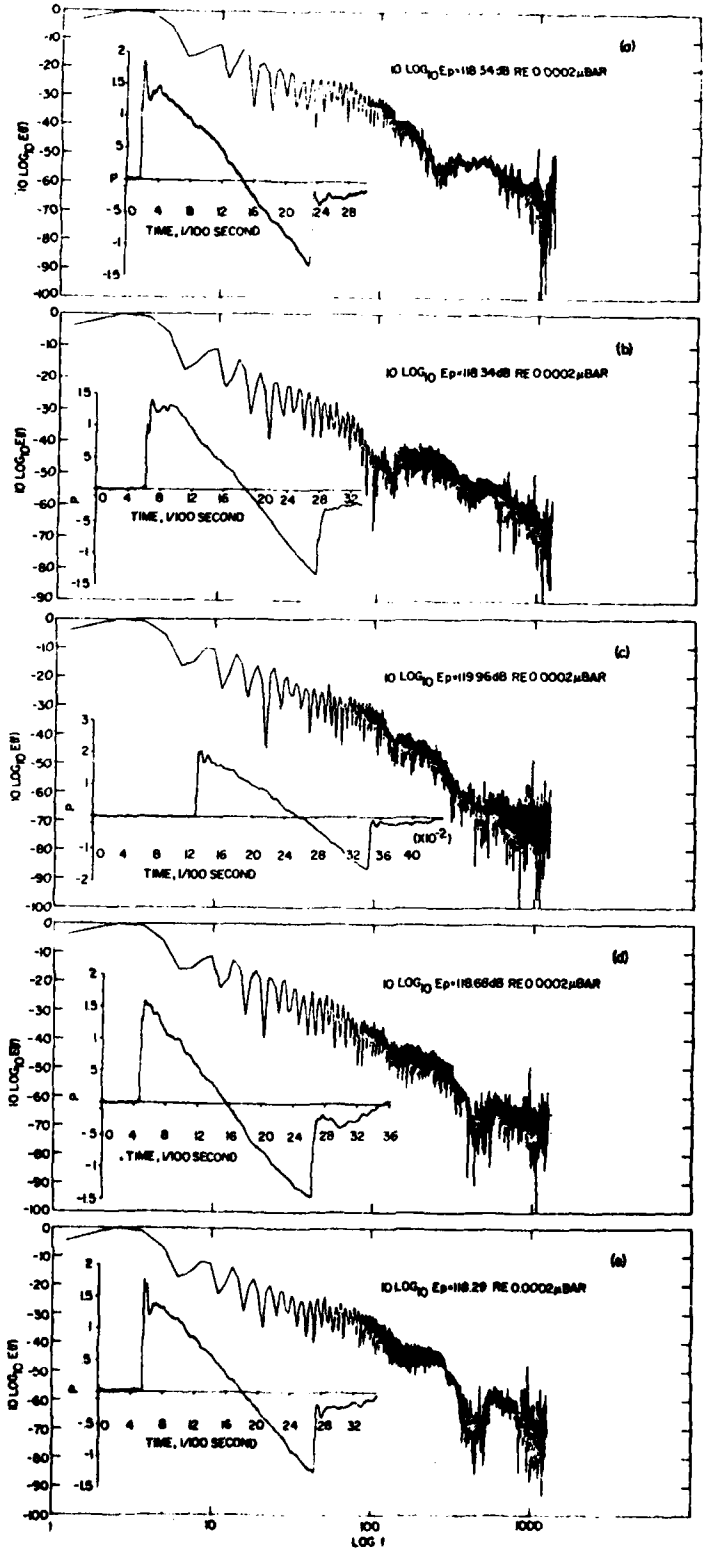

FIG. 1.5 PRESSURE-TIME PLOTS AND ENERGY SPECTRA FOR FIVE MICROPHONE RECORDINGS OF MISSION 123-1 FLOWN BY B-58 AIRCRAFT (REF. 1).

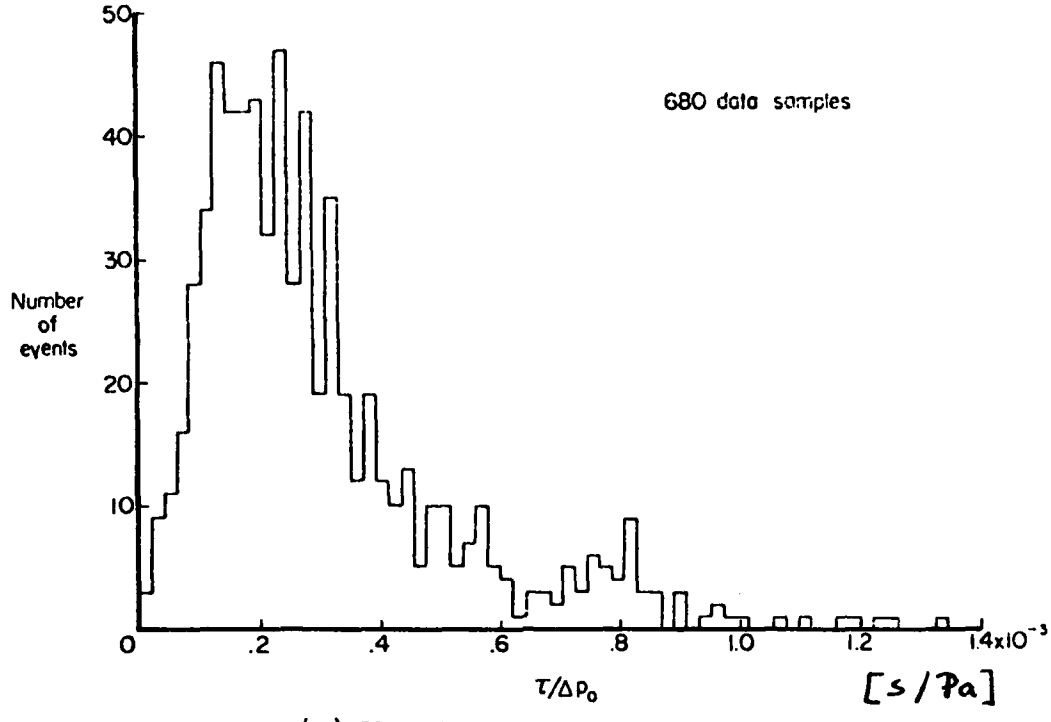

(a) Rise time per unit overpressure.

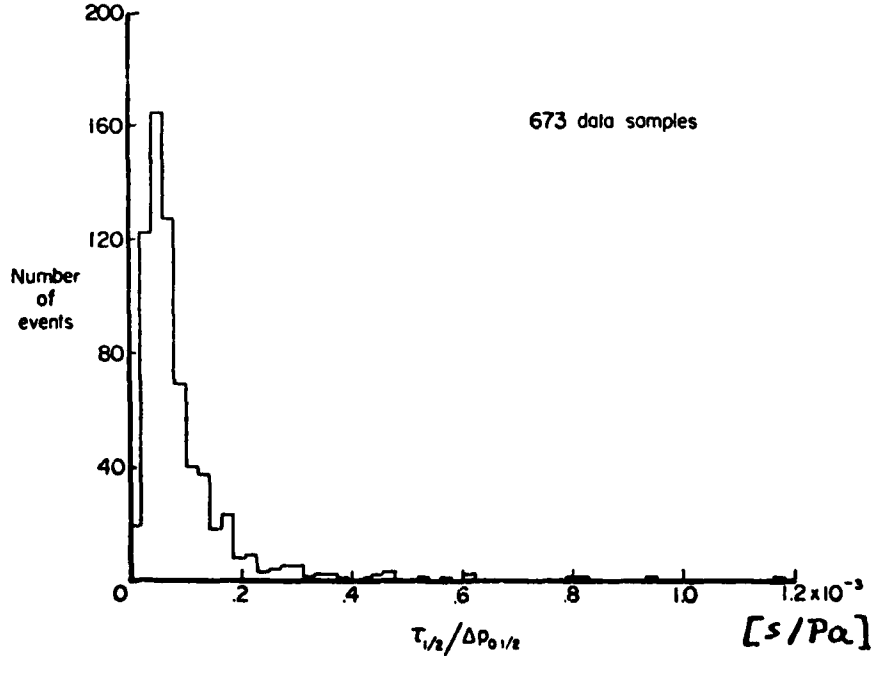

(b) Rise time to half amplitude.

FIG. 1.6 HISTOGRAMS OF SONIC-BOOM DATA FROM SR-71 AIRCRAFT AT M = 3 AT ALTITUDES TO 24,384m (REF. 4).

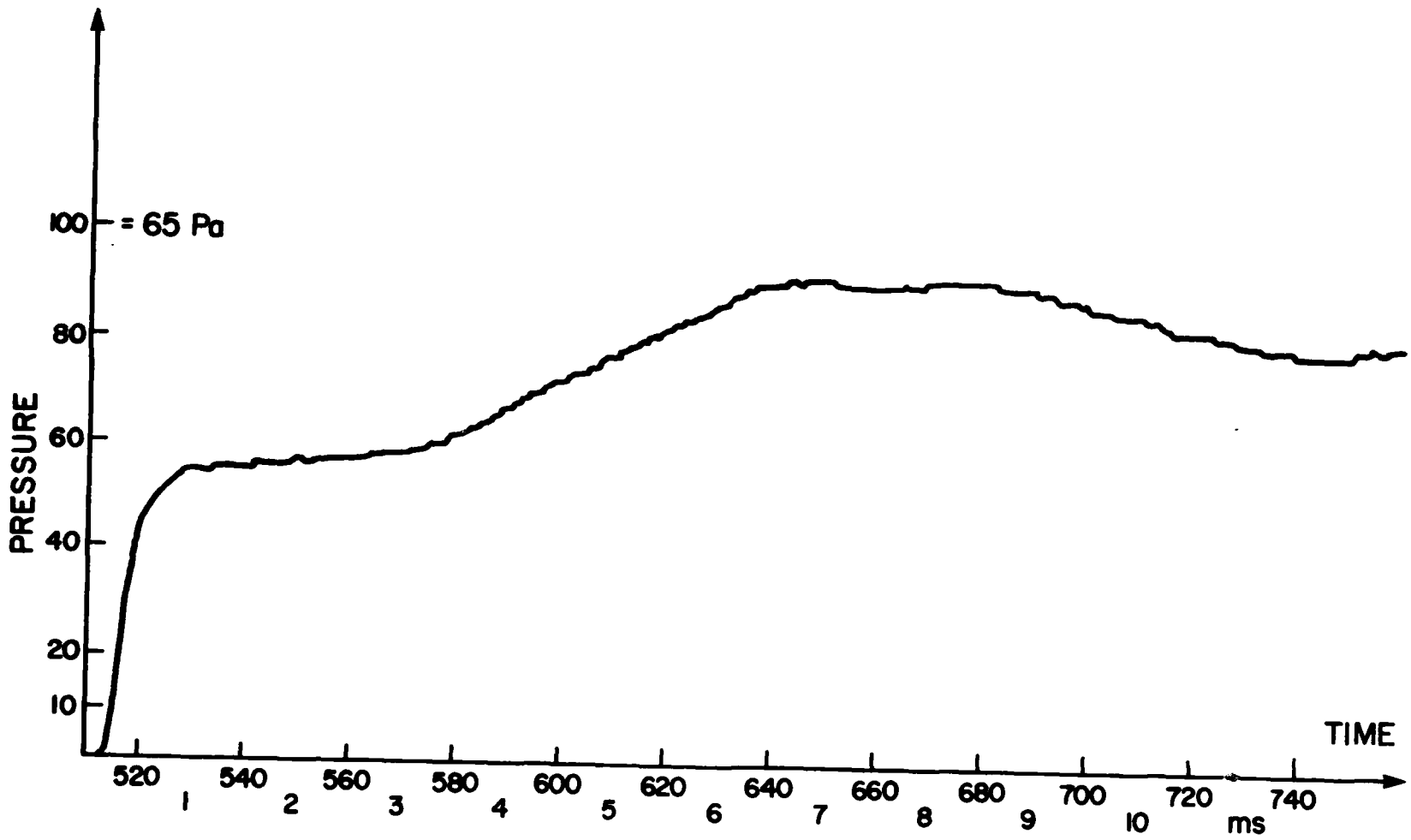

FIG. 1.7(a) RAE SONIC BOOM RUN 105/9/1 1945 ft = 593m (REF. 8).

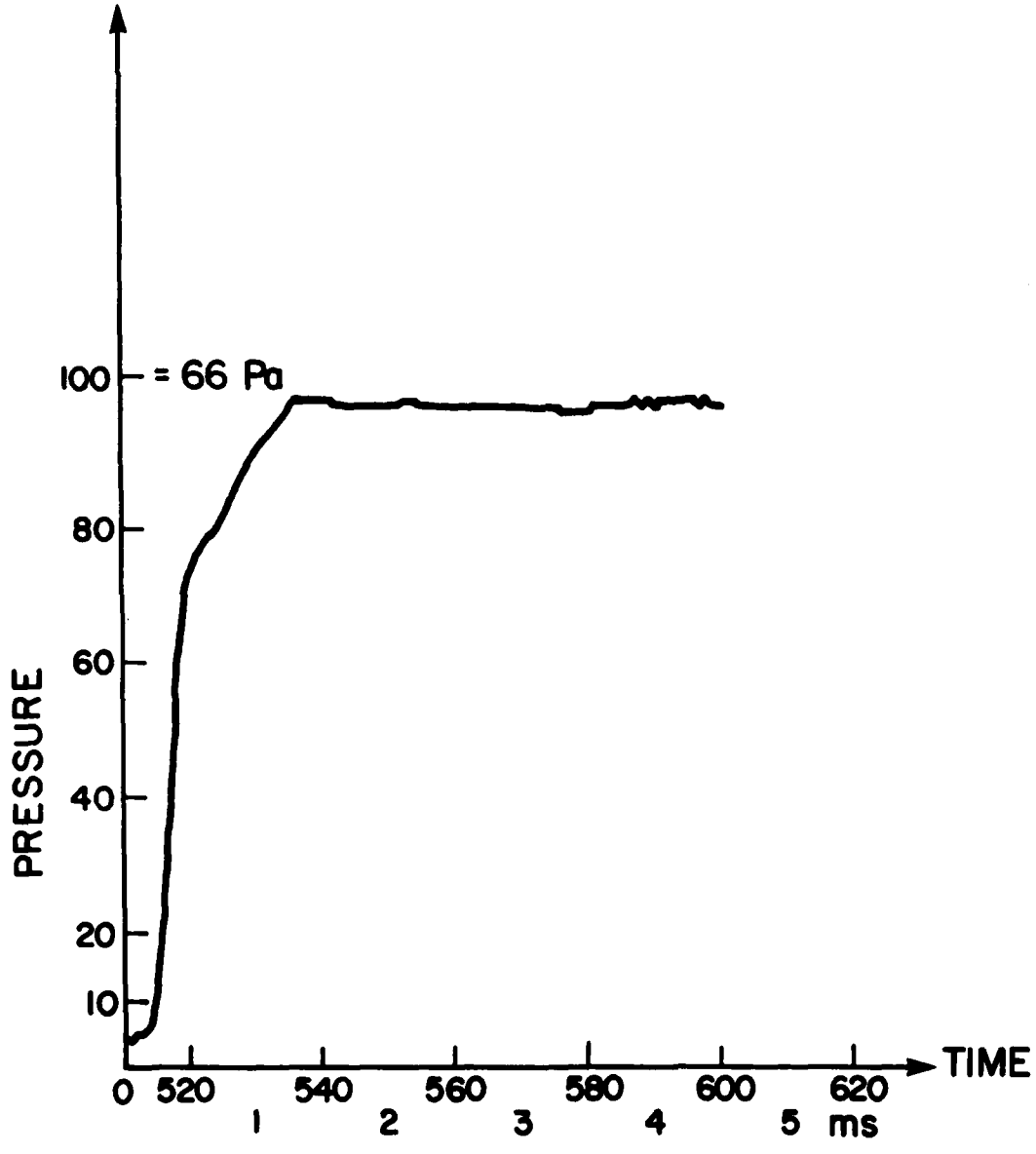

FIG. 1.7(b) RAE SONIC BOOM RUN 105/9/2 1377 ft = 420m (REF. 8).

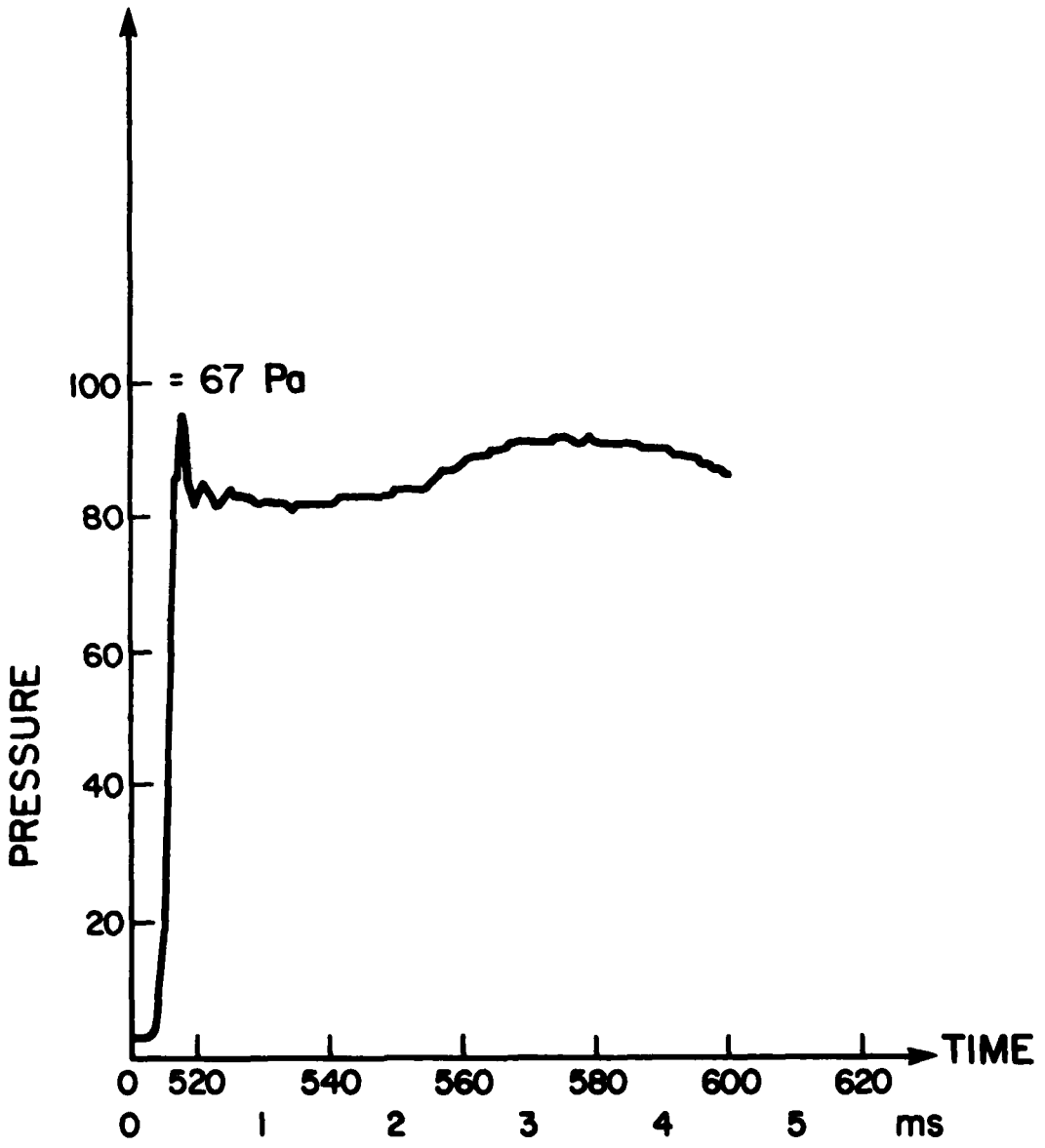

FIG. 1.7(c) RAE SONIC BOOM RUN 105/9/3 943 ft = 287m (REF. 8).

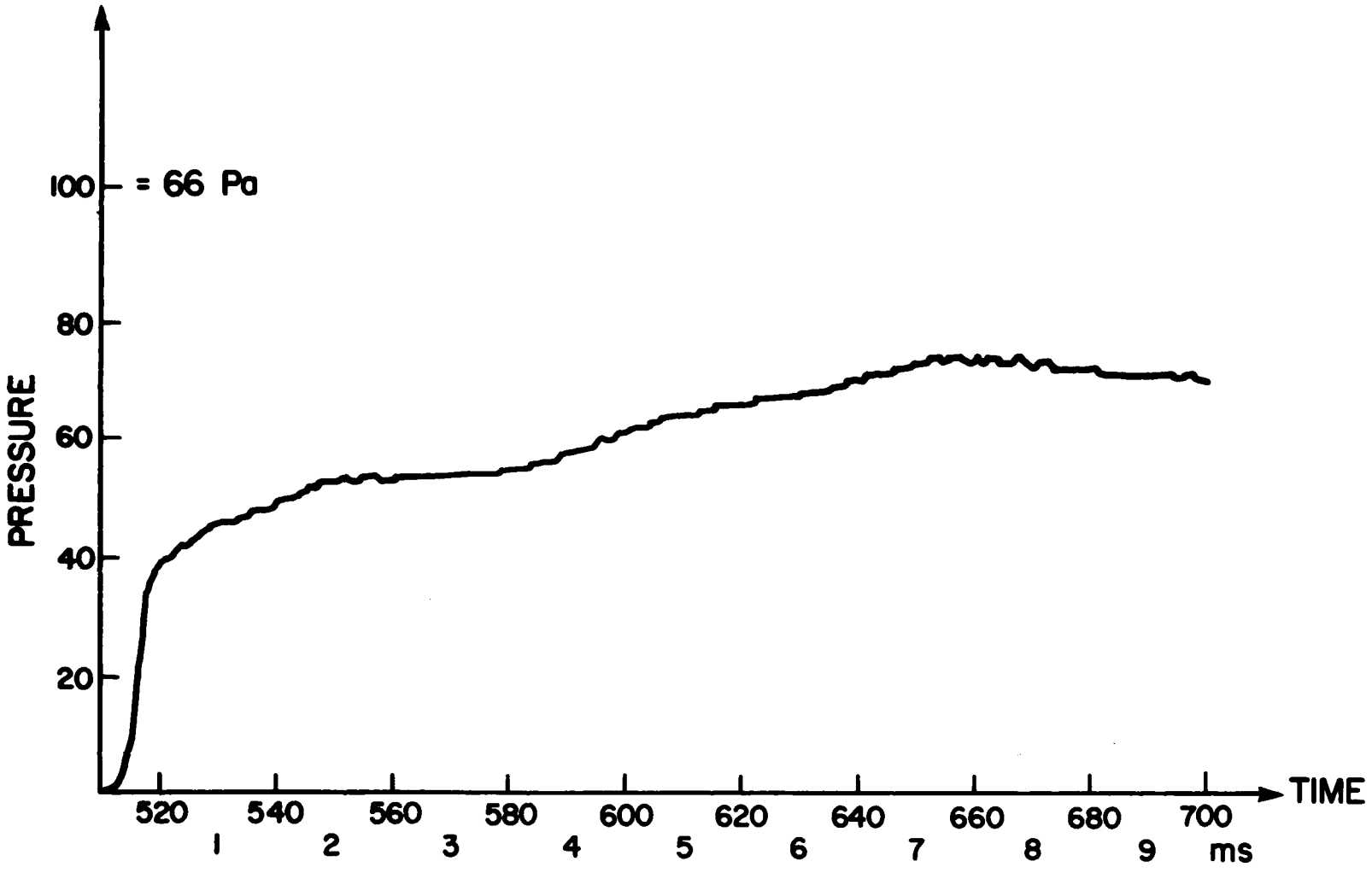

FIG. 1.7(d) RAE SONIC BOOM RUN 105/9/4 472 ft = 144m (REF. 8).

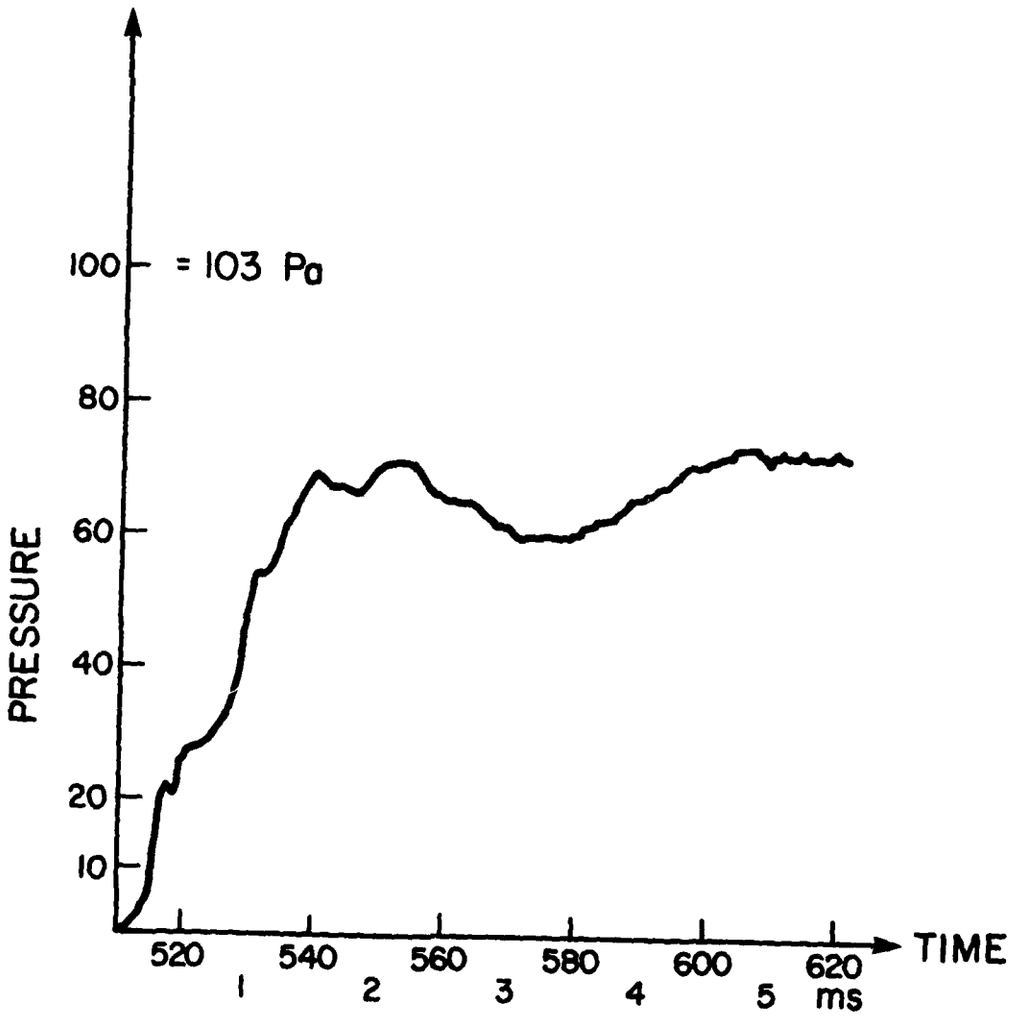

FIG. 1.7(e) RAE SONIC BOOM RUN 105/9/5 GROUND (REF. 8).

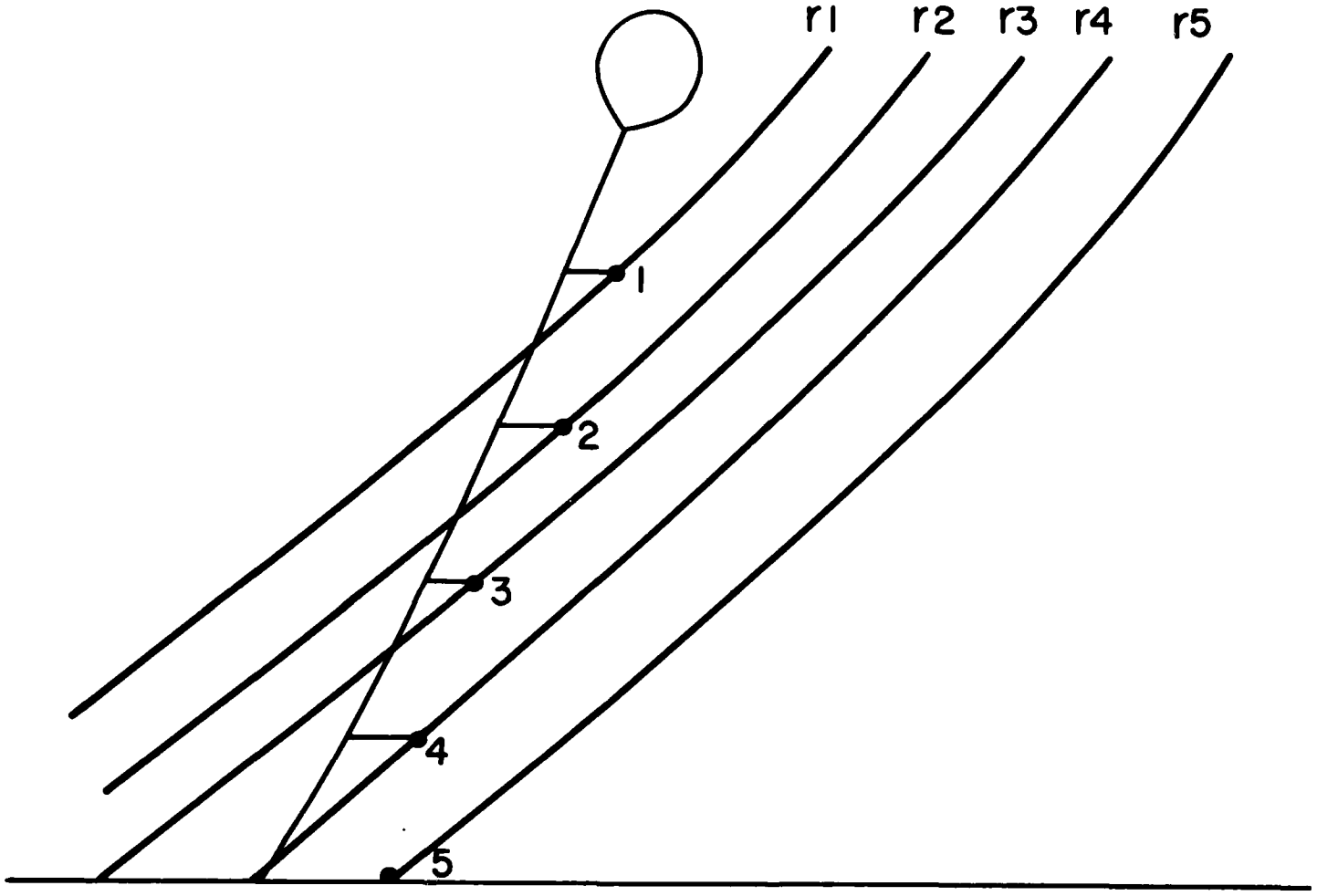

FIG. 1.8 SKETCH SHOWING THE BALLOON, TETHER AND FIVE MICROPHONES. THE FIVE LINES r1 TO r5 ILLUSTRATE HOW THE RAY PATHS OF THE MEASURED BOOMS CAN DIFFER.

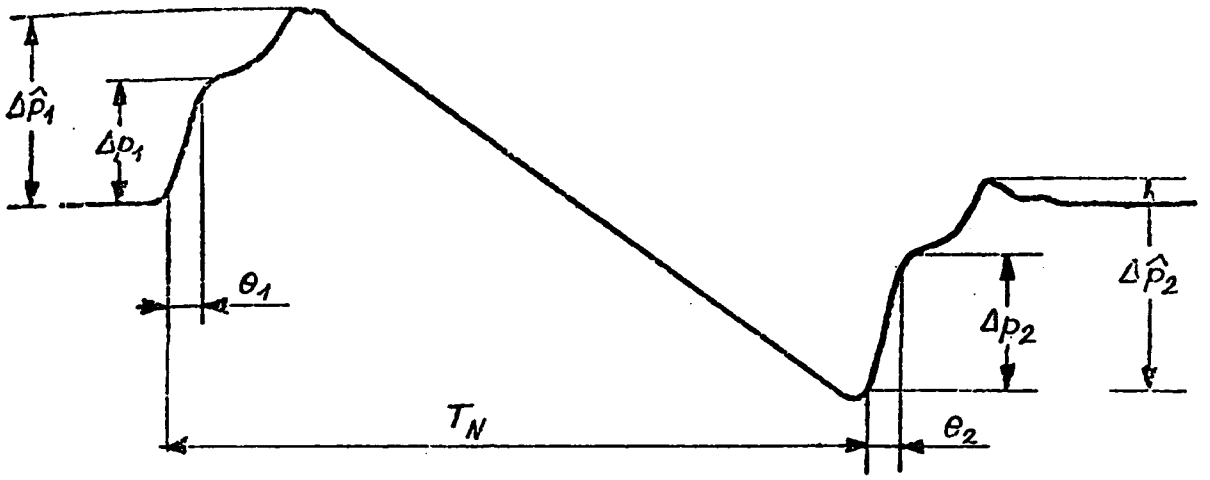

T_N Intervalle de temps entre les 2 chocs

$\Delta\hat{p}_1$ Valeur maximale de la surpression du 1er choc

Δp_1 Saut de pression de la partie la plus raide du 1er choc

θ_1 Temps de montée de la partie la plus raide du 1er choc (de 10 à 90% de Δp_1)

$\Delta\hat{p}_2$ Valeur maximale du saut de pression du 2^{e} choc

Δp_2 Saut de pression de la partie la plus raide du 2^{e} choc

θ_2 Temps de montée de la partie la plus raide du 2^{e} choc (de 10 à 90% de Δp_2)

FIG. 1.9 DÉFINITION DES PARAMÈTRES DÉPOUILLÉS (REF. 9).

Vols à basse altitude

Signature	1er Choc	2ème Choc
Vol 8 Passage 4		
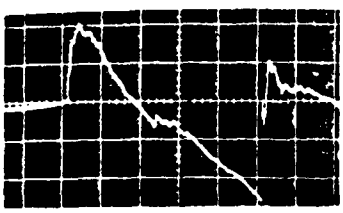	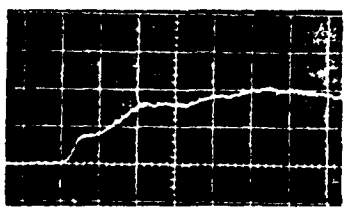	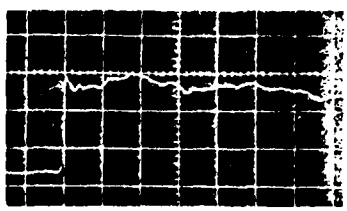
20 ms/div	1 ms/div	0,2 ms/div
Vol 9 Passage 1		
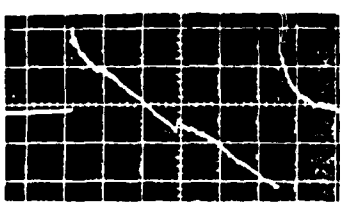	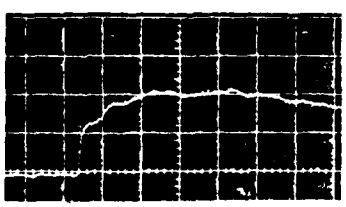	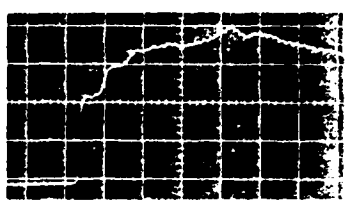
20 ms/div	0,2 ms/div	0,2 ms/div
Vol 9 Passage 3		
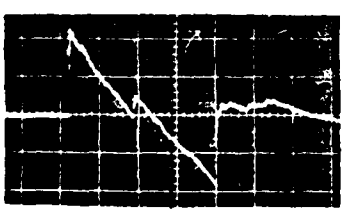	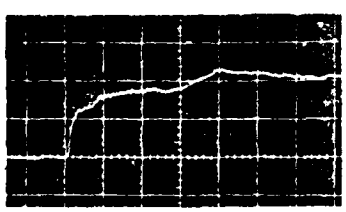	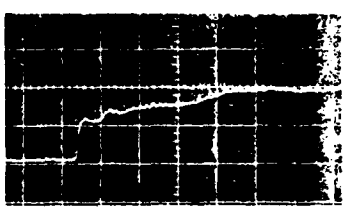
20 ms/div	0,2 ms/div	0,2 ms/div
Vol 9 Passage 4		
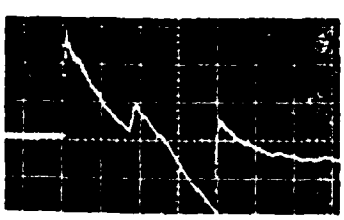	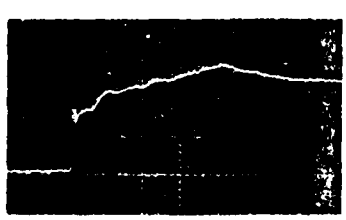	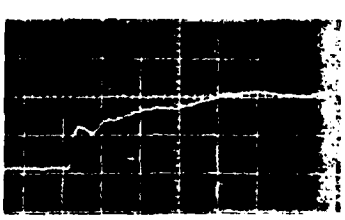
20 ms/div	0,2 ms/div	0,2 ms/div

FIG. 1.10 MIRAGE III BOOMS (REF. 9).

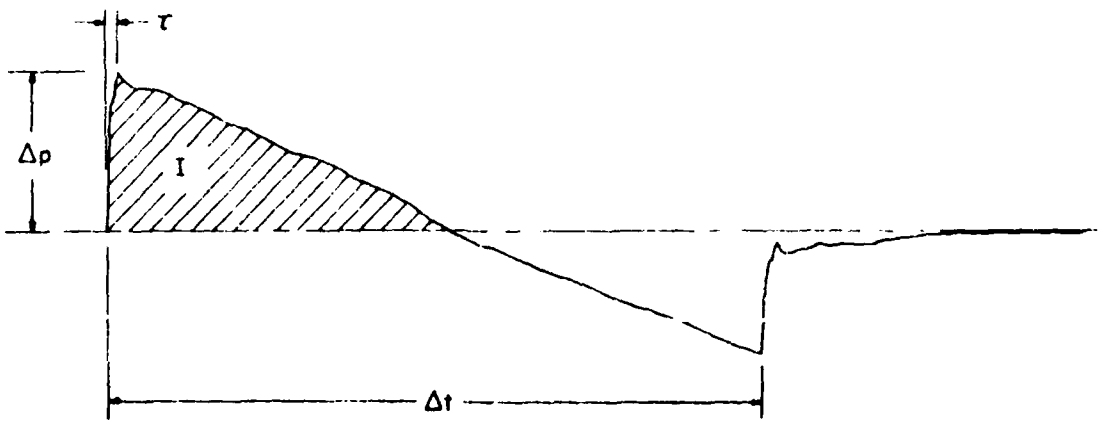

FIG. 1.11 DEFINITION OF RISE TIME IN THE AMERICAN EXPERIMENTAL STUDIES (REF. 1).

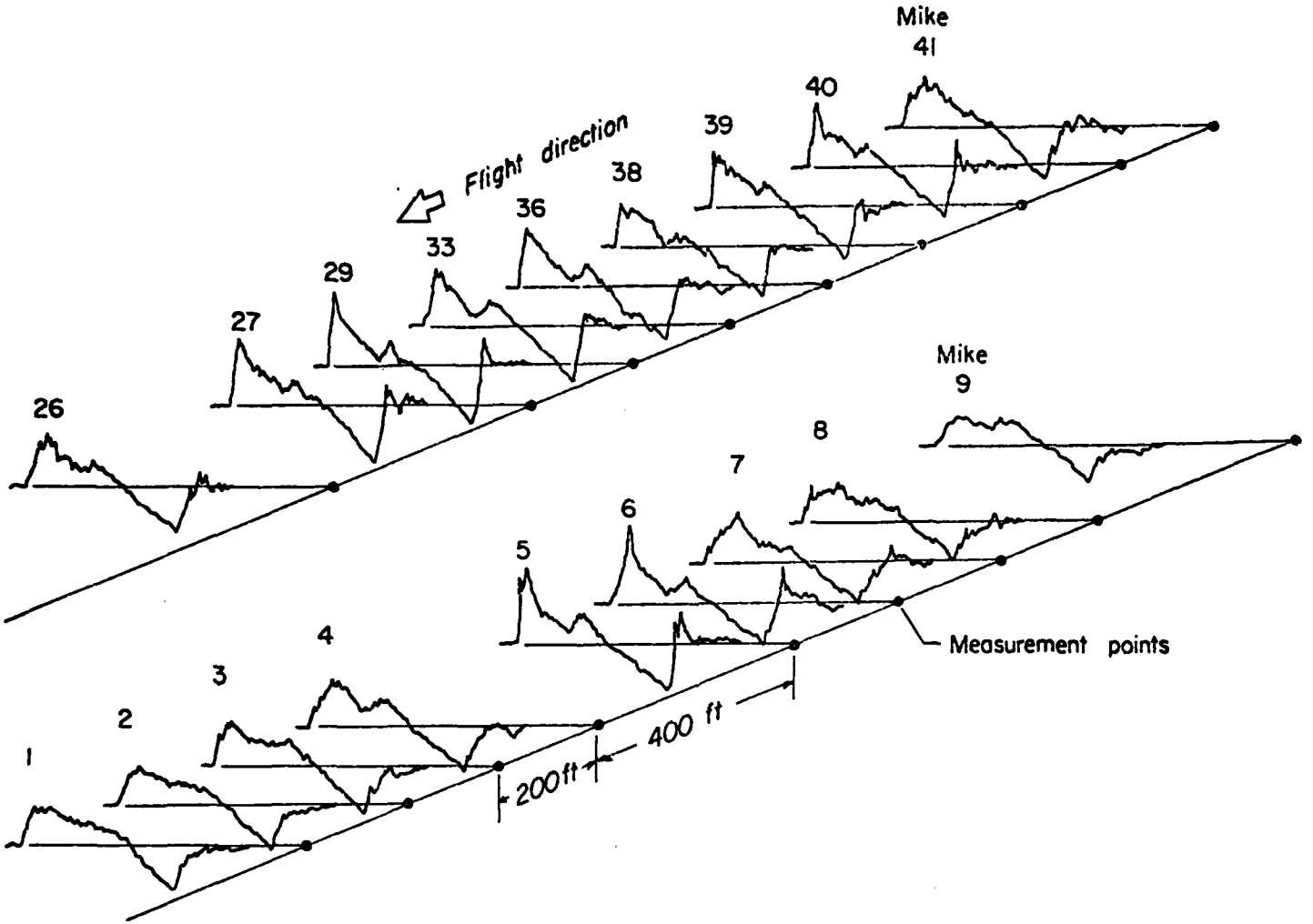

FIG. 1.12 SONIC-BOOM PRESSURE SIGNATURES AS MEASURED BY SEVERAL MICROPHONES SPACED AT 200-ft (60.96m) INTERVALS ALONG THE 8000-ft (2438m) LINEAR ARRAY FOR A FIGHTER AIRPLANE IN STEADY, LEVEL FLIGHT AT A MACH NUMBER OF 1.31 AND AN ALTITUDE OF 30,800 ft (9388m) (REF. 4).

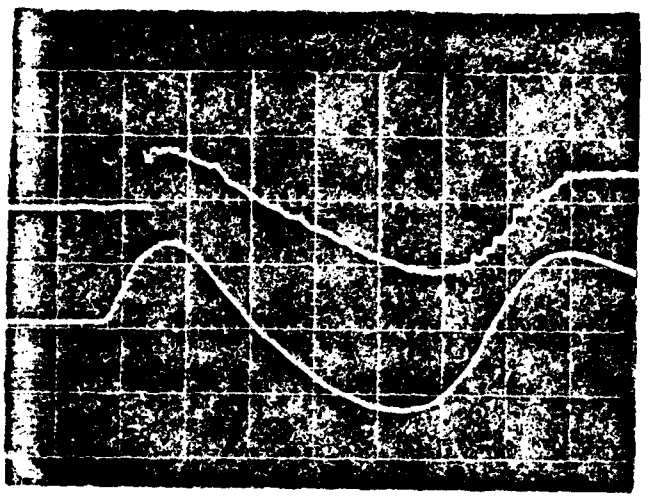

FIG. 1.13 WAVEFORMS PRODUCED BY PORTABLE SONIC-BOOM SIMULATOR PRIOR TO INSTALLATION OF LOW-PASS ACOUSTIC FILTER (REF. 31).

Driver pressure = 5 atm; distance = 30m; horizontal = 0.5 ms/div; vertical = 100 N/m^2/div; top trace 1.64m above ground; bottom trace 0.033m above ground.

EFFET SUR LE PROFIL DE L'ONDE D'UN GRADIENT DE TEMPERATURE DANS LE MILIEU AVAL.

i) Conditions normales (sans gradient de température).

$\Delta p_1 = 10,5$ mbar

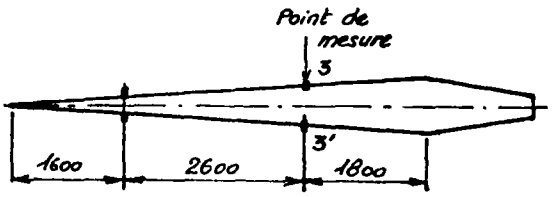

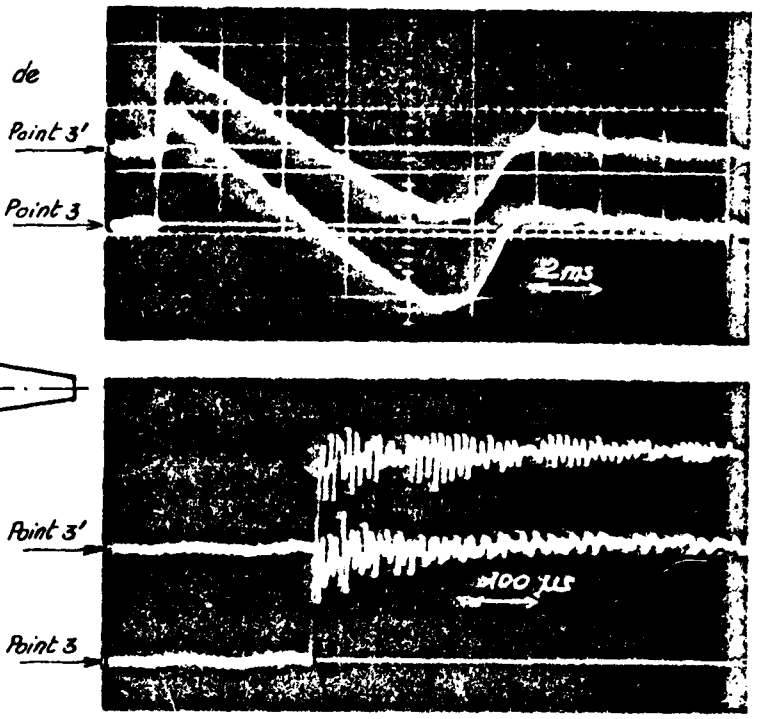

ii) avec un gradient de température normal à l'axe du tube

$\Delta p_1 = 10,5$ mbar

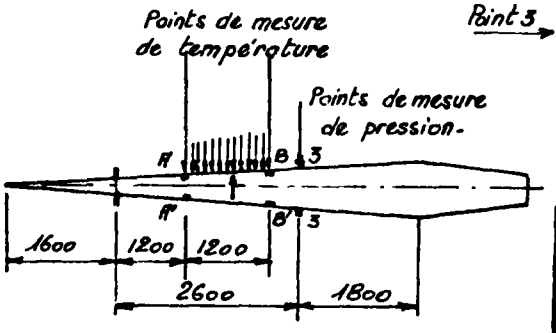

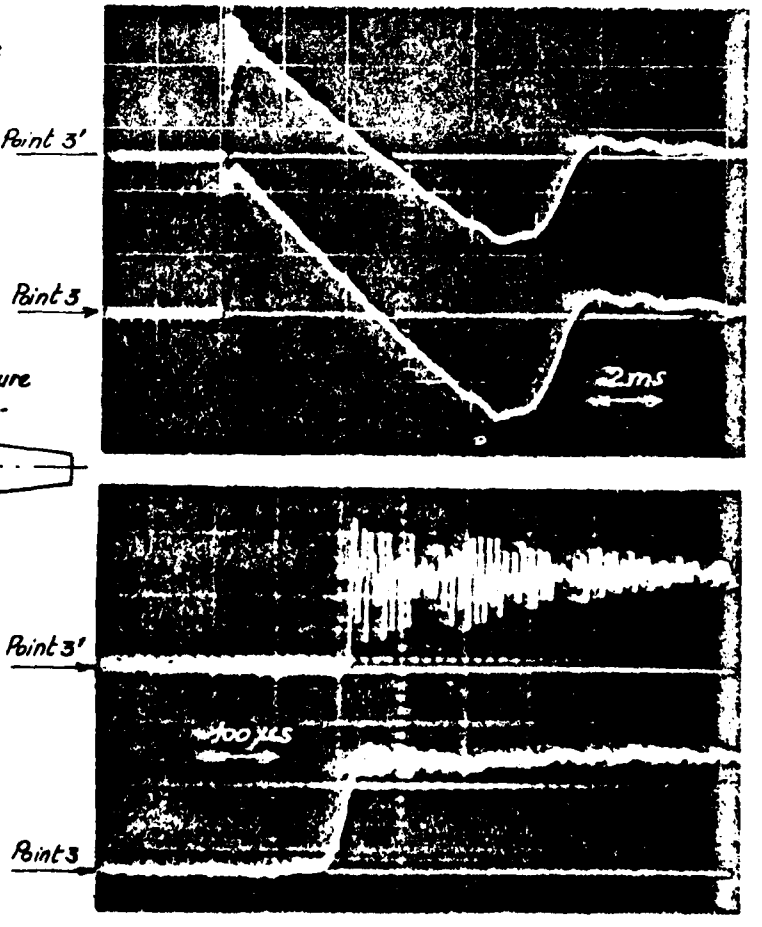

FIG. 1.14(a)

DIFFERENCE DE TEMPERATURE ENTRE PAROIS SUPERIEURE ET INFERIEURE.
ENTRE A ET A': 10°C
ENTRE B ET B': 15°C
(REF. 33).

i) Comparaison des signaux enregistrés avec un gradient de température normal à l'axe du tube avec ceux obtenus en l'absence de gradient (enregistrements de la planche précédente)

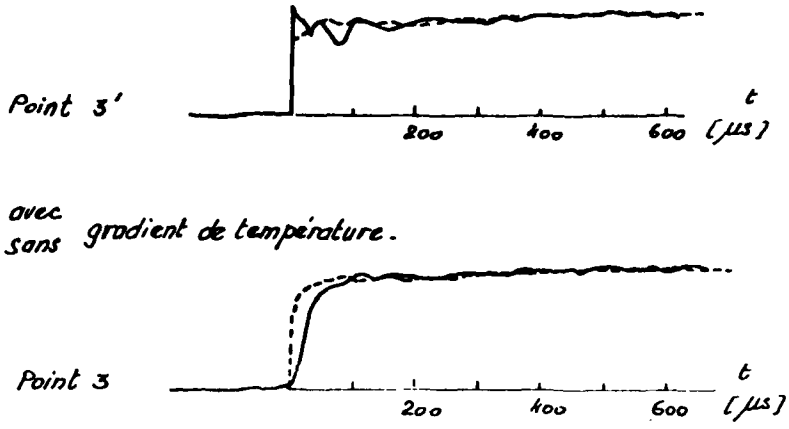

ii) Autre exemple d'enregistrement réalisé avec un gradient de température normal à l'axe.

Δp_i = 10,5 mbar.

Différence de température entre les parois supérieure et inférieure :
entre A et A' : 3,8 °C
entre B et B' : 6 °C

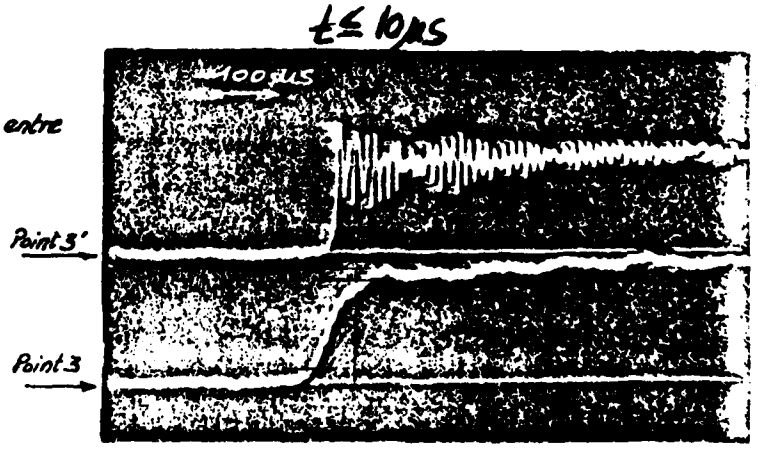

FIG. 1.14(b) EFFET SUR LE PROFIL DE L'ONDE D'UN GRADIENT DE TEMPERATURE DANS LE MILIEU AVAL (REF. 33).

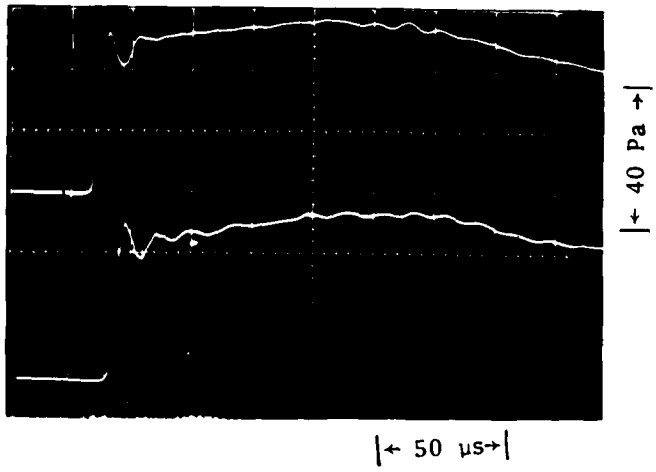

FIG. 2.1 MICROPHONE RESPONSE TEST. THE TWO MICROPHONES ARE MOUNTED 50 mm APART AT THE SAME DISTANCE FROM THE APEX OF THE HORN. BOTH MICROPHONES HAVE PROTECTION GRIDS MOUNTED.

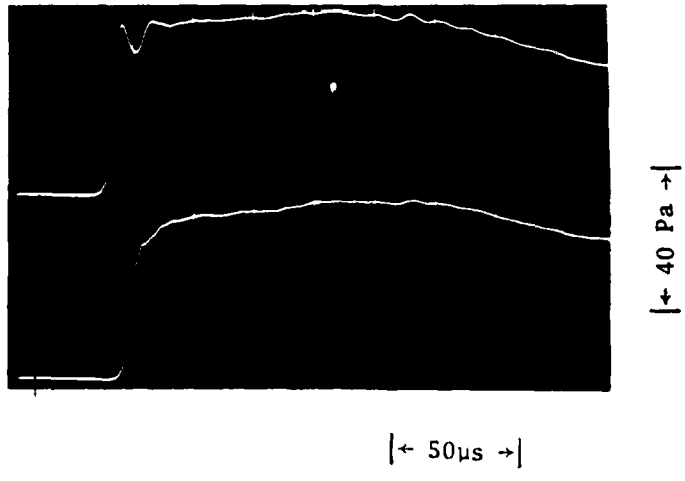

FIG. 2.2 MICROPHONE RESPONSE TEST. THE TWO MICROPHONES ARE MOUNTED 50 mm APART AT THE SAME DISTANCE FROM THE APEX OF THE HORN. BOTTOM MICROPHONE DOES NOT HAVE A PROTECTION GRID.

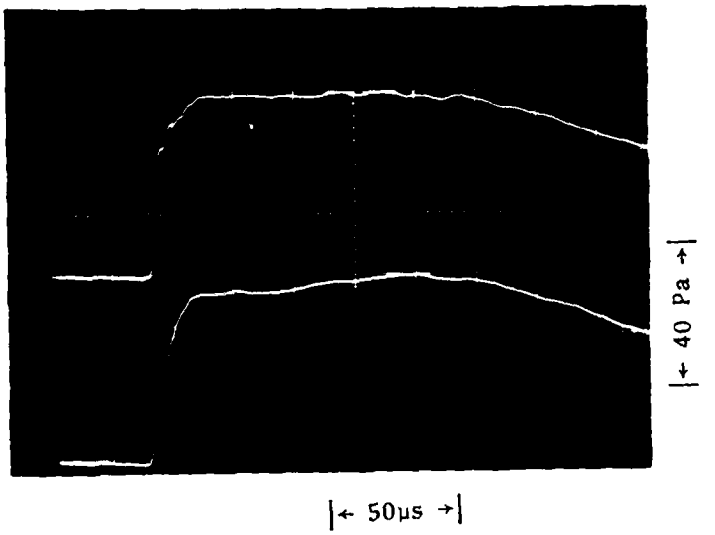

FIG. 2.3 MICROPHONE RESPONSE TEST. THE TWO MICROPHONES ARE MOUNTED 50 mm APART AT THE SAME DISTANCE FROM THE APEX OF THE HORN. THE TOP TRACE IS FROM A MICROPHONE WITHOUT PROTECTION GRID AT 0 DEGREE INCIDENCE. THE BOTTOM TRACE IS FROM A MICROPHONE WITHOUT PROTECTION GRID AT 90-DEGREE INCIDENCE.

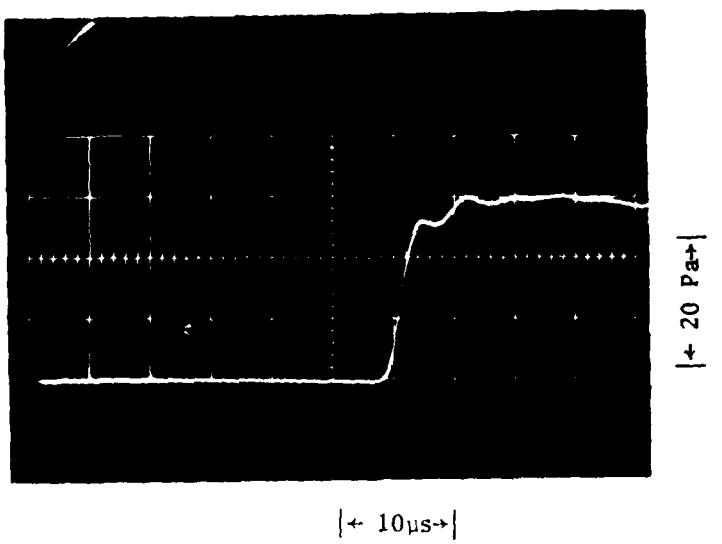

FIG. 2.4 MICROPHONE RESPONSE TEST. THE MICROPHONE IS WITHOUT PROTECTION GRID, SHOWING A RIPPLE OF ABOUT 135 kHz.

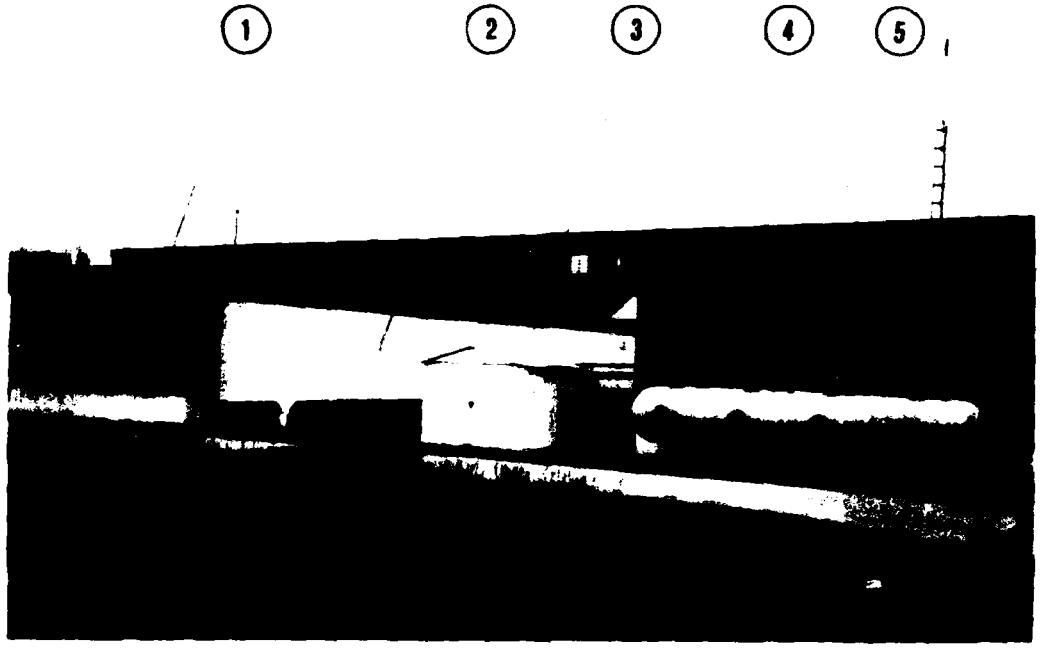

FIG. 2.5 AN OUTSIDE VIEW OF THE TRAVELLING-WAVE SONIC BOOM SIMULATOR.

1. Test room
2. Travelling-wave horn
3. Compressor shed
4. Control room
5. Reservoir tanks

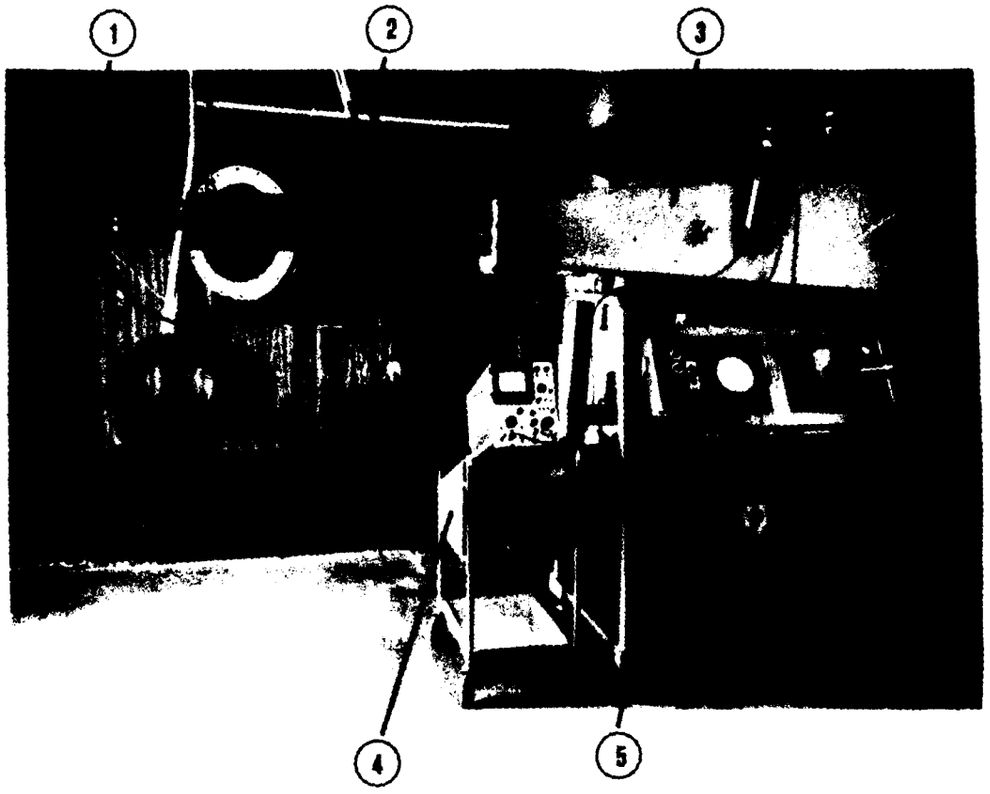

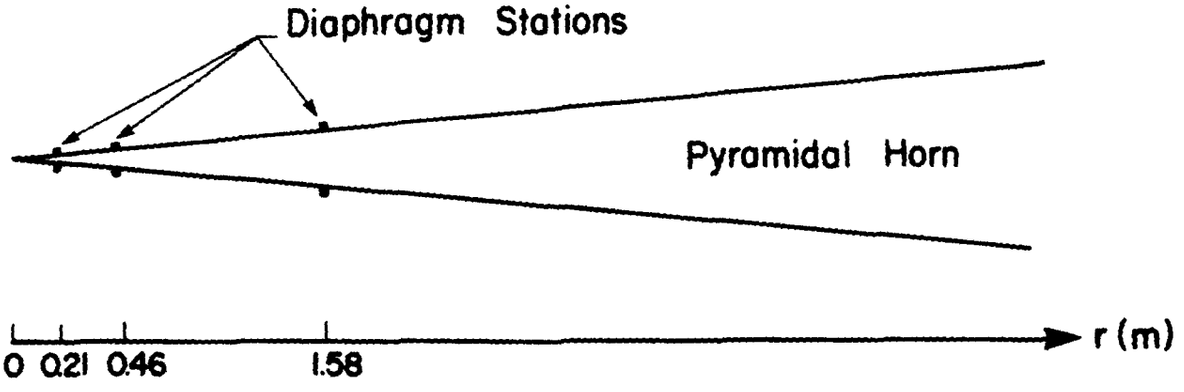

FIG. 2.6 INTERIOR OF CONTROL ROOM, SHOWING THE SHOCK-TUBE DRIVERS AND DIAPHRAGM STATIONS.

1. 0.21m driver
2. 1.58m driver
3. 25-mm thick steel section
4. Recording oscilloscope
5. Pressure control panel

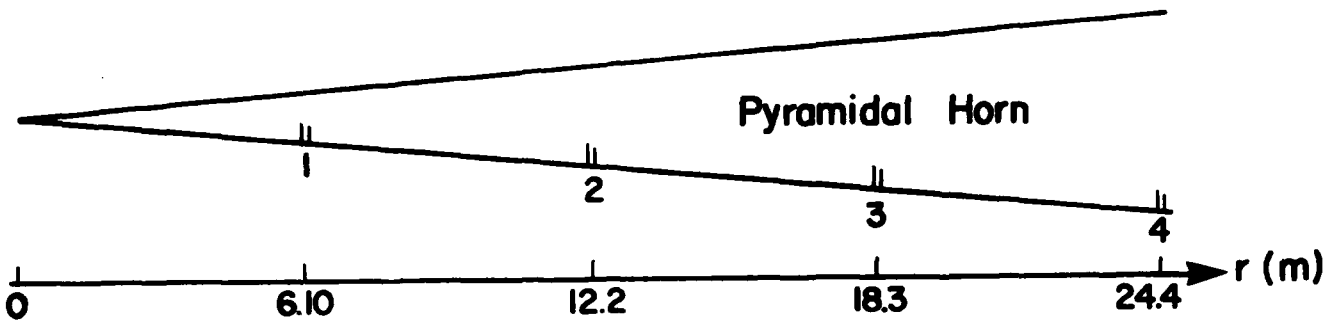

FIG. 2.7 HUMIDITY AND TEMPERATURE SENSORS IN THE PYRAMIDAL HORN.
1-4 SENSOR STATIONS.

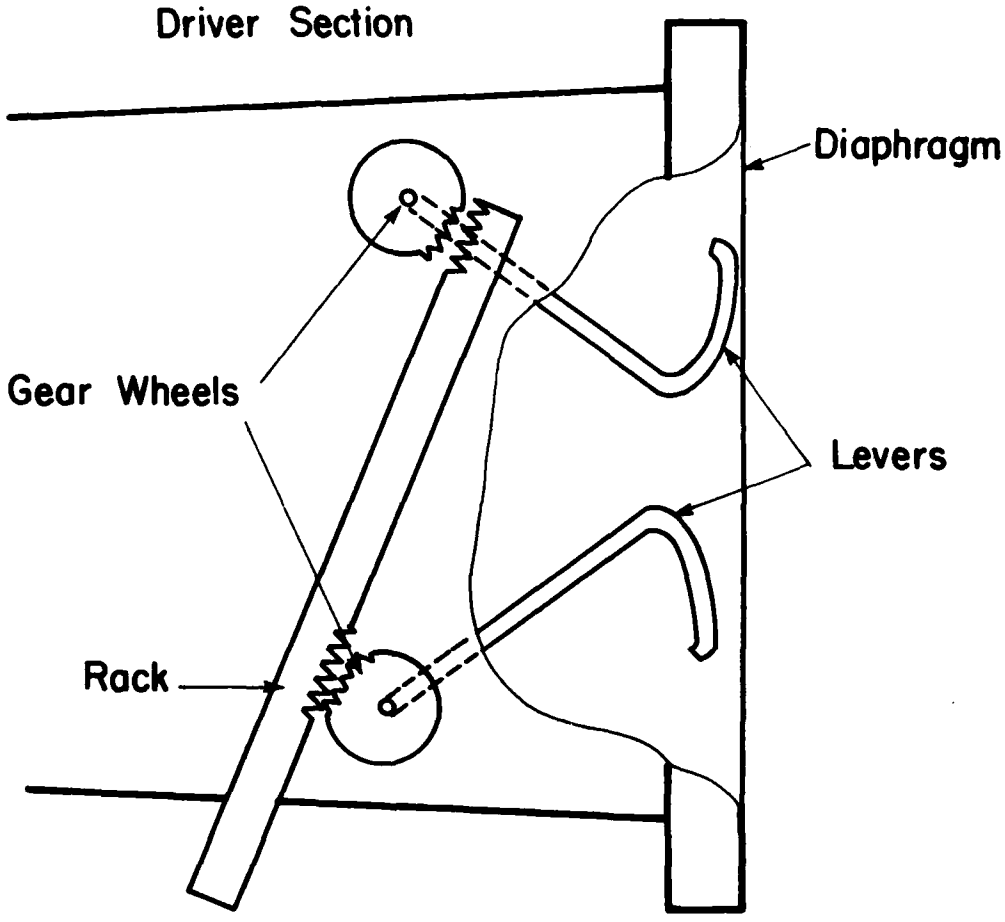

FIG. 2.8 DIAPHRAGM BREAKER MECHANISM. PUSHING THE RACK (AT THE ARROW) THE TWO GEAR WHEELS ARE TURNED IN OPPOSITE DIRECTIONS OF ROTATION, SIMULTANEOUSLY TURNING THE LEVERS (FOUR) MOUNTED INSIDE THE DRIVER SECTION, THEREBY BREAKING THE DIAPHRAGM.

R = 21.3 m

p = 48.8 Pa

t = 475 μs

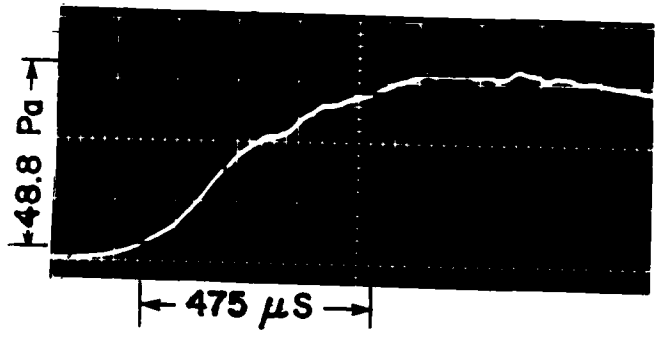

FIG. 2.9 WAVEFRONT OBTAINED IN PYRAMIDAL SHOCK TUBE WITH 1.58m DRIVER.

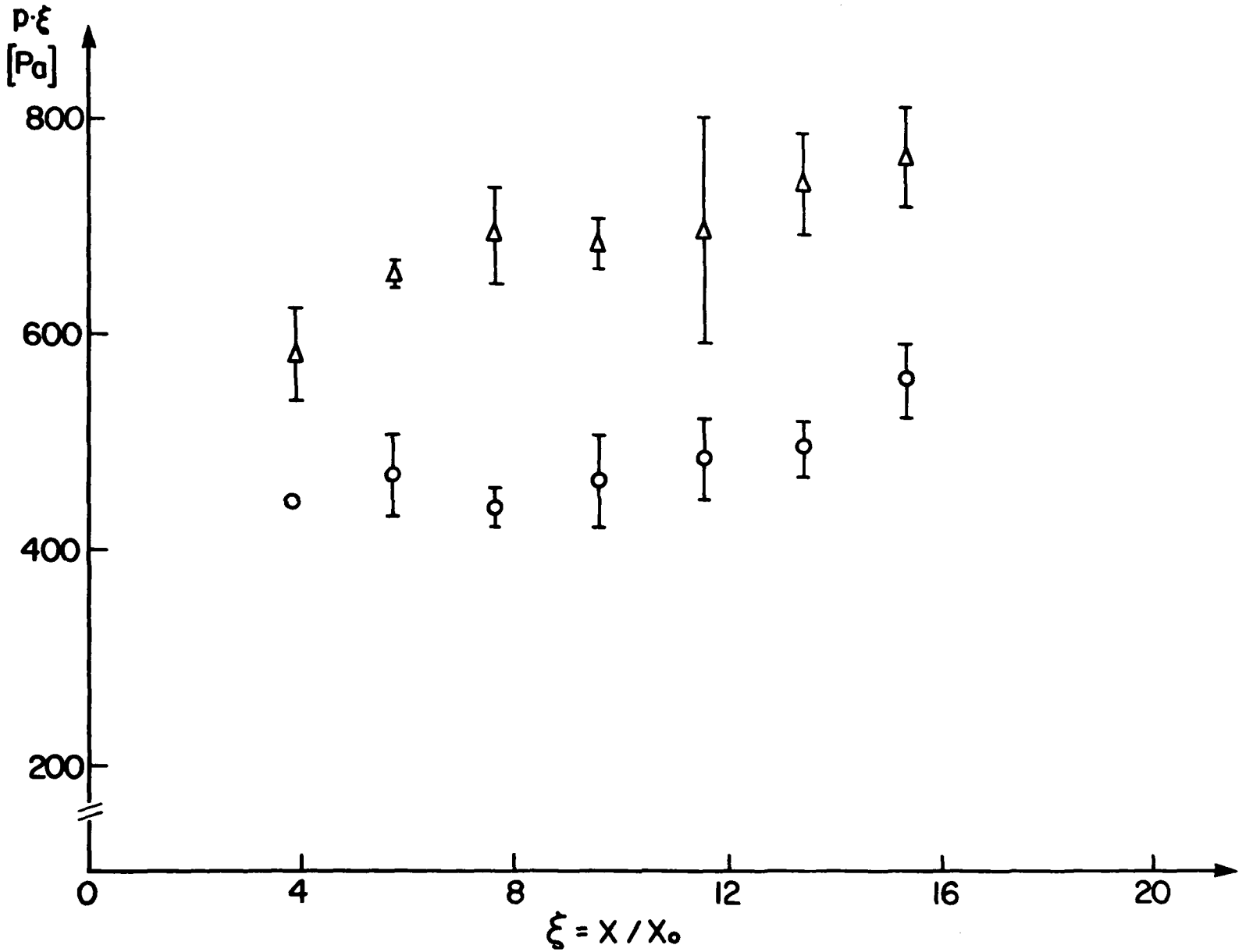

FIG. 2.10 PEAK-OVERPRESSURE VARIATION FOR N-WAVES IN SIMULATOR SHOCK-TUBE MODE. DRIVER LENGTH x_o = 1.58m.

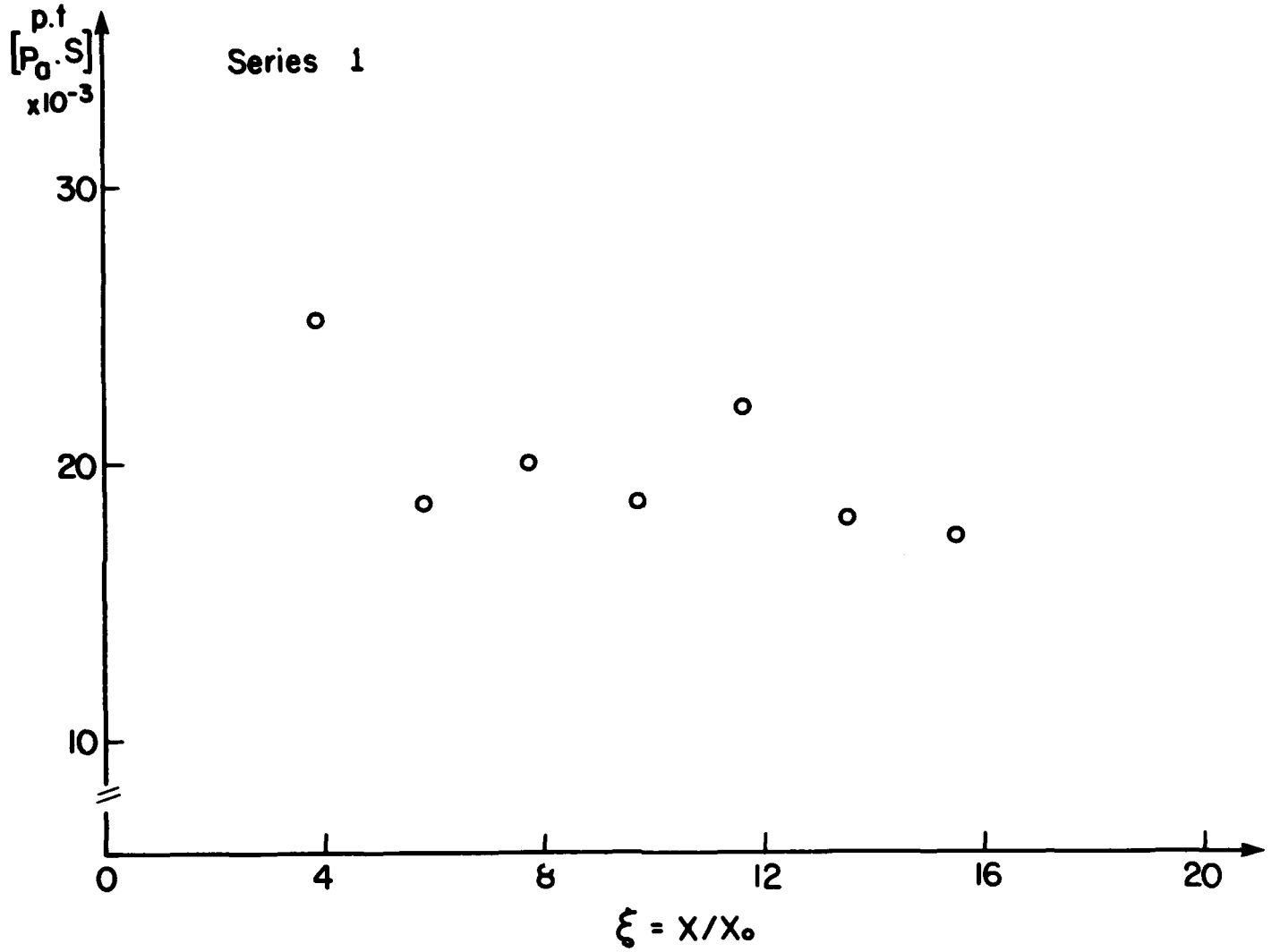

FIG. 2.11 STEEPENING OF FRONT SHOCK IN N-WAVE SIMULATOR.

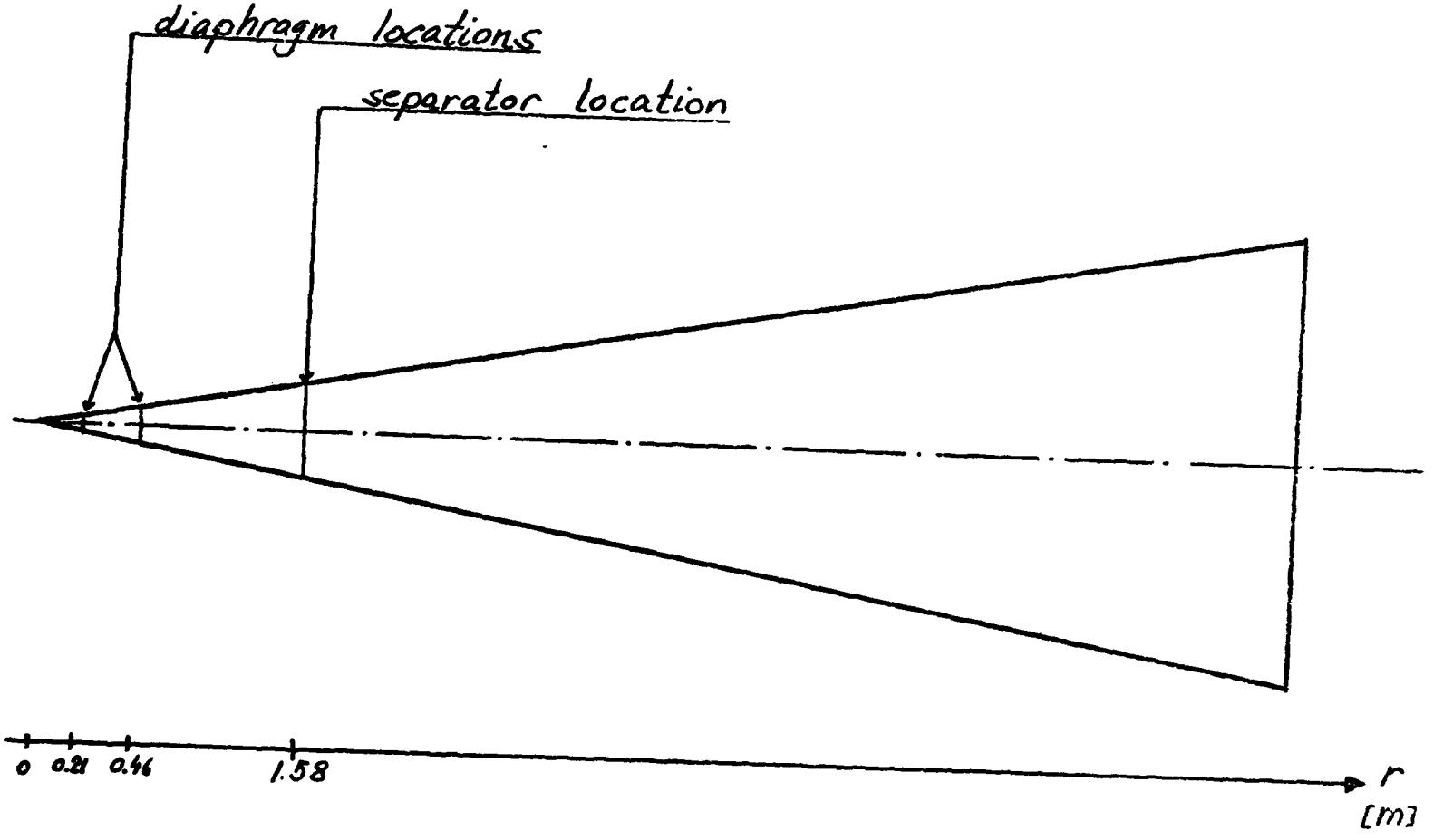

FIG. 2.12 SKETCH OF PYRAMIDAL HORN WITH DIAPHRAGM AND SEPARATOR LOCATIONS.

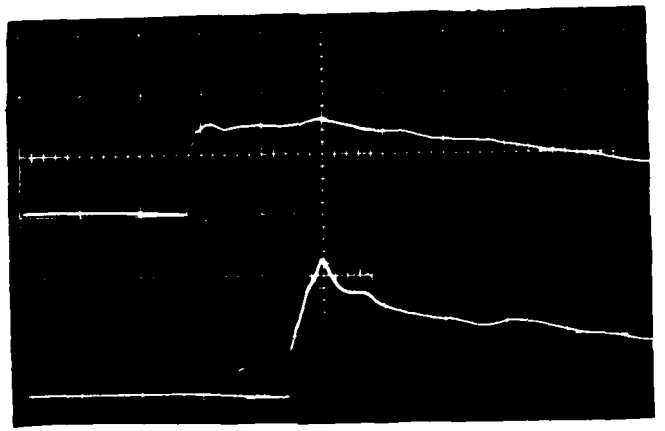

p_w = 90 Pa
t_w = 50 μs

FIG. 2.13 PRESSURE-TIME HISTORIES FOR SPHERICITY CHECK.
TOP TRACE: ON HORN AXIS - c
BOTTOM TRACE: 1/6 DISTANCE (CENTRE-TO-WALL) FROM THE WALL - w

FIG. 2.14 SERIES 6

O - MEASURED ON HORN AXIS
O - MEASURED NEAR WALL (1/6 OF DISTANCE AXIS - WALL

DRIVER LENGTH X_o = 0.46m
INITIAL OVERPRESSURE 15,500 Pa

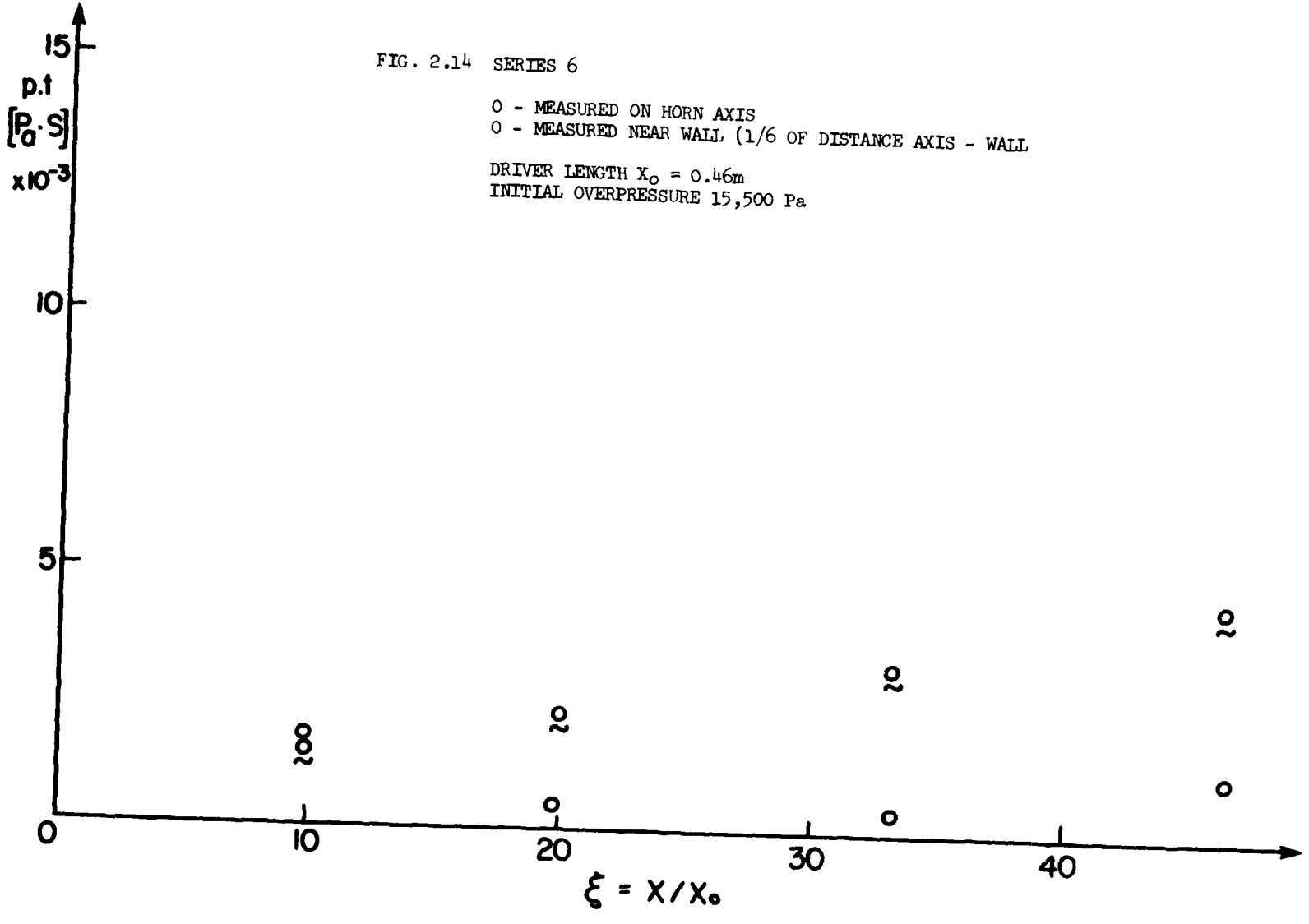

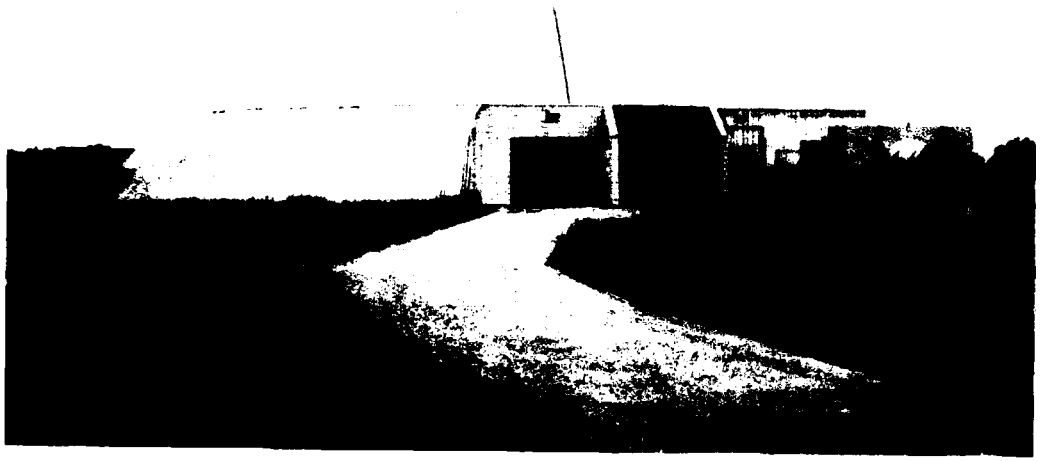

FIG. 2.15 UTIAS AIR CUSHION VEHICLE DOME.

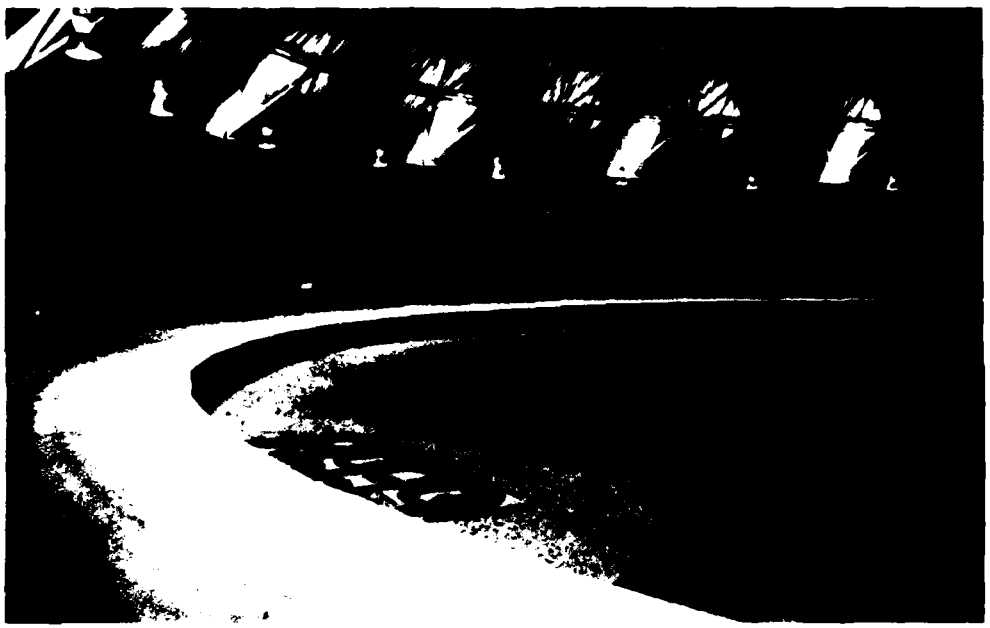

FIG. 2.16 UTIAS AIR CUSHION VEHICLE (ACV) DOME INTERIOR.

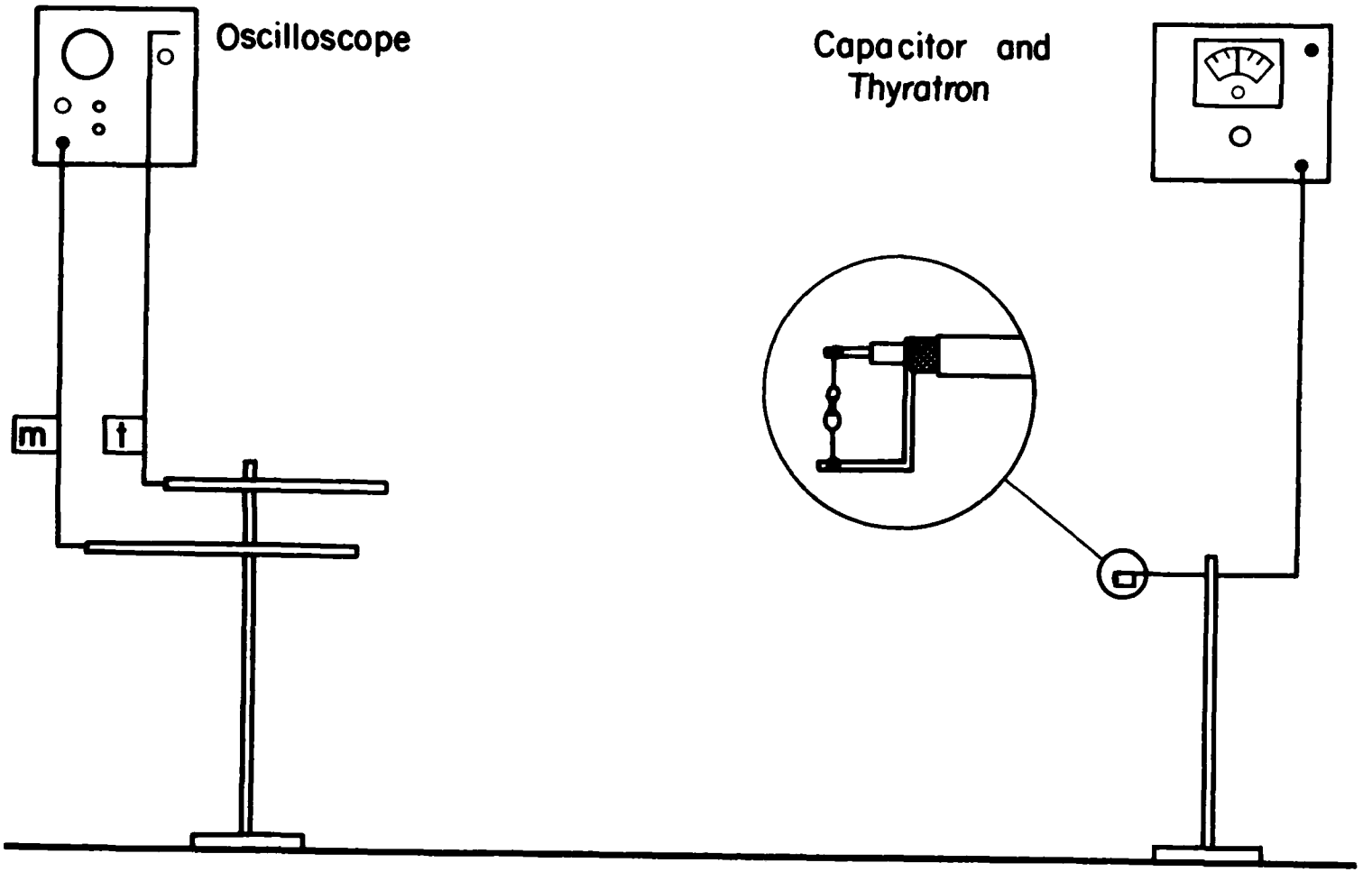

FIG. 2.17 EXPERIMENTAL SET-UP FOR SPARK AND EXPLODING-WIRE EXPERIMENTS.
m - MEASURING MICROPHONE AT THE END OF A ROD
t - TRIGGERING MICROPHONE

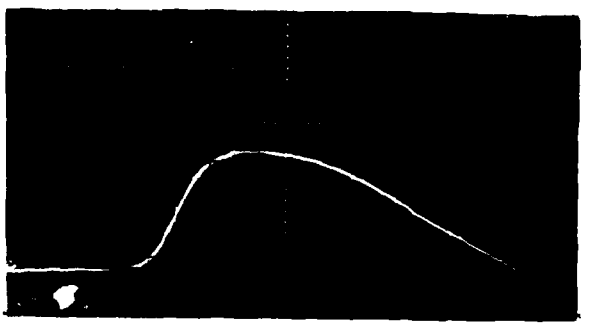

5 mV/div
10 μs/div

5 mV/div
50 μ /div

FIG. 2.18 TYPICAL OSCILLOGRAPHS OF FRONT SHOCK AND FULL N-WAVE GENERATED BY SPARK.

UPPER TRACE: t_f = 11.2 μs, p_f = 6.92 Pa, 5 kV, R = 21.56m
LOWER TRACE: t_r = 58.6 μs, p_f = 7.18 Pa, p_r = 6.03 Pa

S = 4.4 kV

R = 4.08 m

p_f = 64.8 Pa

p_r = 42.0 Pa

t_r = 30.9 μs

20 μs/div

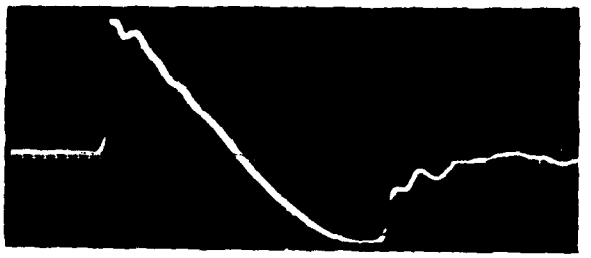

R = 4.85 m

p_f = 47.2 Pa

p_r = 28.7 Pa

t_r = 34.9 μs

20 μs/div

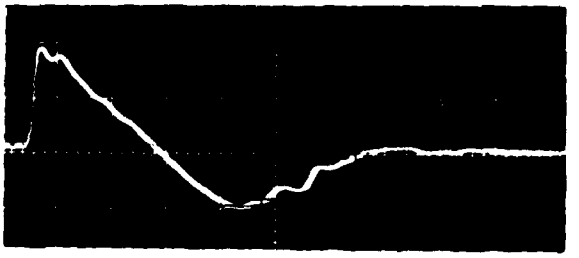

R = 9.76 m

p_f = 20.0 Pa

t_f = 5.1 μs

5 μs/div

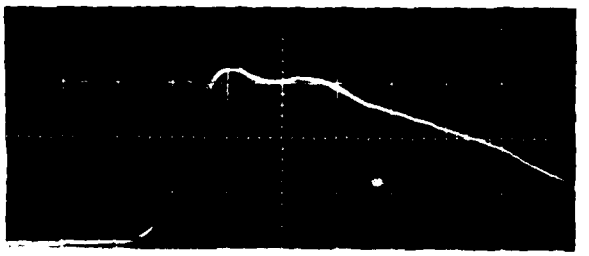

R = 15.6 m

p_f = 10.7 Pa

t_f = 9.15 μs

10 μs/div

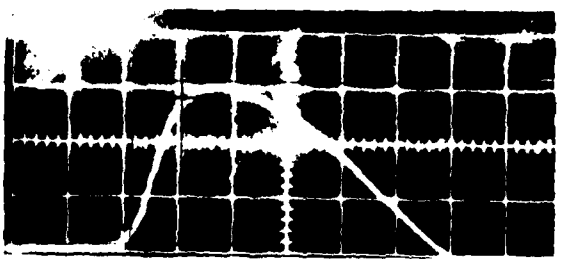

R = 21.6 m

p_f = 4.79 Pa

t_f = 11.2 μs

10 μs/div

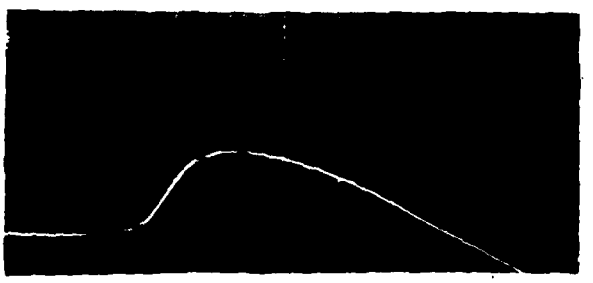

FIG. 2.19(a) SPARK-GENERATED N-WAVES.

S = 5.0 kV

R = 4.08 m
p_f = 67.8 Pa
p_r = 47.9 Pa
t_r = 23.4 μs
20 μs/div

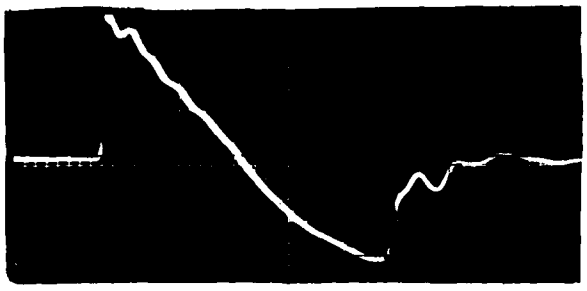

R = 4.44 m
p_f = 56 Pa
p_r = 36.1 Pa
t_f ≅ 2.6 μs
t_r = 24.0 μs
20 μs/div

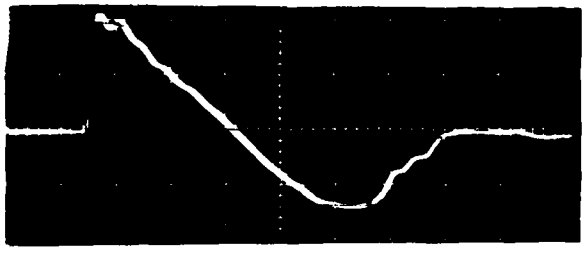

R = 9.76 m
p_f = 22.4 Pa
t_f = 4.64 μs
5 μs/div

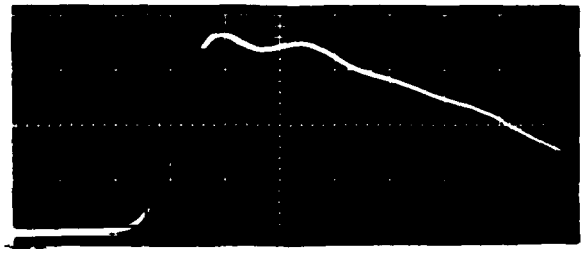

R = 15.6 m
p_f = 14.0 Pa
t_f = 7.44 μs
10 μs/div

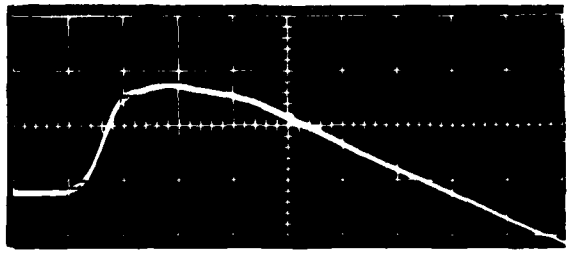

R = 21.56 m
p_f = 7.45 Pa
t_f = 11.2 μs
10 μs/div

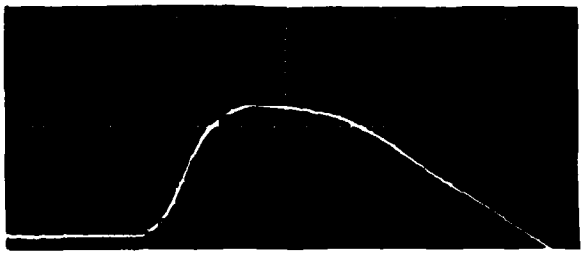

FIG. 2.19(b) SPARK GENERATED N-WAVES.

S = 6.0 kV

R = 4.08 m
p_f = 76.6 Pa
p_r = 55.3 Pa
t_r = 30.9 μs
20 μs/div

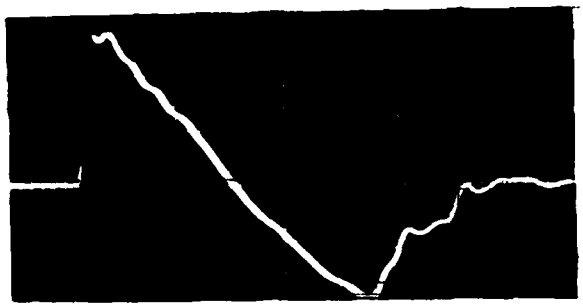

R = 4.85 m
p_f = 56.7 Pa
p_r = 30.9 Pa
t_f ~ 2 μs
t_r = 20.0 μs
20 μs/div

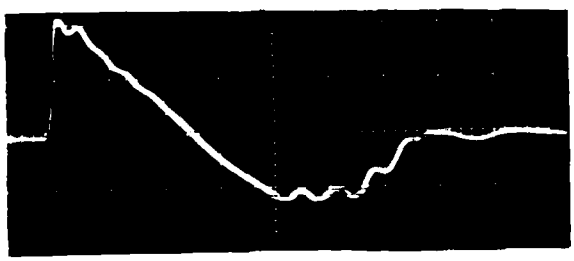

R = 9.76 m
p_f = 28.4 Pa
t_f = 4.78 μs
5 μs/div

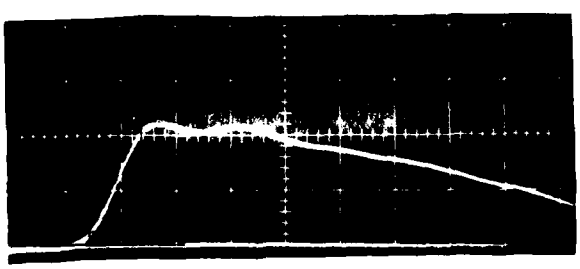

R = 15.6 m
p_f = 15.9 Pa
t_f = 7.15 μs
10 μs/div

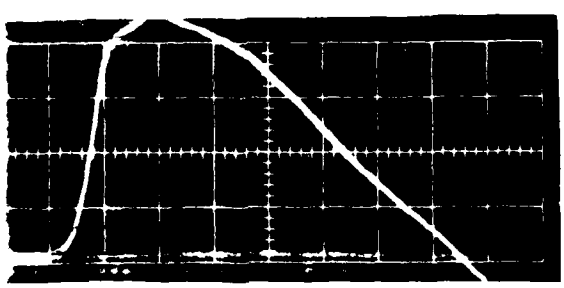

R = 21.56 m
p_f = 8.16 Pa
t_f = 11.7 μs
10 μs/div

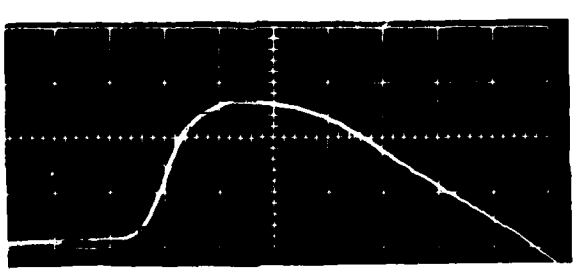

FIG. 2.19(c) SPARK-GENERATED N-WAVES.

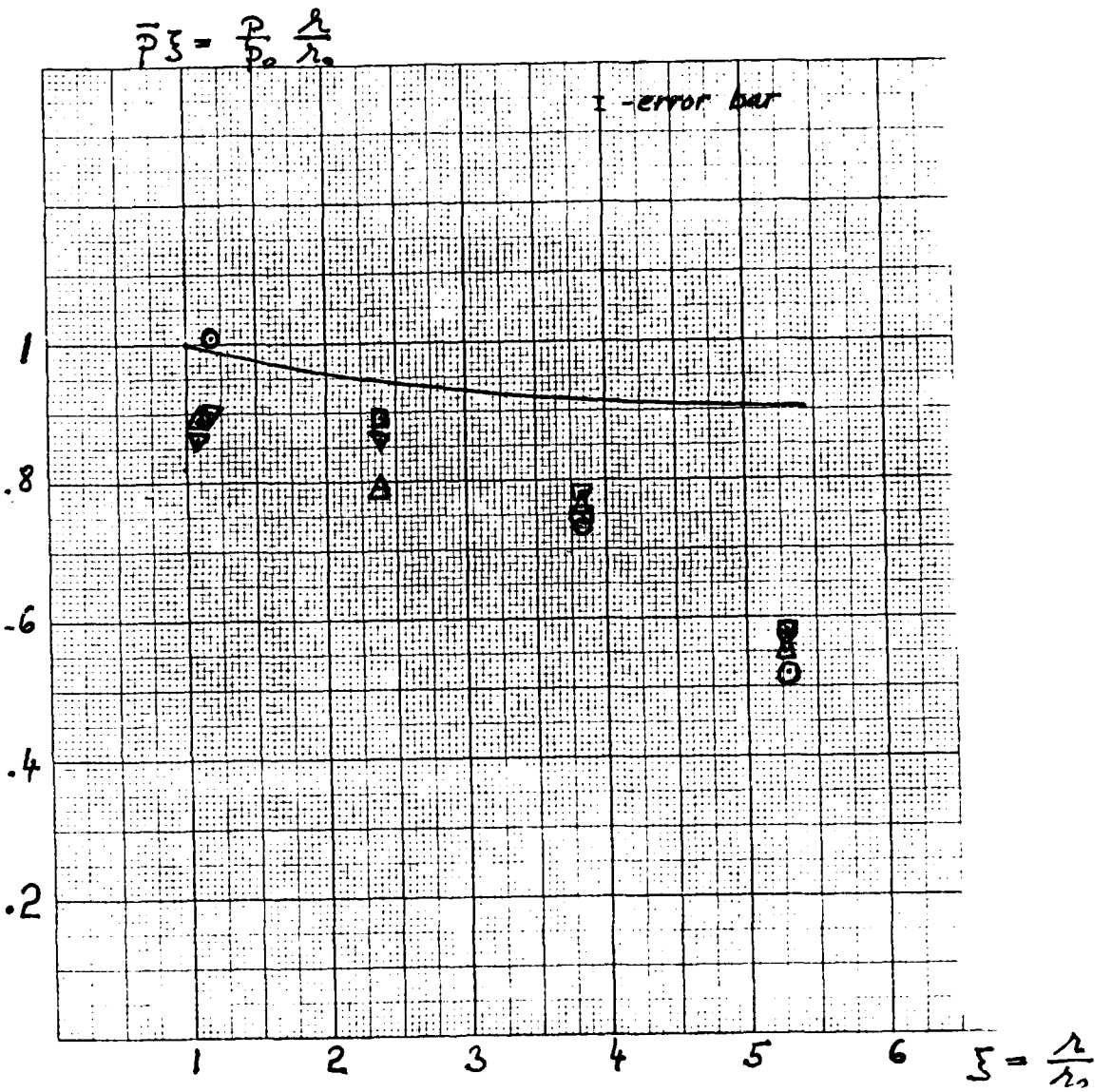

FIG. 2.19(d) NONDIMENSIONALIZED PEAK OVERPRESSURE VERSUS DISTANCE OF FRONT SHOCKS IN SPARK-GENERATED N-WAVES. TOTAL OF 100 MEASURED PRESSURES AT THE SOURCE STRENGTHS S = 4.4 kV, S = 5.0 kV, S = 5.4 kV, S = 6.0 kV, r_o = 4.08m.

ℓ = 2.5 cm

p_f = 45.8 Pa
p_r = 32.2 Pa
t_r = 32.2 μs
T = 239 μs
50 μs/div

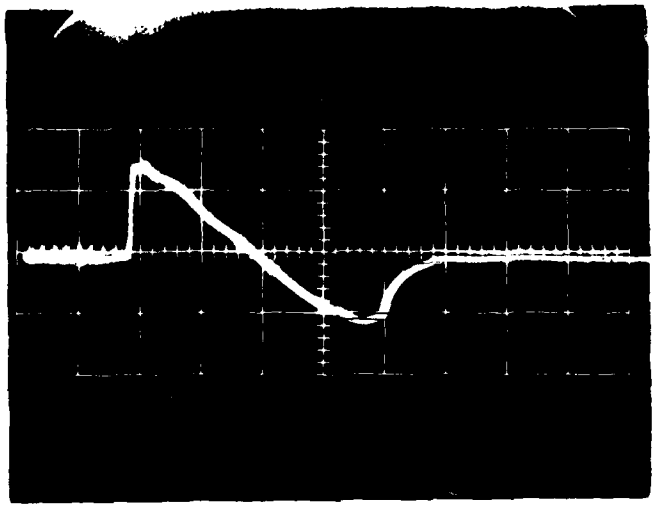

ℓ = 6.0 cm

p_f = 48.3 Pa
p_r = 39.0 Pa
T = 197 μs
50 μs/div

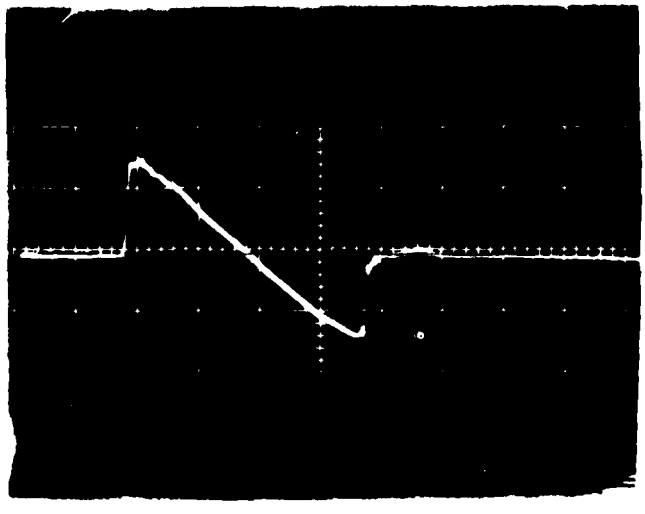

FIG. 2.20 EFFECTS OF EXPLODING-WIRE LENGTH ON N-WAVE SYMMETRY AND RISE TIME.

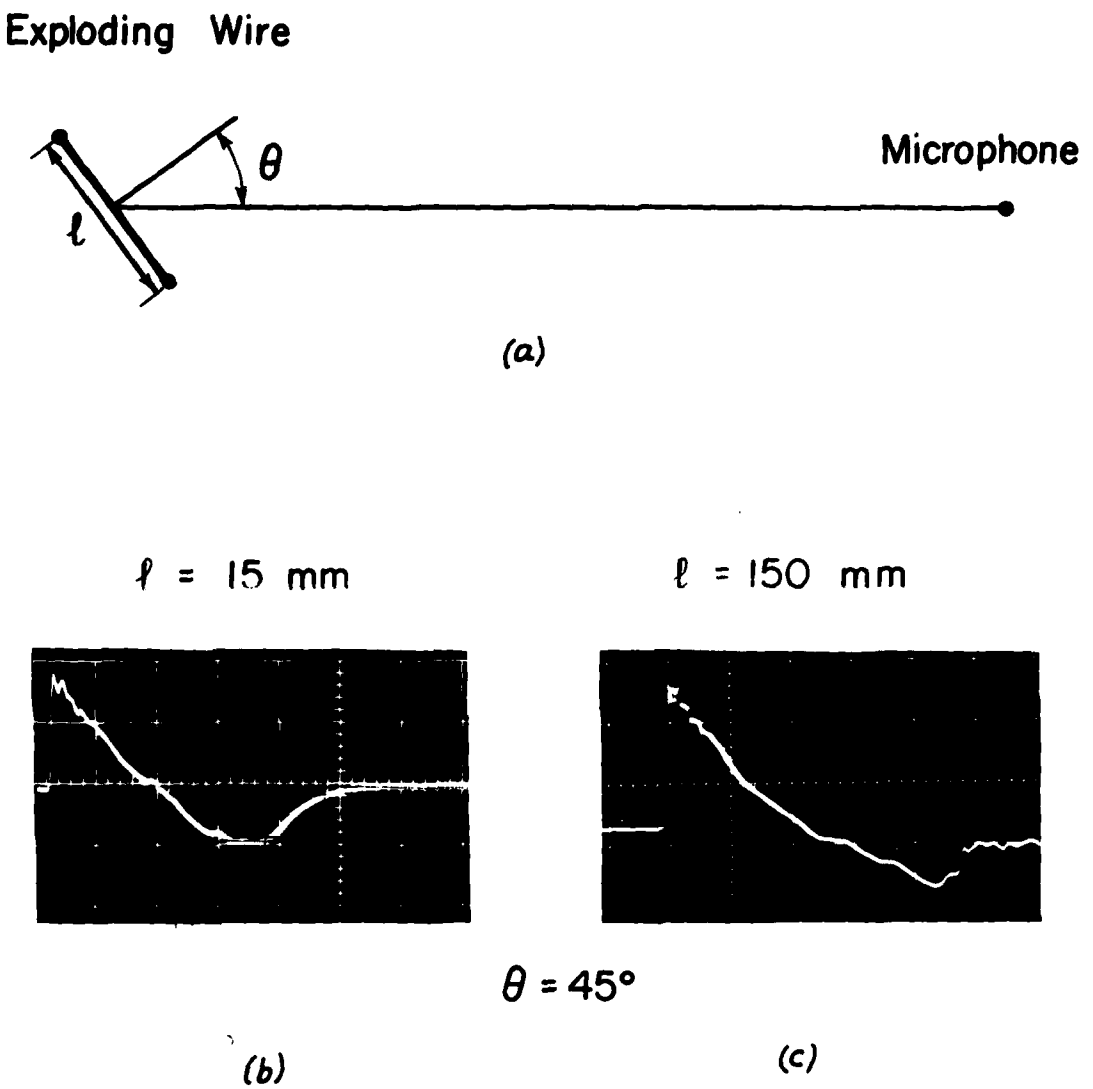

FIG. 2.21 EFFECTS OF EXPLODING-WIRE LENGTHS AND ORIENTATION ON N-WAVES.

(b) p_f = 227 Pa, p_r = 108 Pa, t_r = 50 μs, 50 μs/div
(c) 50 μs/div.

S = 4.6 kV , ℓ = 5 cm

R = 24.3 m

p_f = 19.3 Pa
t_f = 14.0 μs
p_r = 14.7 Pa
t_r = 16.8 μs
T = 175 μs
50 μs/div

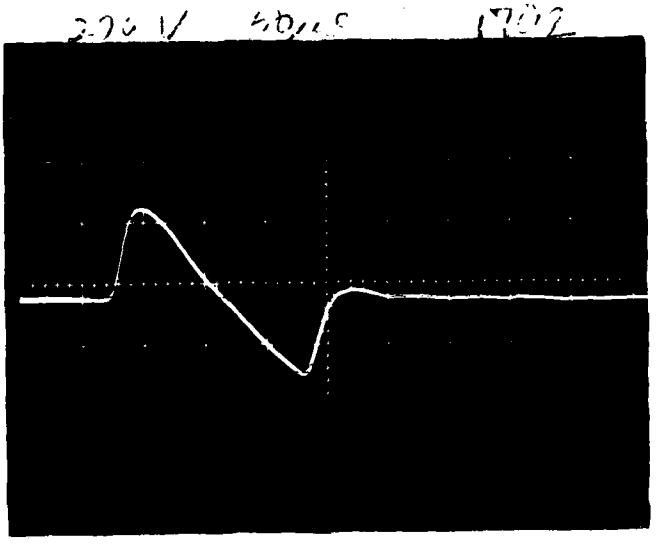

R = 29.3 m

p_f = 15.3 Pa
t_f = 15.4 μs
p_r = 13.7 Pa
t_r = 19.6 μs
T = 197 μs
50 μs/div

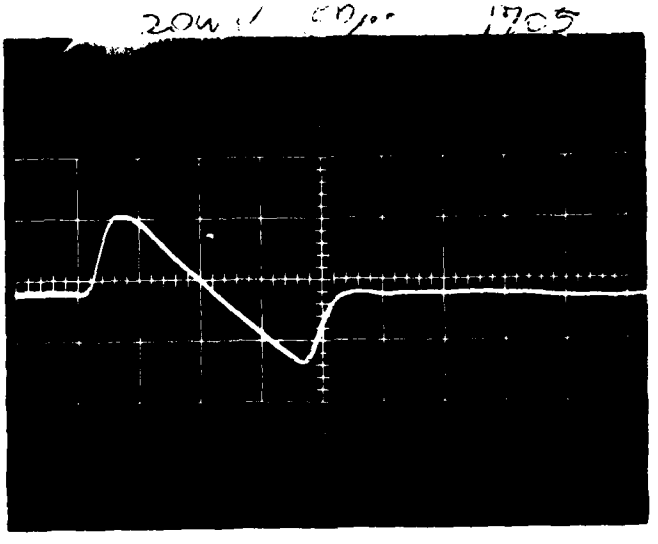

FIG. 2.22(a) EXPLODING-WIRE N-WAVES.

S = 6.0 kV , R = 24.3 m , ℓ = 5 cm

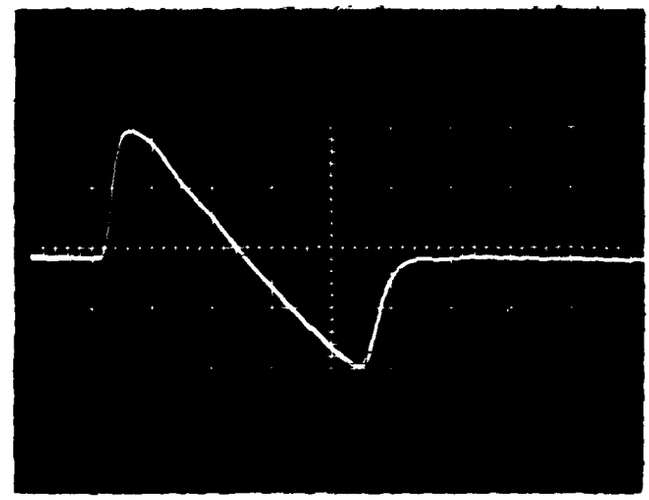

p_f = 25.6 Pa
t_f = 9.8 μs
p_r = 21.5 Pa
t_r = 23.1 μs
T = 254 μs
50 μs/div

R = 29.3 m

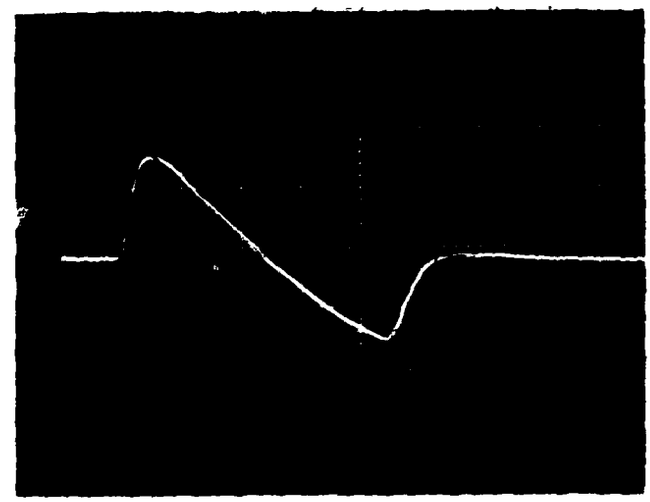

p_f = 20.0 Pa
t_f = 12.6 μs
p_r = 16.6 Pa
t_r = 35.0 μs
T = 262 μs
50 μs/div

FIG. 2.22(b) EXPLODING-WIRE N-WAVES.

APPENDIX A

MICROPHONE RESPONSE

Consideration is given to a microphone response to waves impinging on the diaphragm under various angles of incidence θ between the normal of the wavefront and the normal of the diaphragm, as shown in Fig. A1. The free-field response at incidence of a Brüel & Kjaer type microphone, as shown in the upper curve (a) in Fig. A2, is obtained when a uniform pressure is applied to the microphone diaphragm. The free-field response is the response of the microphone to a free sound field impinging on the diaphragm. The free-field correction is the difference between the two types of response, and it is caused by the mechanical presence of the microphone in the sound field. This diffraction is dependent on the angle of incidence, as shown in Fig. A2 (Ref. 39). It is seen that the free-field correction is greatest for 0° incidence, decreasing with increasing angle. This means that the frequency response of a microphone in a free field is dependent on the angle of incidence. Figure A2 shows the pressure response for a 4135 Brüel & Kjaer microphone as a solid line; above it is the free-field response for zero incidence which is flat within ± 1 dB up to $f_{max}^{4125}(0)$ = 140 kHz. The free-field response for the microphone at 90° incidence, also shown in Fig. A2, shows a frequency response which is flat within ± 1 dB up to $f_{max}^{4135}(90)$ = 12 kHz. This illustrates that the angle of incidence can decrease the bandwidth by a decade.

The impulse pressure response of the type 4135 Brüel & Kjaer microphone is shown in Fig. A3 to have a rise time from 10% to 90% of maximum amplitude of t_{4136} = 5.4 μs. A typical microphone 4136 has a characteristic upper frequency f_{4136} = 70 kHz; see Fig. A2 (Ref. 41), whereas for 4135, f_{4135} = 130 kHz (Fig. A2). The rise time of type 4135 is then estimated to be $t_{4135} = (f_{4136}/f_{4135})\, t_{4136}$ or t_{4135} = 2.9 μs. It should be noted that the microphones have virtually no ringing; see Fig. A3.

We assume that the rise time due to an impulse of a uniform pressure is equal to the rise time of a free-field impulse at 0° incidence, i.e., $t_{4135}(0)$ = 2.9 μs. The rise time for 90° incidence can be calculated now, $t_{4135}(90) = [f_{max}^{4135}(0)/f_{max}^{4135}(90)]\, t_{4135}(0)$, hence $t_{4135}(90)$ = 33.8 μs.

When thin shock fronts are to be measured by a transducer of diameter d of the sensing surface, the angle of incidence has another effect as shown in Fig. A1. The shock front of thickness h has a normal propagation speed c at the angle θ to the normal of the microphone diaphragm. For a point microphone, d ~ 0, the measured rise time would be $t_s = h/c$, the rise time of the shock. For an infinitely thin shock, h ~ 0, the rise time would be the traversing time $t_{tr}(\theta) = \bar{d}/c = d \sin\theta/c$. Hence the rise time for a finite thickness shock-wave measured by a finite diameter microphone at an angle of incidence θ is $t_m(\theta) = t_{tr}(\theta) + t_s$. Note that for θ = 0, the lower limit on $t_m(0)$ is the microphone rise time, say in the present case $t_m(0) \geq t_{4135}$.

Hence if $t_s < t_{4135}$ we have

$$t_m^{4135}(\theta) = t_{tr}(\theta) + t_{4135}(\theta)$$

The microphone rise time is at 0 incidence $t_m^{4135}(0) = 2.90$ μs, at 90 incidence $t_m^{4135}(90) = 52.6$ μs.

The 1.0 cm-dia Brüel & Kjaer microphone type 4146 has been widely used in sonic-boom field-measurements. Its high frequency response is the same as for type 4144, and the rise time will be the same. The rise time of type 4144 is, as shown in Fig. A3, $t_{4144} = 35$ μs and $t_{4145} = 35$ μs, which is for uniformly distributed pressure instantaneously applied to the diaphragm. The angle of incidence dependency on the free-field response is seen in Fig. A4 where the difference between 0 and 90 degree incidence shows a shift in the -1 dB frequency from $f_{max}^{4146}(0) = 13$ kHz to $f_{max}^{4146}(90) = 7.8$ kHz. The free-field response at 90 incidence is seen to follow the pressure response until 10 kHz, hence $t_{4146}(90) = 7.8$ kHz. The free field re ponse at 90 incidence is seen to follow the pressure response until 10 kHz; hence $t_{4146}(90) = 35$ μs, and

$$t_{4146}(0) = [f_{max}^{4146}(90)/f_{max}^{4146}(0)]\cdot t_{4146}(90) = 21 \text{ μs}$$

The traversing time at T = 285°K is $t_{tr}(\theta) = 70.3 \sin\theta$ μs. The rise time of the type 4146 microphone is for 90 incidence $t_m^{4146}(90) = 105$ μs, for 0 incidence $t_m^{4146}(0) = 21$ μs.

From the above estimates it is seen that the angle of incidence is a very important parameter in the detection of shocks by condenser microphones.

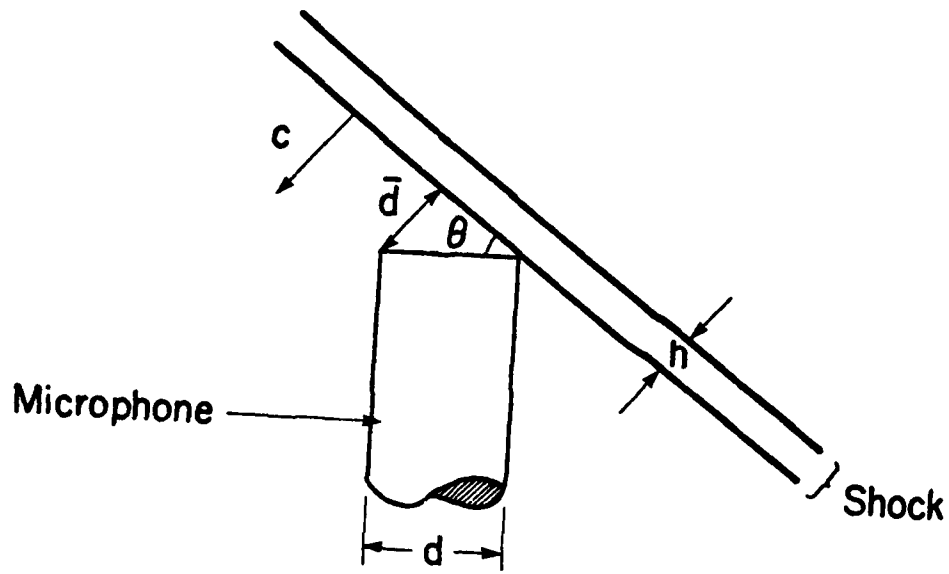

FIG. A1 A SHOCK OF THICKNESS h AND SPEED c IMPINGES ON A MICROPHONE OF DIAMETER d UNDER AN ANGLE OF INCIDENCE θ.

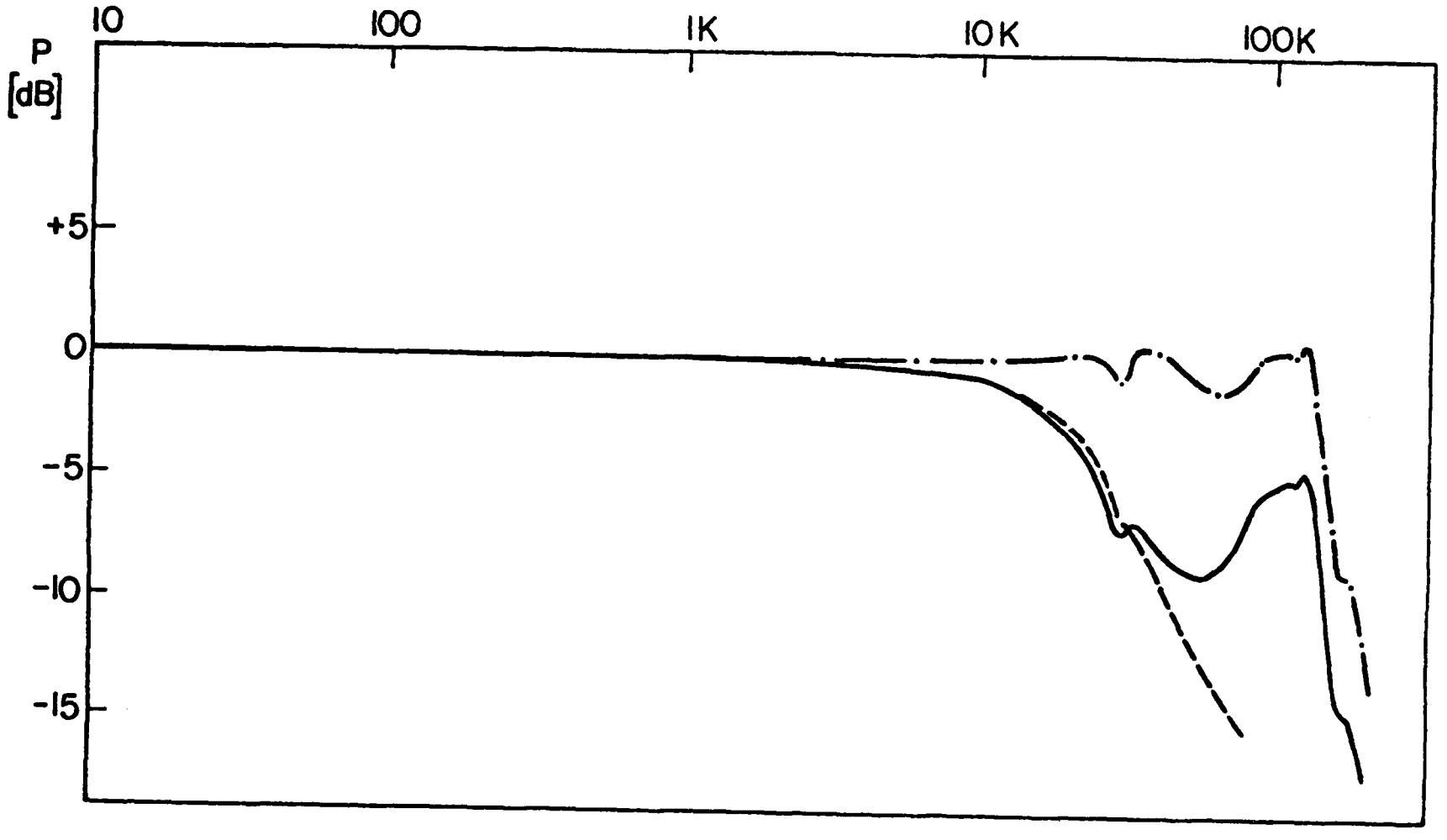

FIG. A2 FREQUENCY RESPONSE OF BRÜEL & KJAER MICROPHONE TYPE 4135 (REF. 39).

(a) ———— PRESSURE RESPONSE, TYPE 4135
(b) —·—·— FREE FIELD RESPONSE, 0° INCIDENCE
(c) – – – – FREE FIELD RESPONSE, 90° INCIDENCE

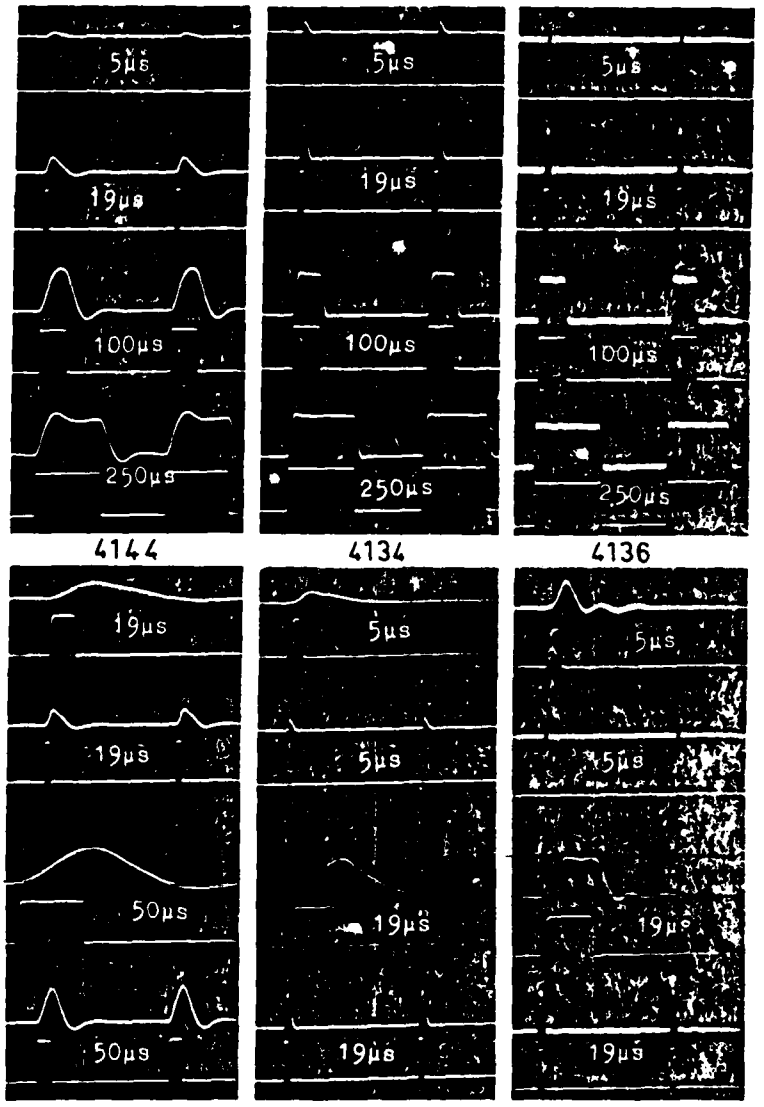

FIG. A3 COMPARISON OF THE PULSE RESPONSES OF SOME B & K MICROPHONES. FROM LEFT TO RIGHT: 1 INCH TYPE 4144, 1/2 INCH TYPE 4134, 1/4 INCH TYPE 4136 (REF. 40).

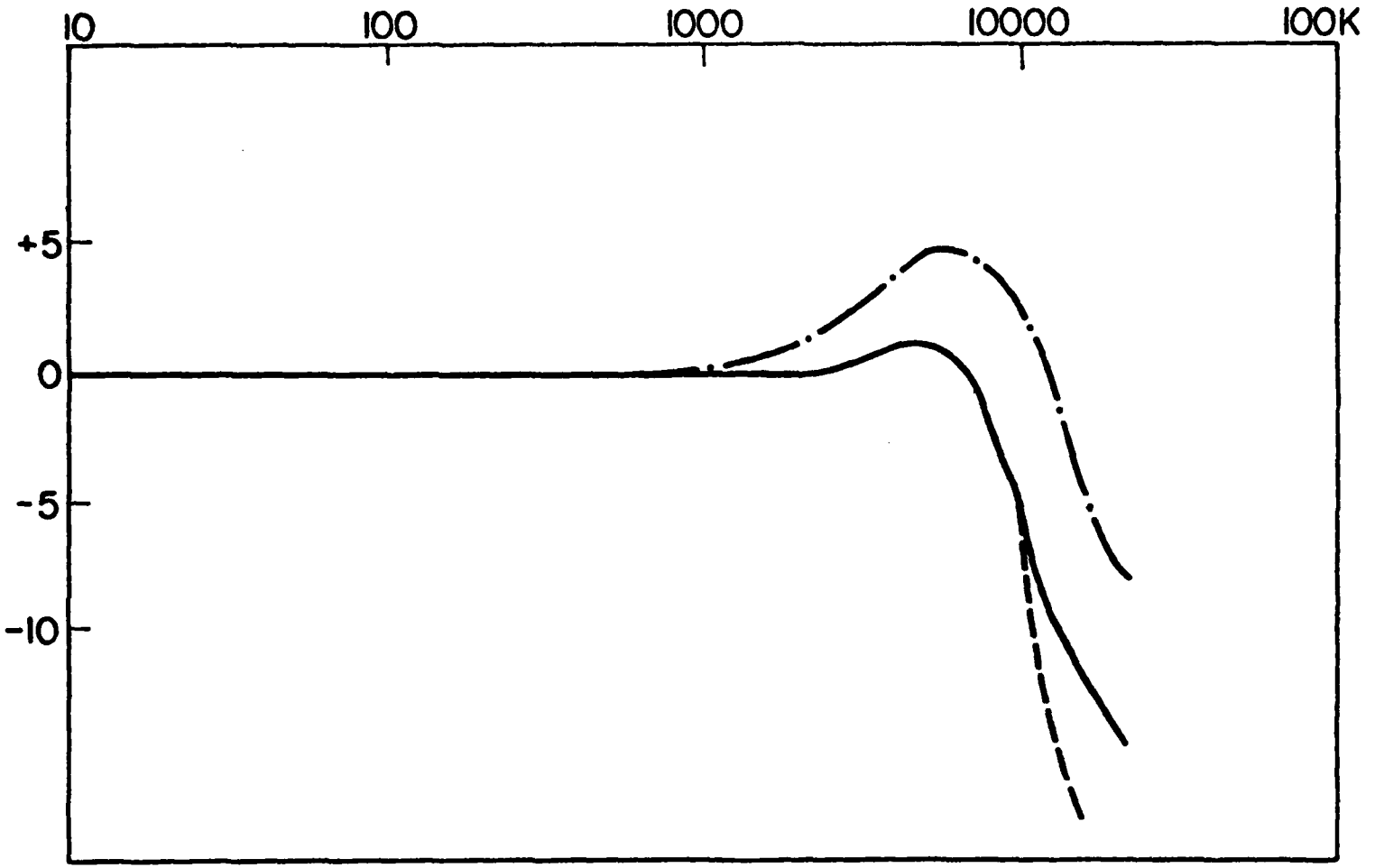

FIG. A4 FREQUENCY RESPONSE OF BRÜEL & KJAER MICROPHONE TYPE 4144 (REF. 40).

(a) ———— PRESSURE RESPONSE
(b) —·—·— FREE FIELD RESPONSE, 0° INCIDENCE
(c) – – – – FREE FIELD RESPONSE, 90° INCIDENCE

APPENDIX B

BULK PRESENTATION OF SPARK AND EXPLODING WIRE EXPERIMENTS

Each run is numbered.

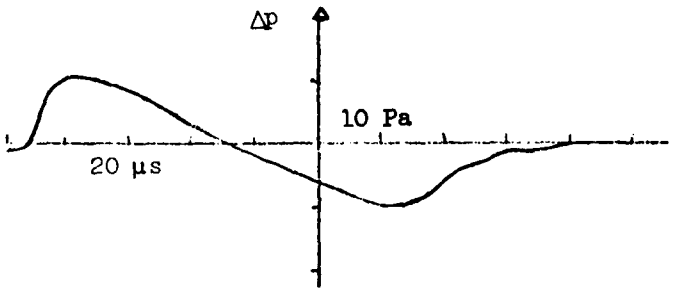

T_d = 11.7°C RH = 70%
T_w = 9.3°C
R = 11.75 m Run 903

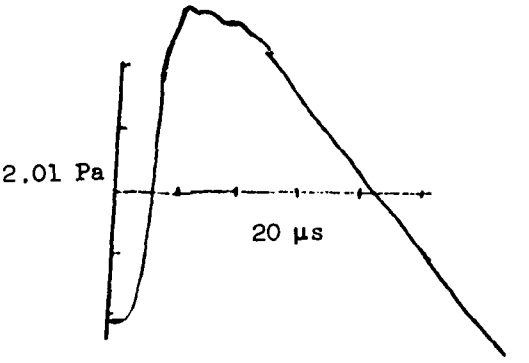

Cu - wire
R = 11.75 m Run 1002

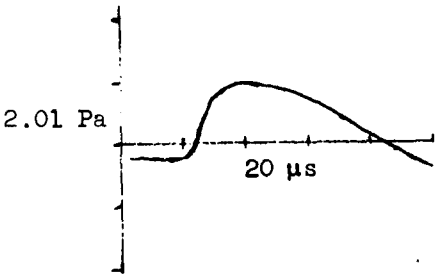

T_d = 11.7°C RH = 60%
T_w = 7.78°C
R = 11.75 m Run 1001

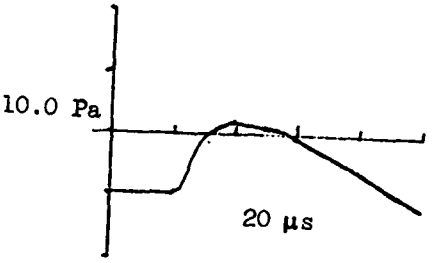

Spark Run 1003
R = 11.75m

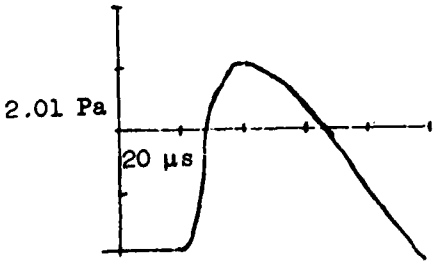

Run 1001

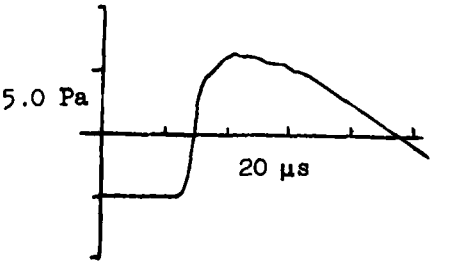

Cu - wire Run 1004
R = 18.5m

FIG. B1

FIG. B2

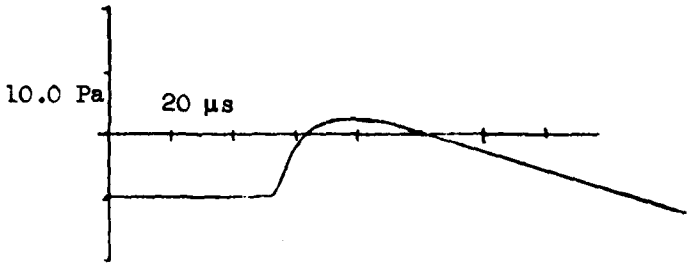

Cu - wire Run 1005

R = 18.50m

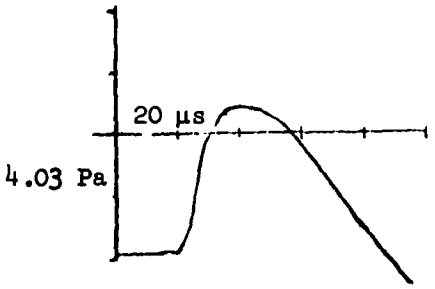

T_d = 15.6°C RH = 50%
T_w = 10.0°C
R = 12.5 m Run 1108

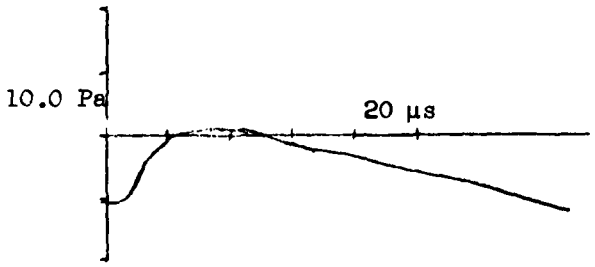

Ni - wire Run 1006

R = 18.50m

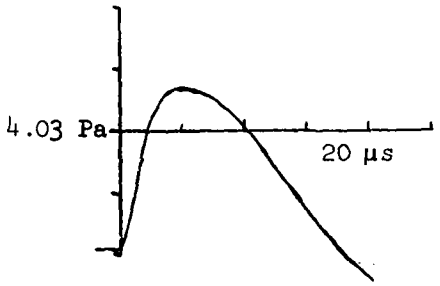

R = 12.5 m Run 1109

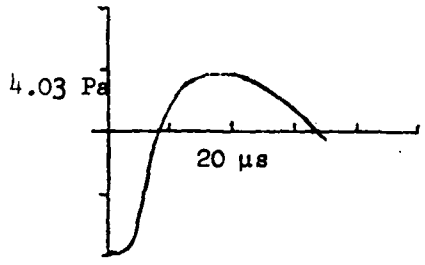

Cu - wire Run 1008

R = 18.5m

FIG. B3

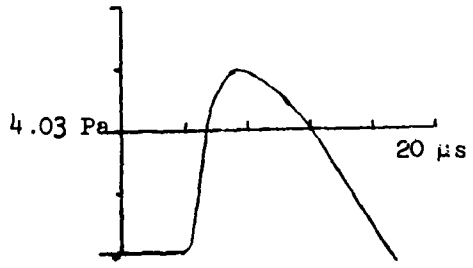

R = 12.5 m Run 1110

FIG. B4

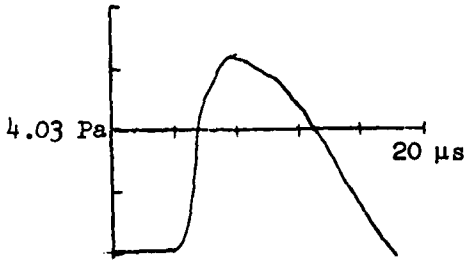

R = 12.5 m Run 1111

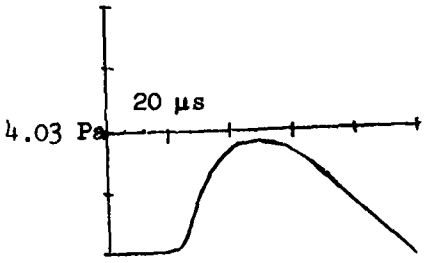

R = 12.5m Run 1114

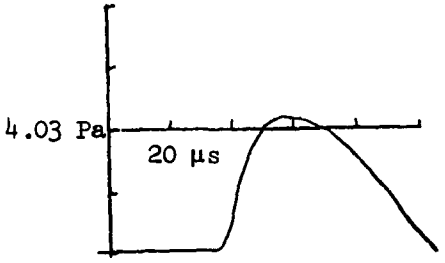

R = 12.5m Run 1112

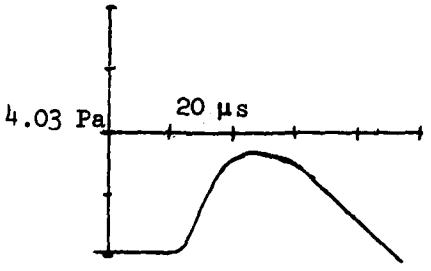

R = 12.5m Run 1115

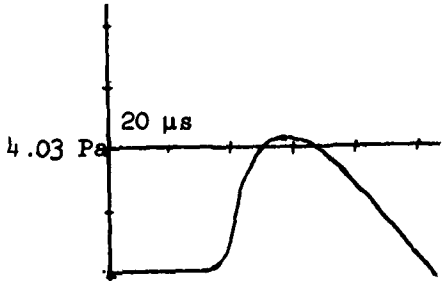

R = 12.5m Run 1113

FIG. B5

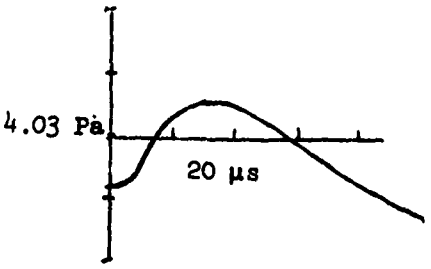

R = 12.5m Run 1116

FIG. B6

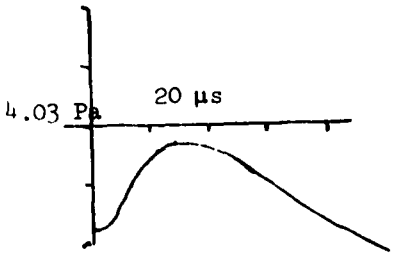

R = 12.5m Run 1117

FIG. B7

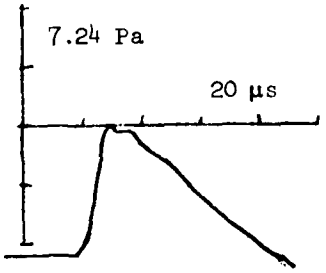

R = 15.2m Run 1204

Free-field mounted 4135
1/4" B&K microphone

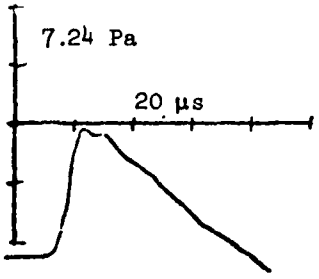

R = 15.2 Run 1206

FIG. B8

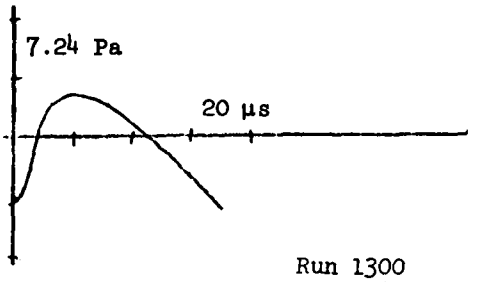

Run 1300

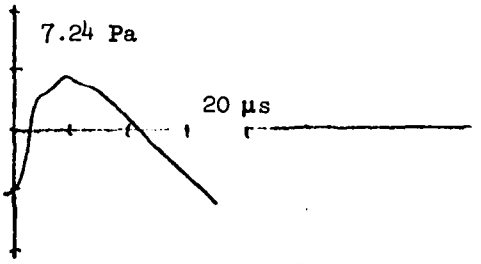

Run 1301

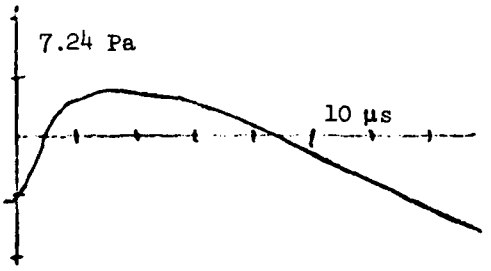

Run 1302

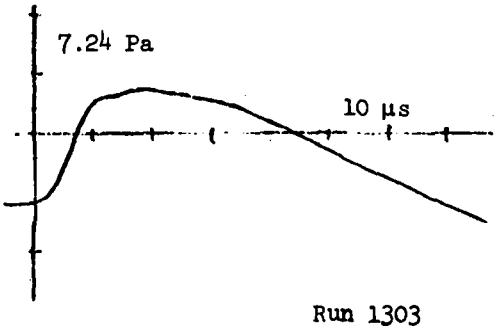

Run 1303

FIG. B9

S = 50 kV
R = 15.6m
T_w = 0 3°C
T_d = 2 5°C
RH = 67%

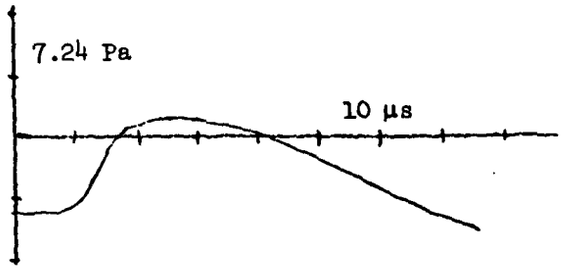

Run 1304

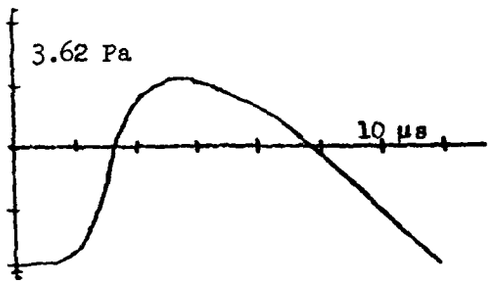

Run 1305

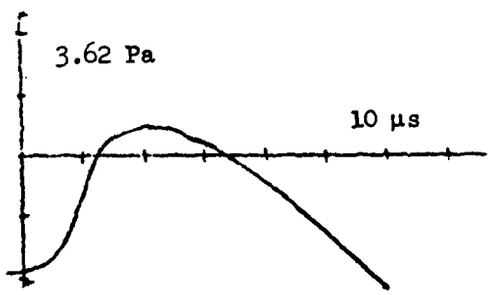

Run 1306

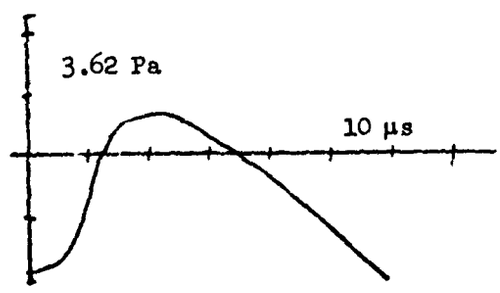

Run 1307

FIG. B10

S = 4.4 kV
T_w = 0.3°C
T_d = 2.5°C
R = 15.6m
RH = 67%

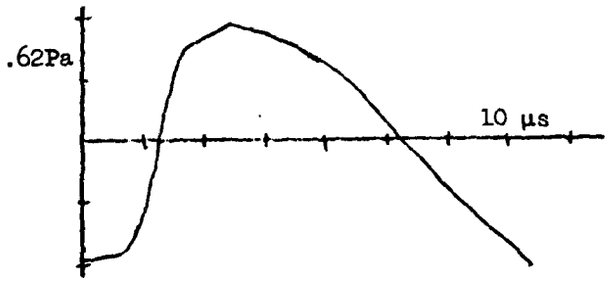

Run 1308

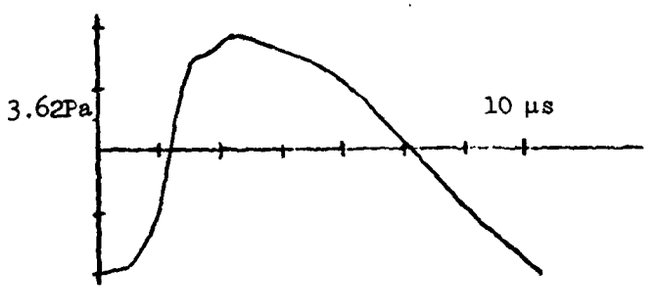

Run 1309

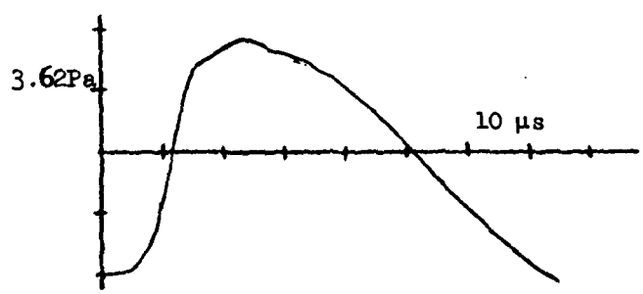

Run 1310

FIG. B11

S = 5.4 kV
T_w = 0.3°C
T_d = 2.5°C
R = 15.6m
RH = 67%

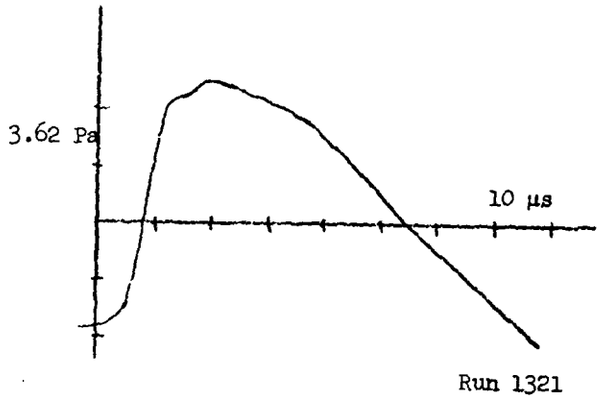

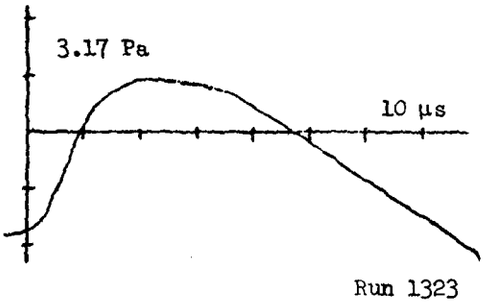

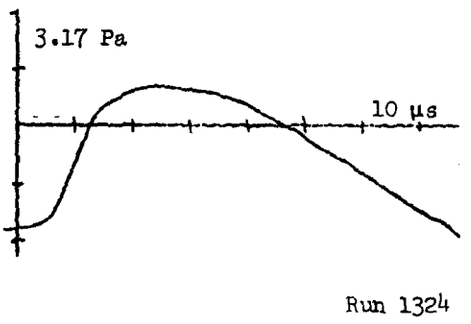

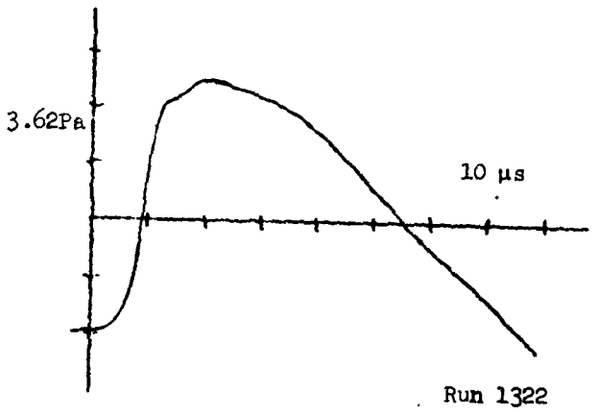

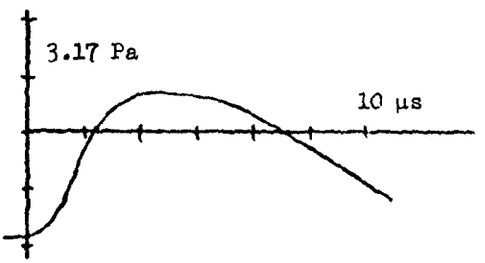

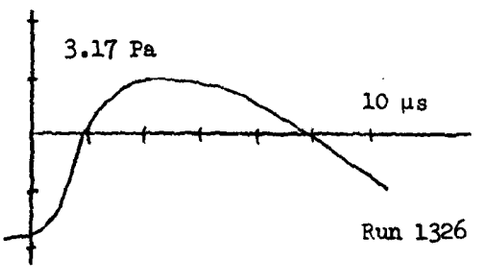

FIG. B12

S = 6.0 kV
R = 15.6m
T_w = 0.3°C
T_d = 2.5°C
RH = 67%

FTG. B13

S = 6.0 kV
R = 21.56m
T_d = 0.6°C
T_w = -1.11°C
RH = 73%

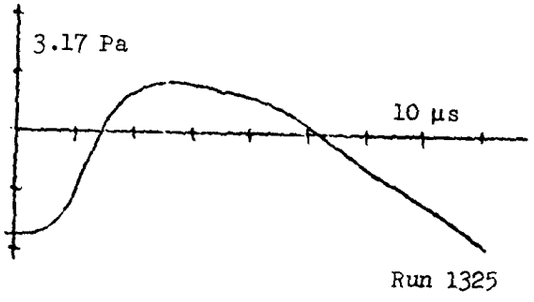

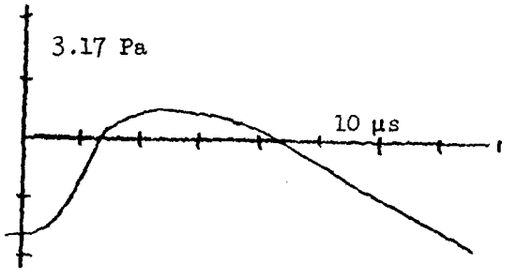

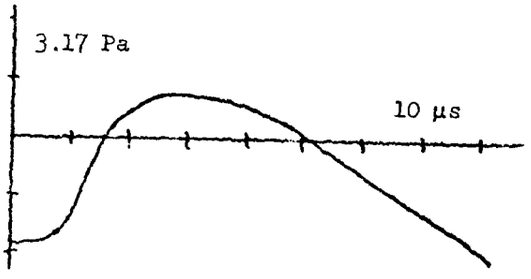

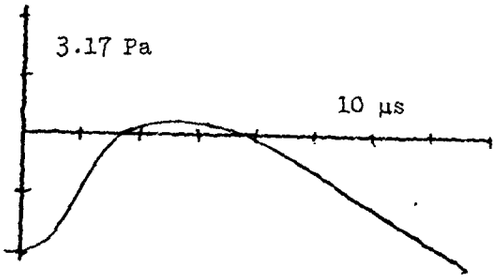

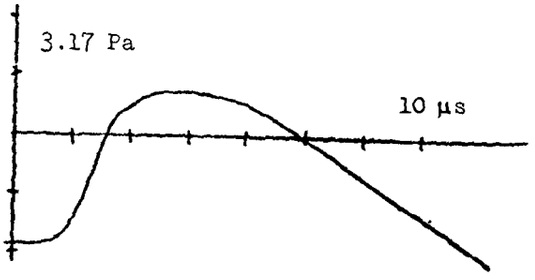

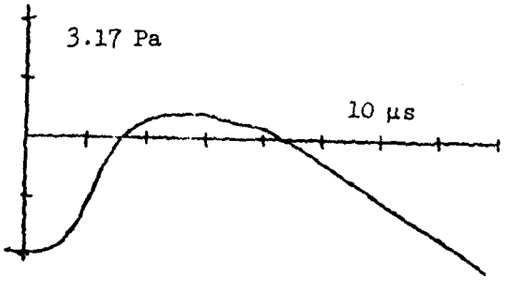

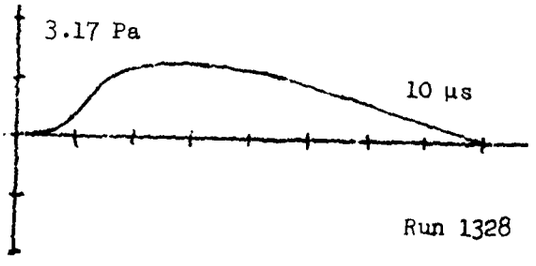

FIG. B14

S = 5.4 kV
R = 21.56m
T_d = 0.6°C
T_w = -1.11°C
RH = 73%

FIG. B15

S = 5.0 kV
R = 21.56m
T_d = 0.6°C
T_w = -1.11°C
RH = 73%

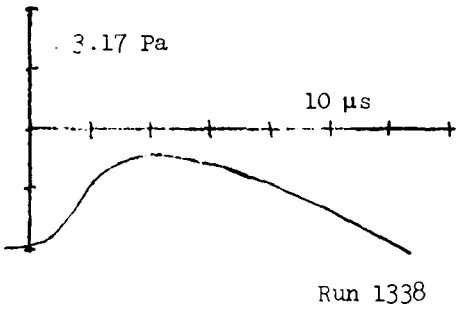

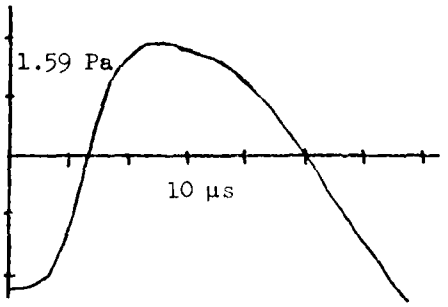

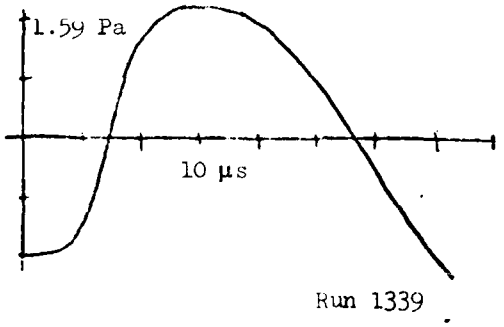

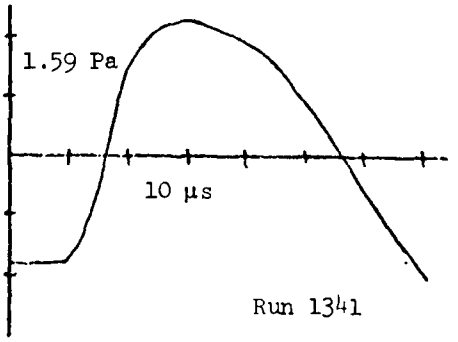

FIG. B16

S = 4.4 kV
R = 21.56m
T_d = 0.6°C
T_w = -1.11°C
RH = 73%

FIG. B17

S = 4.4 kV
R = 21.56m
T_d = 0.6°C
T_w = -1.11°C
RH = 73%

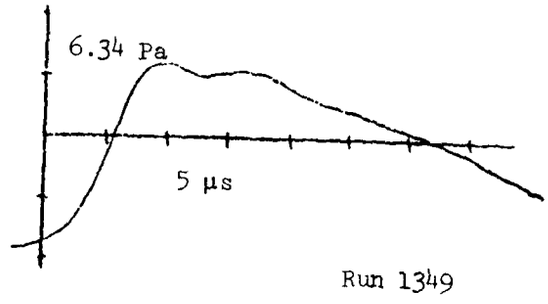

Run 1349

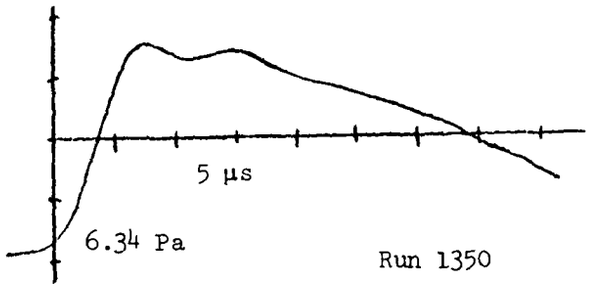

Run 1350

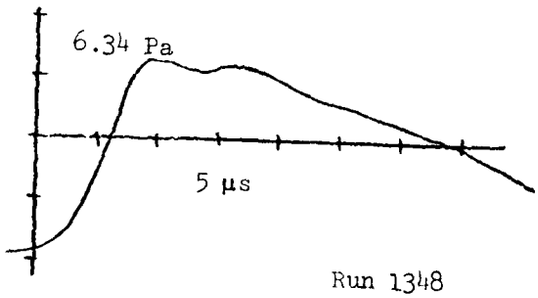

Run 1348

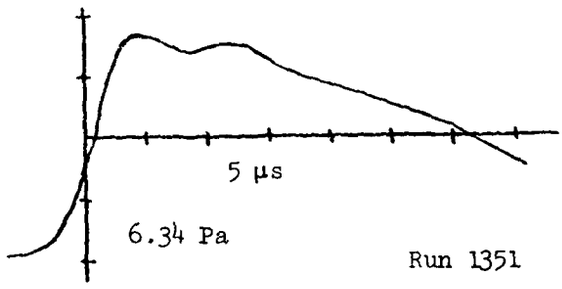

Run 1351

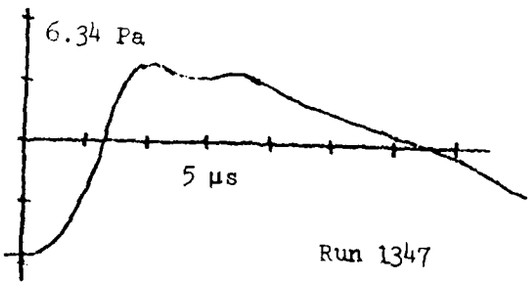

Run 1347

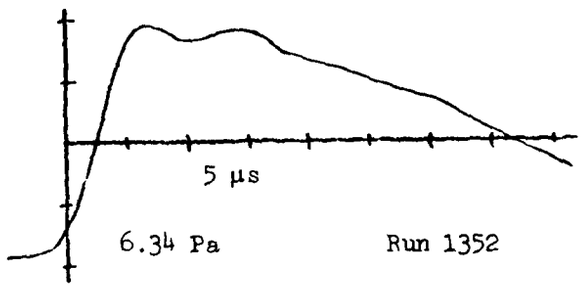

Run 1352

FIG. B18

S = 4.4 kV
R = 9.76m
T_d = 3.1°C
T_w = -0.6°C
RH = 50%

FIG. B19

S = 5.0 kV
R = 9.76m
T_d = 3.1°C
T_w = -0.6°C
RH = 50%

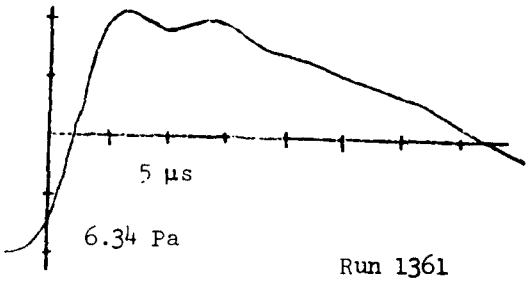

Run 1361

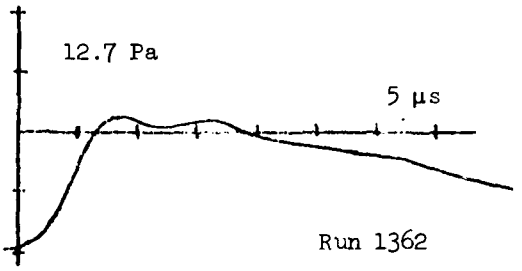

Run 1362

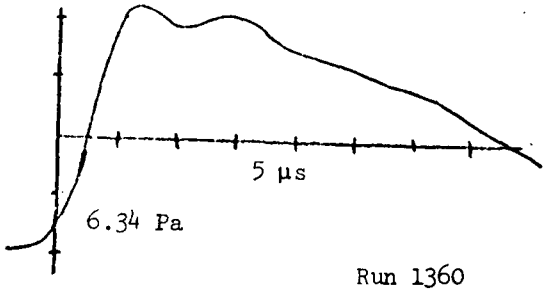

Run 1360

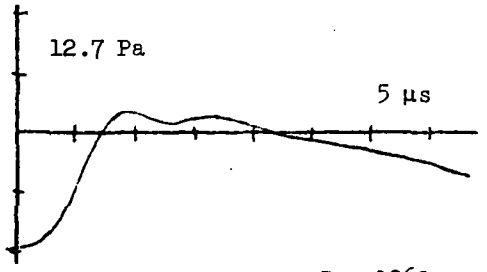

Run 1363

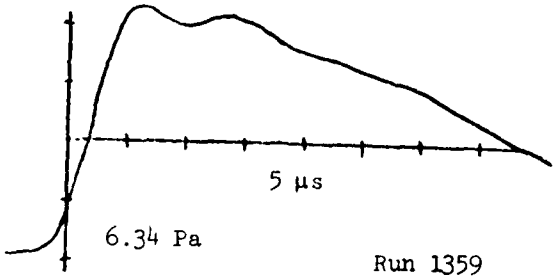

Run 1359

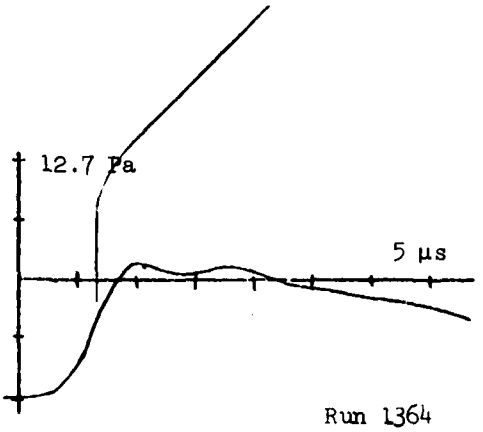

Run 1364

FIG. B20

S = 5.4 kV
R = 9.76m
T_d = 3.1°C
T_w = -0.6°C
RH = 50%

FIG. B21

S = 6.0 kV
R = 9.76m
T_d = 3.1°C
T_w = -0.6°C
RH = 50%

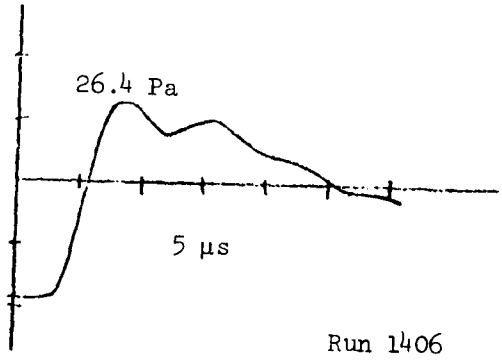

Run 1406

FIG. B22

S = 6.0 kV
R = 4.08m
T_d = 3.1°C
T_w = -0.6°C
RH = 50%

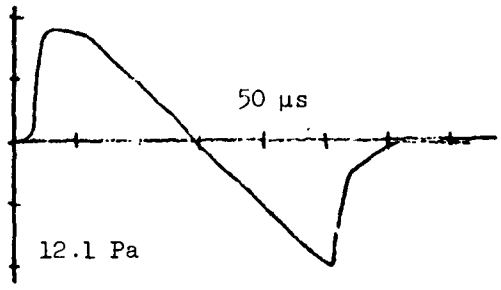

ℓ = 5cm
S = 6.0 kV

Run 1601

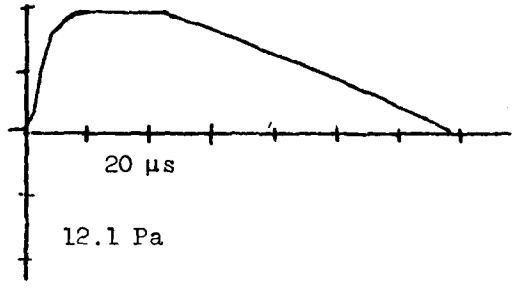

ℓ = 5 cm
S = 6.0 kV

Run 1602

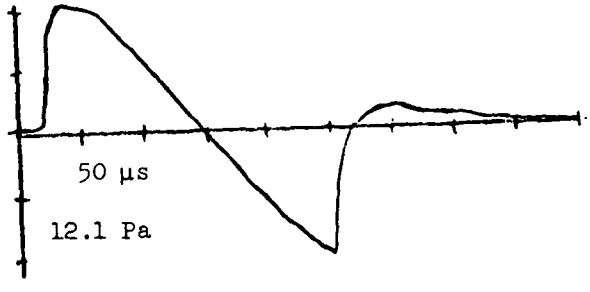

ℓ = 12 cm
S = 6.0 kV

Run 1603

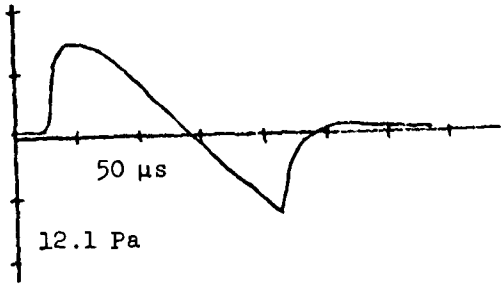

ℓ = 5 cm
S = 4.6 kV

Run 1604

FIG. B23

R = 27.6m
T_d = 4°C
RH = 75%

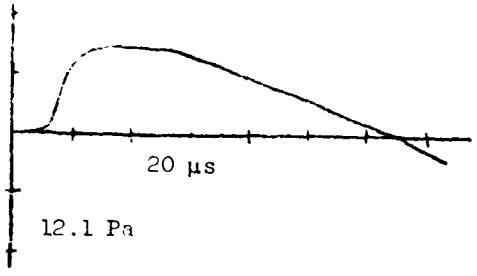

ℓ = 5cm
S = 4.6 kV Run 1605

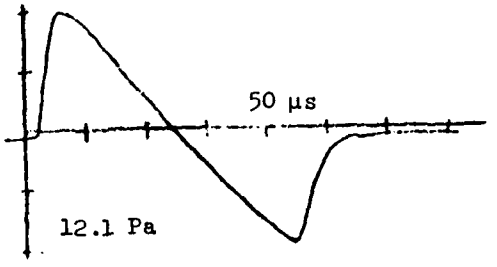

S = 6.0 kV
R = 24.3m
ℓ = 5 cm Run 1701

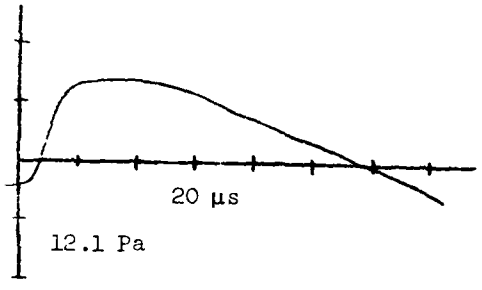

ℓ = 5cm
S = 6.0 kV Run 1606

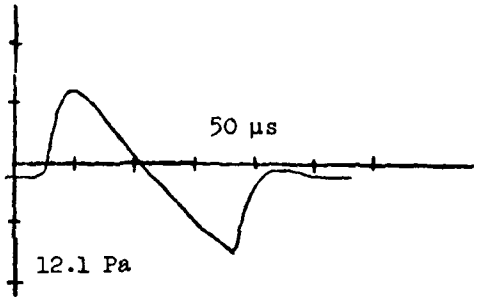

S = 4.6 kV
R = 24.3m
ℓ = 5cm Run 1702

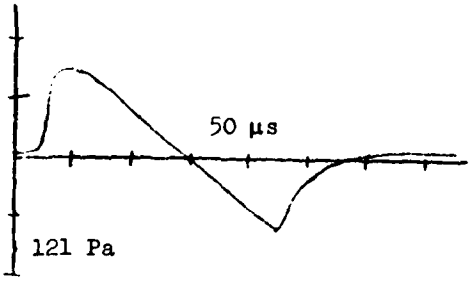

ℓ = 2 cm
S = 6.0 kV Run 1607

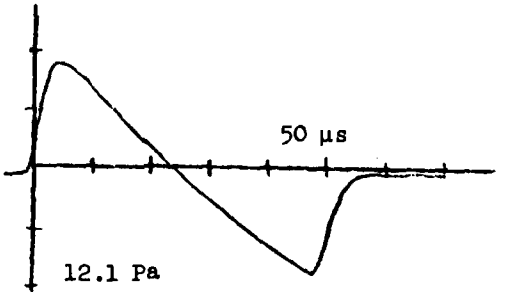

S = 7.0 kV
R = 29.3m
ℓ = 5 cm Run 1703

FIG. B24

R = 27.6m
T = 277 K
RH = 75%

FIG. B25

T_d = 7°C
RH = 87.5%

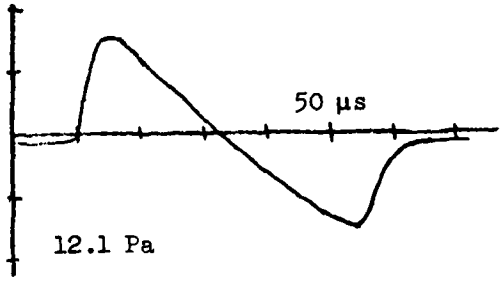

S = 6.0 kV
R = 29.3m
ℓ = 5 cm

Run 1704

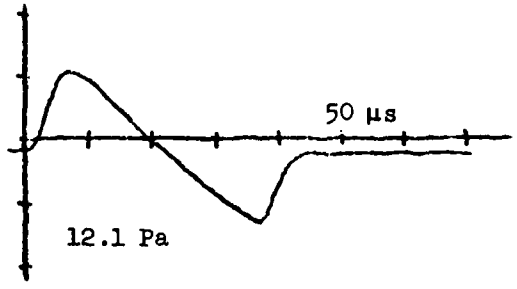

S = 4.6 kV
R = 29.3m
ℓ = 5 cm

Run 1705

FIG. B26

T_d = 7°C
RH = 87.5%

UTIAS Technical Note No. 229

Institute for Aerospace Studies, University of Toronto (UTIAS)
4925 Dufferin Street, Downsview, Ontario, Canada, M3H 5T6

AN EXPERIMENTAL INVESTIGATION OF RISE TIMES OF VERY WEAK SHOCK WAVES

Holst-Jensen, Ole

1. Sonic Boom 2. N-Waves 3. Exploding Wires 4. Exploding Sparks
5. Travelling-Wave Sonic-Boom Simulator

I. Holst-Jensen, Ole II. UTIAS Technical Note No. 229

The present work has as its main contribution the development of the experimental technique of using exploding wires to generate N-waves. Consideration is also given to N-waves generated by sparks, in the UTIAS Travelling-Wave Sonic-Boom Simulator and from supersonic aircraft.

Available copies of this report are limited. Return this card to UTIAS, if you require a copy.

UTIAS Technical Note No. 229

Institute for Aerospace Studies, University of Toronto (UTIAS)
4925 Dufferin Street, Downsview, Ontario, Canada, M3H 5T6

AN EXPERIMENTAL INVESTIGATION OF RISE TIMES OF VERY WEAK SHOCK WAVES

Holst-Jensen, Ole

1. Sonic Boom 2. N-Waves 3. Exploding Wires 4. Exploding Sparks
5. Travelling-Wave Sonic-Boom Simulator

I. Holst-Jensen, Ole II. UTIAS Technical Note No. 229

The present work has as its main contribution the development of the experimental technique of using exploding wires to generate N-waves. Consideration is also given to N-waves generated by sparks, in the UTIAS Travelling-Wave Sonic-Boom Simulator and from supersonic aircraft.

Available copies of this report are limited. Return this card to UTIAS, if you require a copy.

UTIAS Technical Note No. 229

Institute for Aerospace Studies, University of Toronto (UTIAS)
4925 Dufferin Street, Downsview, Ontario, Canada, M3H 5T6

AN EXPERIMENTAL INVESTIGATION OF RISE TIMES OF VERY WEAK SHOCK WAVES

Holst-Jensen, Ole

1. Sonic Boom 2. N-Waves 3. Exploding Wires 4. Exploding Sparks
5. Travelling-Wave Sonic-Boom Simulator

I. Holst-Jensen, Ole II. UTIAS Technical Note No. 229

The present work has as its main contribution the development of the experimental technique of using exploding wires to generate N-waves. Consideration is also given to N-waves generated by sparks, in the UTIAS Travelling-Wave Sonic-Boom Simulator and from supersonic aircraft.

Available copies of this report are limited. Return this card to UTIAS, if you require a copy.

UTIAS Technical Note No. 229

Institute for Aerospace Studies, University of Toronto (UTIAS)
4925 Dufferin Street, Downsview, Ontario, Canada, M3H 5T6

AN EXPERIMENTAL INVESTIGATION OF RISE TIMES OF VERY WEAK SHOCK WAVES

Holst-Jensen, Ole

1. Sonic Boom 2. N-Waves 3. Exploding Wires 4. Exploding Sparks
5. Travelling-Wave Sonic-Boom Simulator

I. Holst-Jensen, Ole II. UTIAS Technical Note No. 229

The present work has as its main contribution the development of the experimental technique of using exploding wires to generate N-waves. Consideration is also given to N-waves generated by sparks, in the UTIAS Travelling-Wave Sonic-Boom Simulator and from supersonic aircraft.

Available copies of this report are limited. Return this card to UTIAS, if you require a copy.

END

DATE
FILMED

1-82

DTIC